Performance evaluation of WC-12wt%Co as grinding wheel abrasive material by machining a titanium alloy

by

Anton Alexander Enever

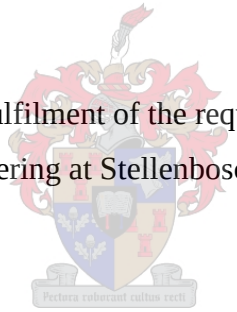

Thesis presented in partial fulfilment of the requirements for the degree Master of Engineering at Stellenbosch University

Supervisor: Dr Gert Adriaan Oosthuizen

Department of Industrial Engineering, Faculty of Engineering, Stellenbosch University

Co-supervisor: Prof Natasha Sacks

School of Chemical and Metallurgical Engineering, Faculty of Engineering, University of the Witwatersrand

March 2016

Declaration

By submitting this thesis electronically, I declare that the entirety of the work contained therein is my own, original work, that I am the sole author thereof (save to the extent explicitly otherwise stated), that reproduction and publication thereof by Stellenbosch University will not infringe any third party rights and that I have not previously in its entirety or in part submitted it for obtaining any qualification.

March 2016

Abstract

Grinding has been the most common machining process for material removal in manufacturing for many decades. The process originated from the realization that harder materials have the ability to abrasively alter the geometry and surface finish of softer materials. It was originally used in construction of buildings by abrasively forming limestone building bricks into desired shapes and sizes. This process has evolved over time to the high precision manufacturing industries of the modern era. High quality and high precision parts are manufactured with the use of grinding wheels, from rough part forming or part cutting to precision automotive engine components such as cam shafts. Most abrasives in modern grinding processes have been developed for general applications, while others are intended for specialised applications. The use of tungsten carbide as abrasive for both general and specialised grinding wheels is not generally implemented in industrial applications or used in published research work.

This carbide falls in the refractory group of materials. When it is mixed and sintered with a ductile metal such as cobalt, molybdenum or nickel, its classification changes to a cemented carbide or cermet (ceramic metal). The amount of metal incorporated in a cermet mainly influences the ductility and transverse rupture strength. A metal content of about 12 wt% (12 weight %) is roughly the midway between a hard and brittle and a ductile cermet, giving tungsten carbide a unique hardness to ductile ratio. The metal that works best with tungsten carbide is cobalt, thus producing the cermet WC-12wt%Co. This specific cermet is commonly used as the base material for machining tools (for lathes and milling machines) due to its high hardness to toughness ratio that is needed for machining hard metals such as tool steels or titanium alloys. The base WC-12wt%Co material can be used as is for machining, but it is commonly coated with layers of other high wear resistant materials (such as titanium nitride, TiN, or titanium carbo-nitride, TiCN).

This study focuses on the custom manufacture of a grinding wheel containing WC-12wt%Co as abrasive material, bonded together by an epoxy resin binder. This type of grinding wheel is not in use in industrial applications and must thus be specially designed and produced. The resin is used as binder, which is the case for many industrially implemented grinding wheels, to ease the production process and make it safer. The grinding wheels that were produced in this study are the smaller variant called mounted points. The performance of these mounted points was determined by the grinding of a titanium alloy and measuring the rate of wear, the surface finish the points produce on the titanium alloy and the surface hardness of the alloy.

Opsomming

Die slyp proses is die mees algemene bewerkingsproses vir die verwydering van materiaal in vervaardigingsprosesse vir baie dekades. Die proses het ontstaan uit die besef dat harder materiale die vermoë het om die geometrie en oppervlakafwerking van sagter material te verander deur slyping. Dit was oorspronklik gebruik in die konstruksie van geboue deur slyp vorming van kalksteen boustene in die benodigde groottes en vorms. Hierdie proses het ontwikkel met verloop van tyd tot die hoë presisie vervaardigingsnywerhede van die moderne era. Hoë gehalte en hoë presisie onderdele word vervaardig met die gebruik van slypwiele wat strek van growwe onderdeel vorming tot presisie motor enjin komponent vervaardiging. Die mees algemene skuurpartikels in moderne slyp prosesse is ontwikkel vir algemene toepassings, terwyl ander bedoel is vir gespesialiseerde toepassings. Die gebruik van wolframkarbied vir beide algemene en gespesialiseerde slyp wiele word nie gewoonlik geïmplimenteer in industrie nie, asook nie in gepubliseerde navorsingswerk nie.

Hierdie karbied materiaal val in die vuurvaste groep van materiale. Wanneer dit gemeng en gebind word met 'n smeebare metaal soos kobalt, molibdeen of nikkel, word die klassifikasie verander na 'n gesementeerde karbied of kermet (keramiek metaal). Die hoeveelheid van die metaal wat gebruik word in die kermet beïnvloed die smeebaarheid daarvan. ‘n Metaal inhoud van sowat 12 gw% (12 gewig %) is rofweg die middeweg wat lei tot 'n unieke hardheid tot taaiheid verhouding. Die metaal wat die beste werk met wolfram karbied is kobalt, dus WC-12gw%Co. Hierdie spesifieke kermet word algemeen gebruik as basis materiaal in bewerking gereedskap (vir draaibanke en freesmasjiene) te danke aan die hoë hardheid en taaiheid verhouding benodig vir die bewerking van harde metale soos verharde staal of titaan allooie. Hierdie basis WC-12gw%Co materiaal kan net so gebruik word vir masjinering, maar word gewoonlik bedek met lae van ander slytwerende materiale (soos titaan nitried, TiN, of karbonitried, TiCN).

Hierdie studie fokus op die spesiale vervaardiging van 'n slypwiel wat WC-12gw%Co as skuurmiddel bevat en wat gebind word met 'n epoksie hars binder. Hierdie tipe slypwiel is nie in gebruik in industriële toepassings nie en moet dus spesiaal ontwerp en vervaardig word. Die hars word gebruik as binder, wat die geval is vir baie industrieel geïmplementeerde slypwiele, om die produksie proses te vereenvoudig en hoër veiligheid te verseker. Die slypwiele wat in hierdie studie geproduseer is, is die kleiner weergawe wat ‘n gemonteer punt genoem word. Die werksverrigtinge van hierdie gemonteerde punte word bepaal deur die slyp van 'n titaan allooi. Die werks verrigtinge is bepaal deur die meting van die tempo van slytasie, die oppervlakafwerking wat die punte produseer op die titaan allooi en die oppervlak hardheid van die allooi aangesien dit gewoonlik deur die slyp proses beïnvloed word.

Acknowledgments

I would first and foremost like to thank God, my Heavenly Father, for the opportunity He provided me to continue my studies and the emotional, psychological and financial aid He provided during the course of my studies (and forever will), Jesus for being my best friend and the Holy Spirit for the guidance He always provides me. Thank You!

Then, I would like to thank my parents (Anton and Maggie Enever) and my brother and his wife (Rudolf and Marie Enever) for their support during my studies. I could not have asked for a better family.

I would also like to thank my house mates, close friends and fellow students (Konstand Spies, Ryno Botha, Coenraad Swanepoel, Janno Van Graan, Christiaan Uys, Christiaan Hattingh, Lourens Delport, Nathan Booysen, Pieter Conradie. Francois Conradie, Ruan de Bruyn and Martin Bezuidenhoudt) for their support and encouragement through the years. Your friendships will forever be cherished.

Then a big thank you to my supervisors (Tiaan Oosthuizen and Natasha Sacks) for their inputs, ideas, suggestions, encouragements and help in completing this thesis. Without them I definitely would not have come as far as I have.

Second to last I would like to thank the Department of Industrial Engineering at Stellenbosch University for their support and input during the course of my studies. A special thank you to the admin ladies (Karina Smith, Anel De Beer and Amelia Henning) for their exceptional organizational skills in helping me get where I need to be in time and assisting in the purchasing of equipment needed for experimentation.

Lastly, the support of the DST-NRF Centre of Excellence in Strong Materials (CoE-SM) towards this research is hereby acknowledged. Opinions expressed and not necessarily to be attributed to the CoE-SM.

Table of Content

List of Figures

List of Tables

Glossary

Abrasive	A hard and wear-resistant material that is used to wear, grind or cut away other materials.
Agglomerate	The clustering together of a few or many particles into a larger solid mass.
Brittle	A brittle structure or material exhibits low ductility, meaning that it exhibits very little plastic deformation before complete failure.
Ceramic	A compound of metallic and non-metallic elements for which the interatomic bonding is predominantly ionic.
Cermet	A composite material consisting of a combination of ceramic and metallic materials, the most common being cemented carbides composed of an extremely hard ceramic bonded together by a ductile metal.
Composite	Any material that consists of two or more sub-materials.
Ductility	A measure of a material's ability to undergo appreciable plastic deformation before fracture.
Fracture Toughness	The measure of a material's resistance to fracture when a crack is present.
Hardness	The measure of a material's resistance to deformation by surface indentation or by abrasion.
Microstructure	The structural features of an alloy that is subject to observation under a microscope.

Mounted Point	Grinding wheel variation consisting of abrasives in various shapes bonded to a central spindle.
Particles/Grains	Individual crystals in a polycrystalline metal or ceramic.
Residual Stress	A stress that persists in a material that is free of external forces or temperature gradients.
Sintering	Particle coalescence of a powder aggregate by diffusion that is accomplished by firing at an elevated temperature.
Toughness	A measure of the amount of energy absorbed by a material as it fractures. Toughness is indicated by the total area under a material's tensile stress-strain curve.
Vitrified/Vitrification (binder)	During firing of a ceramic body, the formation of a liquid phase that upon cooling becomes a glass-bonding matrix.
Workpiece	Term given to the stock material on which machining operations are executed and from which parts are produced.

Nomenclature

a_e	Depth of cut	[mm]
a_p	Grinding width (mounted point width)	[mm]
α	Heat transmission coefficient	[W/m^2*K]
$\bar{b}$	Average undeformed chip width	[mm]
C	Carbon (elemental)	
C	Number of active cutting edges per unit of surface area	
c	Specific heat capacity	[kJ/kg*K]
Co	Cobalt (metal)	
d_{eq}	Equivalent grinding wheel diameter	[m]
d_s	Grinding wheel diameter	[m]
d_w	Workpiece diameter (∞ for surface grinding)	[m]
E	Young's modulus	[MPa]
GR	Grinding ratio	
$\bar{h}$	Average undeformed chip thickness	[mm]
$h_{cu,crit}$	Critical chip thickness	[mm]
h_{eq}	Equivalent chip thickness	[mm]
h_{max}	Maximum chip thickness	[mm]
HK	Knoop hardness	
HV	Vickers hardness	
I_d	Heat of evaporation	[kJ/kg]
K_c	Critical fracture toughness	[MPa$\sqrt{m}$]
$\bar{l}$	Average undeformed chip length	
λ	Thermal conductivity	[W/m*K]
r	Average chip thickness to average chip width ratio	
r	Radius	[m]
r_i	Inner radius	[m]
r_o	Outer radius	[m]
ρ	Density	[g/cm^3]
σ	Surface tension	[N/m]
σ_r	Radial stress	[MPa]
σ_t	Tangential/Tensile stress	[MPa]

ν	Poisson's ratio	
v_c	Cutting speed	[mm/min]
v_{ft}	Workpiece feed speed	[mm/min]
V_g	Grinding wheel material removed	[mm^3]
V_w	Workpiece material volume removed	[mm^3]
W	Tungsten (metal)	
WC-12wt%Co	Tungsten carbide containing 12 weight percent cobalt	
wt%	Weight percentage	
ω	Angular velocity	[rad/s]
μm	Micrometer	

1) Introduction

Modern industrial, aerospace, medical and commercial use of parts and components of high quality and high precision manufactured materials have seen an exponential increase in demand. This high volume demand of parts and components led to manufacturers seeking new high speed machining processes and innovative tool materials. This led to the growth in manufacturing technologies and the search for new materials to improve machining processes.

The use of grinding as a precision and advanced machining method to manufacture parts has been utilised extensively over the past few decades, albeit its limited use for many years prior. The abrasives currently in use have proved their usability and have withstood the test of time, with no major competitor for general purpose applications, except for certain highly specialised grinding processes. The development of tool materials for milling and turning processes has, however, seen constant change and technological improvement. As a result, tungsten carbide has emerged as base material for production of these tools. It has high hardness and can be bonded with a metal for added toughness. These mechanical properties of tungsten carbide are favourable for use as abrasive medium in a grinding wheel.

1.1) Problem Statement

Grinding wheels containing tungsten carbide as abrasive medium are currently not in use for industrial or research based applications. Manufacturers of grinding wheels and grinding related products do not use this carbide as abrasive in the manufacturing of their grinding wheels, but only for the production of grinding burrs, which by classification is not a grinding wheel. The use of tungsten carbide as abrasive medium in grinding wheels specifically, as far as the author is aware of, is not being investigated, which could lead to potentially filling the gap in the market or the research and development of improved grinding wheels.

1.2) Objectives

The objectives of this study are to explore the possibility and performance of grinding wheels containing the cermet tungsten-carbide-cobalt. Such grinding wheels are not in use in industrial applications and it is thus necessary to produce custom designed variants for the purpose of evaluating their effectiveness and efficiency. A moulding and manufacturing process has to be developed to produce the needed grinding wheels with the highest degree of

consistency. The custom produced grinding wheel should then undergo experimental testing in order to evaluate their performance. The parameters pertaining to this evaluation are the wear rate of the grinding wheels as grinding is conducted and the influences of the grinding wheels on the workpiece material in terms of produced surface roughness and hardness.

1.3) Significance of Study

The results from this study will provide an insight into the effectiveness of grinding wheels containing WC-12wt%Co as abrasive medium. There is the possibility of these custom developed grinding wheels having similar or better performance characteristics than their conventional counterparts, which can only be verified through experimentation. The impact of this tough abrasive material could be significant, such as higher part production rates with lower operating costs due to lower wear rates of the grinding wheels. Tighter geometrical tolerances could be achieved while more parts are ground using the same grinding wheel. Despite the high cost of WC-12wt%, the successful implementation of this abrasive could have the greatest benefit of saving costs in the long term.

1.4) Methodology

For the evaluation of the performance characteristics of the grinding wheels, the determination of binder type and binder-to-abrasive ratio will be initially determined. From knowing the composite material characteristics of the grinding wheels during production, a suitable mould will be designed, manufactured and tested. The grinding wheels will then be produced according to design specifications and experimental grinding tests conducted to evaluate their performance. Performance characteristics will be determined by rate of wear of the grinding wheels and the influences they have on the workpiece material.

1.5) Research Roadmap

Chapter one comprises the introduction to the research study. It also includes the study's problem statement, objectives, significance and methodology. These topics should provide the reader with a general overview as to what this study entails. Chapter two is an overview of literature regarding tungsten carbide, cobalt and WC-12wt%Co. The manufacturing and mechanical characteristics of the cermet are covered in this chapter.

Chapter three describes the aspects and dynamics of grinding. It aims at providing as much information regarding the complex machining process as possible, while still keeping the information relevant to the study.

Chapter four is a short and concise overview of titanium, the workpiece material. Its general material and mechanical characteristics are described in this chapter. The actual workpiece material that is used for experimental purposes is an alloy of titanium, Ti6Al4V. A short description of the alloy is also provided.

Chapter five contains the bulk of this research study, which is the research methodology. This chapter explains the steps towards determining the resin-to-abrasive ratio, the grinding wheel geometry, production, mould design and the initial pilot experiment. Then, the full experimental procedure is explained in detail with the data that is recorded and analysed.

Chapter six shows and discusses the experimental results. From these results, the effectiveness and efficiency of the grinding wheels are determined, which are the objectives of the research study. From the results, conclusions are drawn as to whether the cermet WC-12wt%Co performs similar to conventional grinding wheel abrasives, which forms the content of chapter seven. Chapter seven also contains suggestions for future work, including improvements that could be implemented.

2) Background

2.1) WC-12wt%Co

2.1.1) Tungsten Carbide and Cobalt

Tungsten Carbide

Tungsten carbide is a chemical compound that is formed when equal atom quantities of the metal tungsten (W) bonds with the non-metal carbon (C). It is produced in powder form, which can be pressed and sintered into shapes and parts for a variety of uses (the powders are also used to form various alloys). It has approximately twice the stiffness of common steel alloys and is much denser than the commonly used steels of industry. It has comparable hardness to aluminium oxide (Al_2O_3) and can only be polished and finished with an abrasive of superior hardness, such as synthetic diamond. Tungsten carbide falls in the ceramics category of material classifications, which is the hardest known group of materials. Table 1 lists a number of ceramics and their Knoop hardness. Generally, only ceramics with a Knoop hardness exceeding 1000 are used as abrasives in the production of grinding wheels. (Callister 2010)

Table 1 - Approximate Knoop hardness of some ceramic materials – adapted from (Callister 2010)

Material	**Approximate Knoop hardness**
Diamond (carbon)	7000
Boron carbide (B_4C)	2800
Silicon carbide (SiC)	2500
Tungsten carbide (WC)	2100
Aluminium oxide (Al_2O_3)	2100
Quartz (SiO_2)	800
Glass	550

Tungsten carbide has as advantage a high melting point of between 2600°C and 2850°C, and high hardness. It is also the hardest binary carbide at elevated temperatures, has high compressive strength and exhibits high resistance to corrosion and oxidation. The low thermal expansion coefficient and high thermal conductivity of tungsten carbide makes it an attractive

material for the production of high temperature furnace crucibles. It is also used as catalytic electrode for anodic oxidation of hydrogen in fuel cells. (Koc & Kodambaka 2000)

There are various processes for producing tungsten carbide, such as mechanical alloying (or solid state reaction), chemical vapour condensation (*CVC*) and gas-solid reaction methods. The mechanical alloying or solid state reaction method is the most common method for producing tungsten carbide; the alloy reaction is controlled by diffusion and phase transformation of tungsten and carbon. The method involves mixing and heating powdered metallic tungsten and carbon black in a graphite furnace with a controlled atmosphere of hydrogen. Hydrogen gas is used to prevent oxidation of tungsten by preferentially forming water ($H_2 + O_2 = H_2O$). This reaction is greatly dependent on the diffusion of carbon in tungsten, which as a result requires furnace temperatures to be in the range of 1400 - 1800 °C. The solid state reaction technique is able to produce a wide range of WC particle sizes, mostly depending on the initial tungsten powder particle size. The process relies on high temperatures and lengthy reaction times. (Kim & Kim 2004; Medeiros et al. 2001)

The CVC process is able to produce nano-structured tungsten carbide powders (grain sizes of less than 30 nm) with high purity and non-agglomeration properties. This process uses metal organic precursor materials, such as tungsten hexacarbonyl ($W(CO)_6$), as basis from which WC is derived. High-purity carbon monoxide gas is used as carrier gas through a heated evaporator containing the solid $W(CO)_6$ precursor material. The precursor material vapour and carrier gas is passed through the furnace into a collection chamber. The precursor vapour decomposes, reacts in the furnace with the carrier gas and condenses into WC nano-powders in the collection chamber. Tungsten hexacarbonyl vaporizes at an optimized temperature of 120°C. (Kim & Kim 2004)

The gas-solid method is similar to the CVC process, but does not use vaporized tungsten hexacarbonyl. It uses solid ammonium paratungstate (APT), $(NH_4)(H_2W_{12}O_{42}).(H_2O)$, or tungsten blue oxide (TBO), $WO_{2.9}$. Highly pure methane (CH_4) and hydrogen (H_2) gas is used as carbon source and reducer, respectively. Hydrogen is again used to reduce the formation of oxides. Carburization of the solid tungsten source is carried out in a horizontal fixed bed reactor. Reactor temperatures are 850°C for APT and 820°C for TBO and soaking times for both cases are 2 hours. During the process, the gas flows through the reactor, forming WC nano-sized particles that are collected afterwards. (Medeiros et al. 2001; Koc & Kodambaka 2000)

Cobalt

Cobalt is a metal found in the Earth's crust only in chemically combined form, except for small amounts deposited in alloys of natural meteoric iron. The pure form is produced by reductive smelting, is hard and has a lustrous silver-grey colour. Cobalt is primarily used in its metal form and for the preparation of magnetic, wear-resistant and high-strength alloys. The compound cobalt silicate and cobalt(II) aluminate are pigments and give a distinctive deep blue colour to glass, ceramics, inks, paints and varnishes.

2.1.2) WC-xCo

When tungsten carbide and cobalt powders are combined and sintered, the resultant is termed a cemented carbide, cermet (ceramic-metal) or hardmetal composite. The composition of this composite material mostly influences the mechanical properties of it. Cobalt is the best binder for tungsten carbide due to its excellent wetting of the WC during liquid phase sintering, whereas other metals work better with other carbides, such as nickel with TiC and/or Cr_3C_2. Nickel also works well as binder with tungsten carbide and is regularly used. Tungsten carbide is the most widely used carbide for wear resistant applications and has an estimated 20 million kilograms per annum world market. (Medeiros et al. 2001; Koc & Kodambaka 2000)

Tungsten carbide and cobalt is mixed thoroughly in powder form in a wetted state in a mixing machine (such as a ball mill), forming a homogeneous sludge. When a ball mill is used, the milling process further refines particle size. To prevent oxidation, the sludge is dried in an atmosphere controlled environment or in a vacuum. The thoroughly mixed and dried powder can then be further processed and parts manufactured from it. Figure 1 shows the relationship between hardness and toughness of various tool materials, with cemented carbides lying roughly in the centre. (Callister 2010; da Silva et al. 2001)

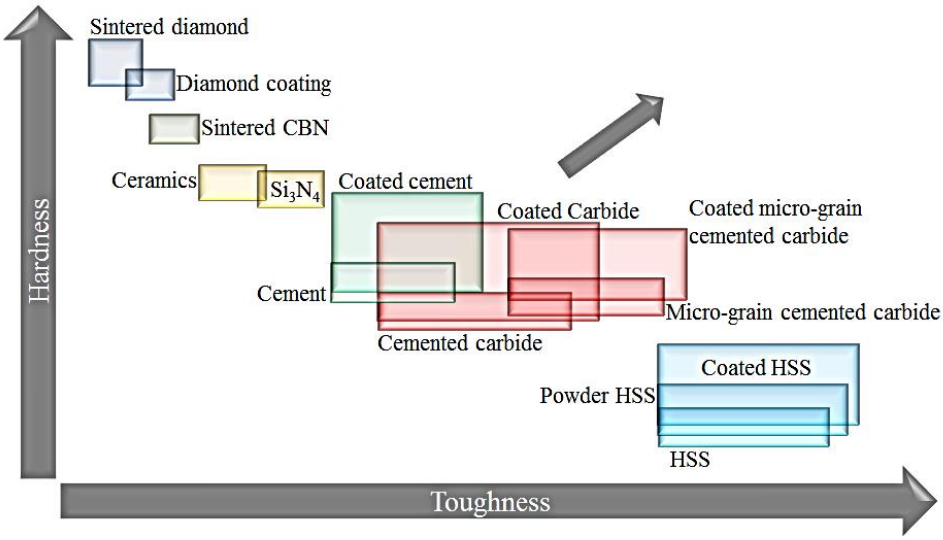

Figure 1 - Relationship between hardness and toughness for various tool materials – adapted from (Oosthuizen et al. 2010)

WC-Co is extensively used in cutting tools for hardened steels and titanium alloys. The carbide particles act as the abrasive to cut a workpiece material, but are themselves too brittle to withstand the cutting forces. The cermet's toughness comes from the ductile metal matrix the carbide particles are embedded in. This matrix isolates carbide particles, thereby preventing particle-to-particle crack propagation. The carbide particles are refractory to withstand the high machining temperatures accompanying machining processes; conventional and grinding alike. Figure 2 shows a photomicrograph of WC-Co. (Callister 2010)

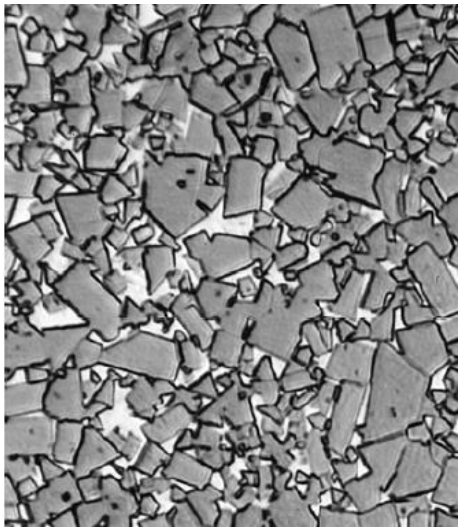

Figure 2 - Photomicrograph showing WC-Co. The lighter areas are the cobalt metal matrix and the darker areas are the tungsten carbide particles (Callister 2010)

For the manufacturing of WC-Co cutting tool inserts, the dried powder mixture is usually compacted into a shape of desired geometry to suit design requirements and then sintered. The most common compaction method for high production volumes of the cemented carbides is cold pressing, which compresses the powder at room temperature in a die. The dies are

designed to be over size in geometry in order to compensate for shrinkage of the compacted powder during high temperature sintering. The dies themselves are sometimes lined with a WC-Co lining in order to reduce wear, especially for high volume production processes, due to the abrasive nature of the compacted carbide particles.

The solid state sintering process of WC and Co takes place in three stages: (1) at the sintering temperature the molten Co spreads out over the WC particles to cover their surfaces, (2) the liquid Co agglomerates particles of WC that are close together and (3) the resulting agglomerates form a network which sinter together to form larger particles. For the industrial applications it is used in, tungsten carbide is not the hardest carbide and neither is cobalt the toughest metal, but together WC-Co is the best system for hard metal machining. The reason for the good coupling between tungsten carbide and cobalt is:

1) a reported zero degree WC-Co system dihedral angle,
2) cobalt dissolves tungsten carbide, but not the other way around, and
3) WC-Co has a ternary eutectic reaction at 1275°C.

Characteristics (1) and (2) contribute to WC-Co's good sinterability, which also helps to increase the adherence between the WC and Co phases. The third characteristic allows WC-Co to be sintered typically at 1350°C, which is well below the melting temperature of cobalt (1495°C). (da Silva et al. 2001)

The composition (average cobalt phase thickness and cobalt content) and WC particle size of WC-Co greatly affects the tribological, mechanical and thermal properties of the cermet. Generally for use in industry, WC particle size ranges from 0.1 μm to 10 μm with a cobalt content of about 4–30 wt%. The decrease of WC particle size increases the hardness of WC-Co. It has been found, however, that although wear resistance is increased with a decrease in WC grain size, coarser grades of WC with a hardness range of 1000-1600 HV have shown superior wear resistance. The decrease in WC grain size does not therefore always improve the wear resistance of the cermet. In a study by Saito et al. it was found that the specific wear rate of WC-Co increased with cobalt content and WC grain size. It should be noted that this is a rare occurrence and not the norm. (Saito et al. 2006; Picas et al. 2009; Kim & Kim 2004; Medeiros et al. 2001)

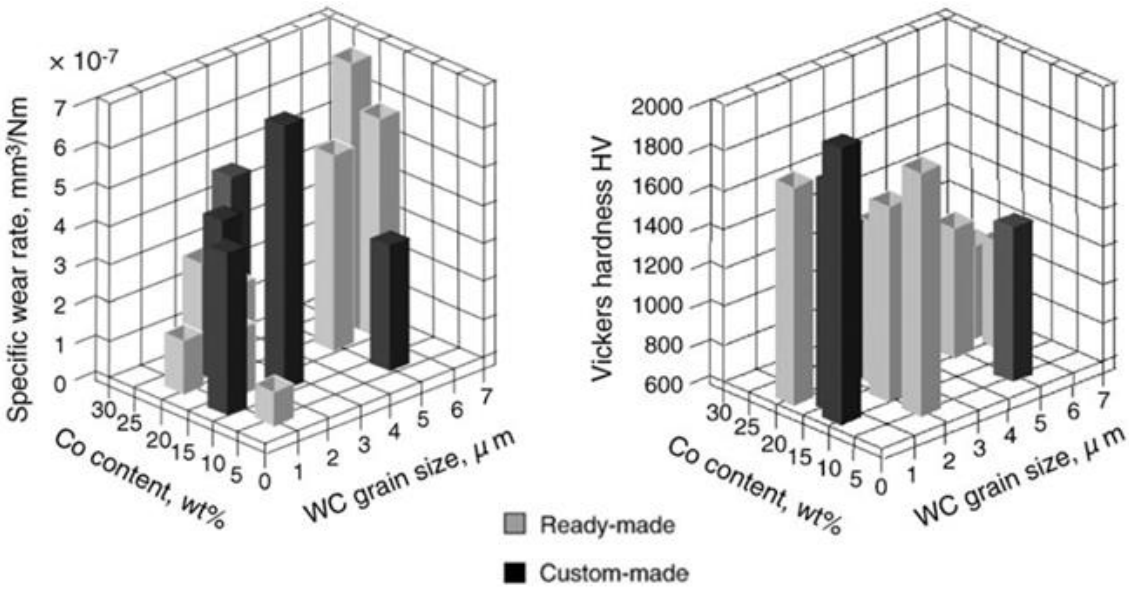

Figure 3 - Relationship between cobalt content, tungsten carbide grain size and the specific wear rate and hardness of WC-Co - adapted from (Saito et al. 2006)

Figure 3 shows the relationship between the cobalt content and tungsten carbide grain size and the specific wear rate and hardness of the cermet WC-Co. The *Ready-made* and *Custom-made* grades referred to in the figure are that of commercially available and lab produced cermet grades respectively. (Saito et al. 2006)

The fracture toughness of WC-Co is of high importance in the application of the cermet due to the risk of brittle failure. The severity of wear is largely controlled by the fracture toughness, which is related to the cermet's composition and carbide grain size. The fracture toughness increases with an increase in cobalt binder, Ferreira et al. demonstrated that the fracture toughness of a WC-Co cermet sample with high cobalt content did not produce fracture cracks and consequent failure under standard fracture toughness testing as was observed in a low cobalt content sample. (Ferreira et al. 2009; Shetty et al. 1985)

For use in this study, a composition of 12 wt% cobalt is used (WC-12wt%Co). This composition has an ideal hardness-to-toughness ratio and is expected to have good fracture toughness while effectively cutting/machining a hardened workpiece material.

2.2) Grinding

Grinding is a material removal process making use of geometrically nondefined tool edges, or abrasive particles, which are bonded together in a grinding wheel to cut (machine) a material into shape. The abrasive particles are randomly shaped and arranged in the grinding wheel with the cutting edges undescribed with reference to a single particle, and thus nondefined. The grinding wheel is disk-shaped and rotates at high rotational velocities, exposing a multitude of cutting edges to the workpiece material per unit time. (Grote & Antonsson 2009)

Machining with a grinding wheel occurs on either the periphery or the face of the grinding wheel. Material removal is accomplished by feeding the workpiece material relative to the grinding wheel, producing a surface shape on the workpiece. There are six main classifications of the grinding process which is related to the produced surface shape. These are surface, peripheral, thread, gear, profile and form grinding, where peripheral grinding is the most common. The various grinding processes can be seen in Figure 4.

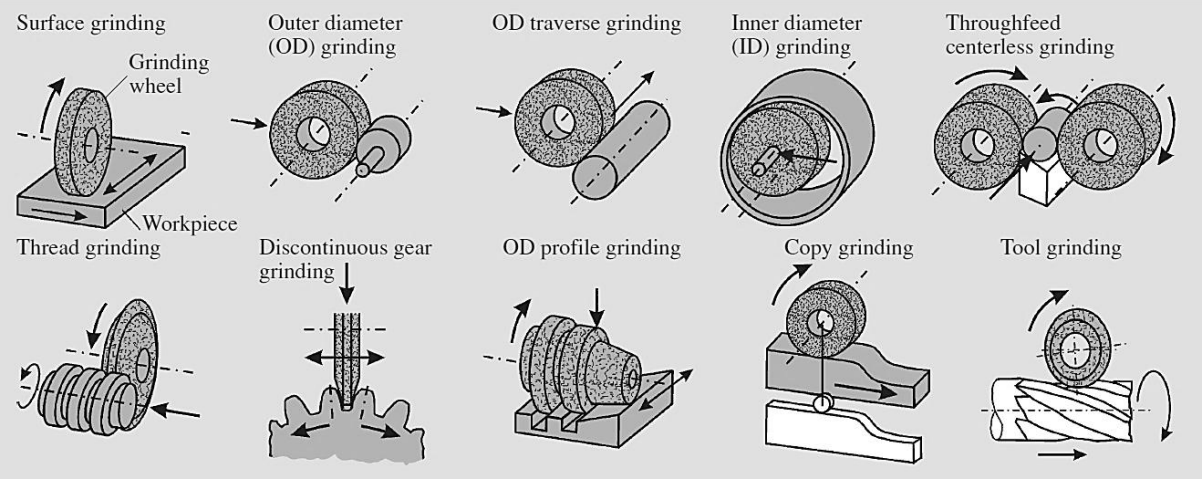

Figure 4 - Various grinding processes (Grote & Antonsson 2009)

2.2.1) General Grinding Wheel Design

A grinding wheel simply consists of three components; the abrasive particles, the binder and air gaps. This composition is true for all grinding wheels, except metallically bonded grinding wheels which do not have any air pores/gaps within its structure. Various grinding wheel characteristics can be achieved by altering the fractional constituent composition. The composition of a grinding wheel is indicated by the international standards (ISO) identification system, which consists of numbers and letters in a specific sequence that defines

the abrasive, grain size, grade and binder. A depiction of the grinding wheel composition and an example of an identification system can be seen in Figure 5 and Figure 6.

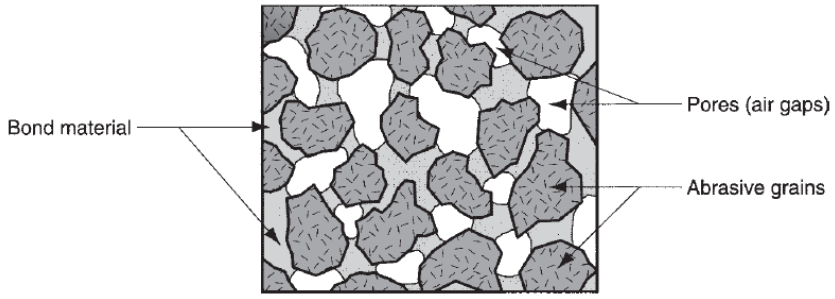

Figure 5 - Composition of the grinding wheel

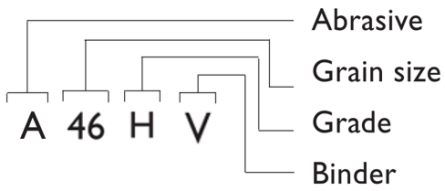

Figure 6 - ISO grinding wheel identification system (Uddeholm 2012)

Abrasive

The abrasive particles that are used in grinding wheels have to fulfil the important requirements of hardness, sharpness, thermal resistivity and chemical stability. Modern abrasives are all synthetic in nature as opposed to natural abrasive materials used for very early grinding wheels. The most common synthetic abrasives used, fulfilling the requirements to a greater or lesser extent, are aluminium oxide (designation A), silicon carbide (designation C), cubic boron nitride (CBN) (designation B) and synthetic diamond (designation SD). These four mainly used abrasives have different applications that are dependent on each abrasive's particular characteristics. The hardness and thermal durability, as partial material characteristics, are shown in Table 2. (Uddeholm 2012)

Table 2 - Partial material abrasive characteristics (Uddeholm 2012)

Abrasive	**Knoop Hardness**	**Thermal Durability in air (ºC)**
Aluminium oxide	2100	2000
Silicon carbide	2500	1200
CBN	4700	1400
Diamond	7000	650

The most commonly used abrasive is aluminium oxide, available in several variants, and is mostly used to grind steels. It can be alloyed with other oxides, of which the most common is titanium oxide, to produce an abrasive with characteristics that enhances hardness, sharpness, thermal resistivity or chemical stability. The characteristics of alloyed aluminium oxide are shown in Table 3. (Uddeholm 2012)

Table 3 - Aluminium oxide variant characteristics (Uddeholm 2012)

Aluminium oxide variant	**Colour**	**Properties**
Normal corundum	Brown, grey	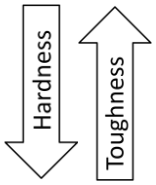
Mixed corundum	Yellow-brown	
Red alumina	Red	
White alumina	White	

It should be noted that the colour of the grinding wheel does not always indicate the type of abrasive used as some manufacturers colour their abrasives and binders. In addition to the alloyed aluminium oxide, there is also another type called an aluminium oxide ceramic or sintered aluminium oxide. This type has a fine crystalline structure, which allows the particles to better retain their sharpness. This higher retention of sharpness requires higher grinding forces for adequate grinding. (Uddeholm 2012)

Silicon carbide is the second most common abrasive and is used for the grinding of cast iron and austenitic steel, but can also be used to grind hardened tool steel. There are two main variants of the abrasive, namely black silicon carbide and a slightly harder green silicon carbide, which is more brittle than the black variant. On the more specialized application side of grinding wheel usage is the cubic boron nitride and synthetic diamond abrasives. These two are manufactured in approximately the same way, but are used for different applications. Cubic boron nitride is primarily used for grinding hardened, high-carbon content tool steel and high-speed steel. The major drawback of CBN is its high price, which is almost twice that of synthetic diamond. Despite the high hardness of synthetic diamond, it is seldom used for grinding tool steel. This is due to the abrasive's low thermal resistivity and is thus primarily used for the grinding of cemented carbides and ceramics. (Uddeholm 2012)

Abrasive grain size

The selection of the correct grinding wheel for a specific application relies greatly on the abrasive grain (particle) size. The sizes of the grains are classified in accordance to an international grain mesh size specification of mesh/inch. This size specification ranges from 8, a coarse grain, to 1200, a superfine grain. A grain mesh size in the range of 24-100 is generally used for grinding tool steel, while 800-1200 size mesh is used for polishing. Since a coarse grain is much larger in comparison to a fine grain, it can remove a larger amount of workpiece material per unit time when grinding large workpieces, softer materials or when the contact surface of the grinding wheel is large. (Uddeholm 2012)

Fine grain sizes on the other hand are used to produce a high quality surface finish when hard materials are ground or when the contact surface of the grinding wheel is small. The produced surface finish or surface smoothness of the workpiece is not only dependant on the grain size, but is also a factor of the grain sharpness, bonding material used and the hardness of the grinding wheel. The grain size to millimeter conversion can be seen in Figure 7. (Uddeholm 2012)

Grain Size Numeral		Dimension mm	Grain Size Numeral		Dimension mm
8		2,83-2,0	90		0.18-0,13
10	very	2,38-1,68	100		0,15-0,11
12	coarse	2,0-1,41	120		0,13-0,09
14		1,68-1,19	150	fine	0,11-0,06
16		1,41-1,0	180		0,09-0,05
20		1,19-0,84	220		0,075-0,045
24	coarse	0,84-0,60	240		0,047-0,043
30		0,71-0,50	280		0,038-0,035
36		0,60-0,42	320		0,031-0,028
46		0,42-0,30	400		0,018-0,016
54		0,35-0,25	500	very fine	0,014-0,012
60	medium	0,30-0,21	600		0,010-0,008
70		0,25-0,18	800		0,008-0,006
80		0,21-0,15	1000		0,005-0,004
			1200		0,004-0,003

Figure 7 - Grain size to millimeter conversion for abrasive particles (Grinding Techniques 2013)

Grinding wheel grade

A grinding wheel's grade refers to its hardness, or how securely the abrasives are held by the binder and does not refer to the hardness of the abrasive used in the grinding wheel. The overall hardness of a grinding wheel, its grade, is primarily determined by the quantity of binder used in the manufacturing of the grinding wheel. A high amount of binder reduces the amount of air gaps and thus produces a harder wheel. The opposite is true for a low amount of

binder. A grinding wheel's grade is indicated by an alphabetical letter, where *A* represents a very soft wheel and *Z* represents a very hard wheel. Some wheel manufacturers might add a numeral after the letter to indicate the distribution of the abrasive grains in the wheel. (Uddeholm 2012)

Grinding wheel binders

There are four types of binders that are used in the manufacturing of grinding wheels. These are vitrified (designation V), resinoid (designation B), rubber (designation R) and metallic (designation M). Vitrified bonding is used for more than 75% of manufactured grinding wheels. The porosity and strength created with this binder gives high stock removal rates and helps in the attainment of high precision. Vitrified bonded grinding wheels are not affected by water, acids, oil or ordinary temperature variations. These grinding wheels are fired at temperatures between 1250°C and 1325°C, are not sensitive to chemical influences and can be stored indefinitely. Sudden temperature changes, shocks and blows should however be avoided. (Grinding Techniques 2013)

Resin bonded grinding wheels are used for high speed wheels in foundries, welding and billet shops. They are also used in cutoff and thread grinding operations. They are commonly manufactured from phenolic resins, but epoxy resins are also widely used. Resin bonded grinding wheels are cured at roughly 180°C and are less sensitive to sudden temperature changes, shocks and blows than vitrified bonded wheels. Lengthy storage and chemical exposure should however be avoided. (Grinding Techniques 2013)

Rubber and metallic wheel binders are mostly used for specialized applications and will thus not be explained in detail. For high specific grinding pressures, such as for control wheels in centreless grinding, a rubber bonding is used. Metallic binders are used in high peripheral speed grinding applications and for bonding diamond and certain CBN wheels. (Uddeholm 2012)

Grinding wheel size and shape

Grinding wheel size and shape adheres to the ISO standards. The specific grinding wheel design standards can be found in the ISO 525, 603 and 8486 documents.

2.2.2) Dynamics of Grinding

As mentioned, grinding is a cutting process where the cutting edges are formed by the grains of abrasive materials. The principle of material removal with a grinding wheel is similar to other chip-cutting machining methods, although various factors deem it necessary to consider the theory of grinding somewhat differently. There are a few special conditions that are applicable to grinding:

- The geometry of the cutting tool is irregular and the abrasive grains are irregularly placed, meaning that cutting, ploughing and sliding will occur. This is illustrated in Figure 8. (Klocke et al. 2005)
- The cutting geometry can change over time as machining goes on. An abrasive grain shatters or breaks free from the binder to generate a new sharp grain, giving the grinding wheel a certain degree of self-sharpening.
- The grains generally have a negative rake (cutting) angle. The irregular "blunt" shapes of the grains mean that their rake angles are often negative.
- A very large number of cutting edges.
- Very high cutting speeds, due to the high rotational velocity of the grinding wheel. Precision grinding as an example has a cutting speed of about 35 m/s (2100 m/min), which is much greater than other cutting processes.
- Very small chips (or swarf) are produced during grinding due to the small depth of cut of each cutting edge.
-

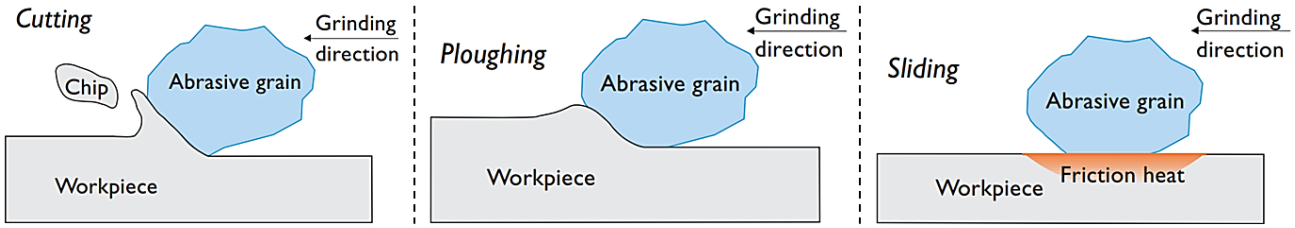

Figure 8 - Different conditions during grinding – adapted from (Uddeholm 2012)

Grinding forces and chip formation

As the abrasive grains cut the workpiece during the grinding process, forces are exerted on each grain, where the total force is that between the grinding wheel and the workpiece. An average force on each grain can be calculated by dividing the overall measured grinding force by the number of cutting edges in contact with the workpiece. The number of cutting edges in contact with the workpiece is dependent on the grinding wheel contact area and the amount of

cutting edges in the grinding path. The grinding forces are responsible for various effects from the degree of self-sharpening of the grinding wheel to its working hardness. (Uddeholm 2012)

Important cutting angles for the formation of chips are the clearance angle α, rake angle γ and wedge angle β and are shown in Figure 9. These angles can only be indicated by statistical parameters such as distributions or mean values. Large contact and friction zones and sharply negative rake angles are formed between the abrasives and workpiece while the cutting edges penetrate only a few microns into the material. The microtopography of the cutting zone (positioning of cutting edges) and geometry of the machined workpiece surface are responsible for the undeformed chip thickness distribution. Elastic and plastic deformations occur alongside chip removal. (Grote & Antonsson 2009)

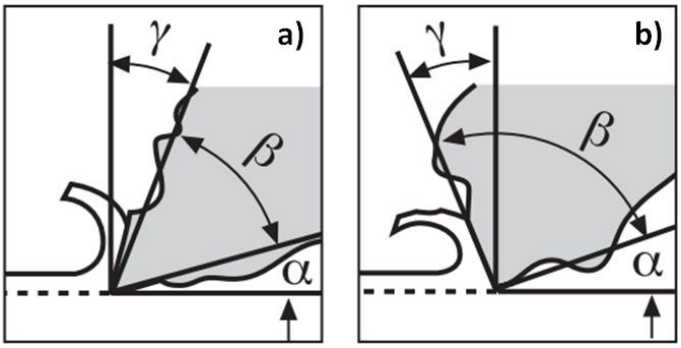

Figure 9 - Abrasive particle cutting angles: clearance angle α, rake angle γ and wedge angle β. a) indicates a positive rake angle while b) indicates a negative rake angle (Grinding Techniques 2013)

A high normal force results between the tool (abrasive particle) and the workpiece at the mainly negative rake angles of the cutting edges. These forces can lead to elastic frame deformation in, or spindle deflection of, the grinding machine, the tool and the workpiece. The amplitude of these deformations can be compared to the normal small feed motions and thus a distinction should be made between the theoretical and actual feed motions as shown in Figure 10 (Grote & Antonsson 2009).

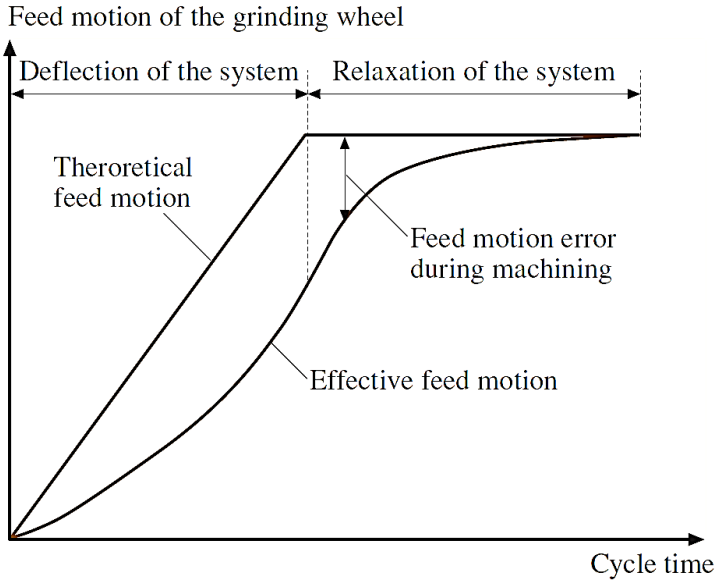

Figure 10 - Grinding system deflection and deformation due to normal force loading – adapted from (Grote & Antonsson 2009)

Chip formation during grinding differs from that of machining with a well-defined tool such as with milling. As an abrasive particle touches the workpiece material and initiates grinding, the workpiece material experiences elastic deformation due to the mostly sharp negative rake angle of the particles. As the particle moves deeper into the workpiece material, plastic deformation occurs before actual chip removal takes place. During this process, a large amount of friction occurs between the abrasive particles and the workpiece material. The phases of chip formation are shown in Figure 11. (Grote & Antonsson 2009)

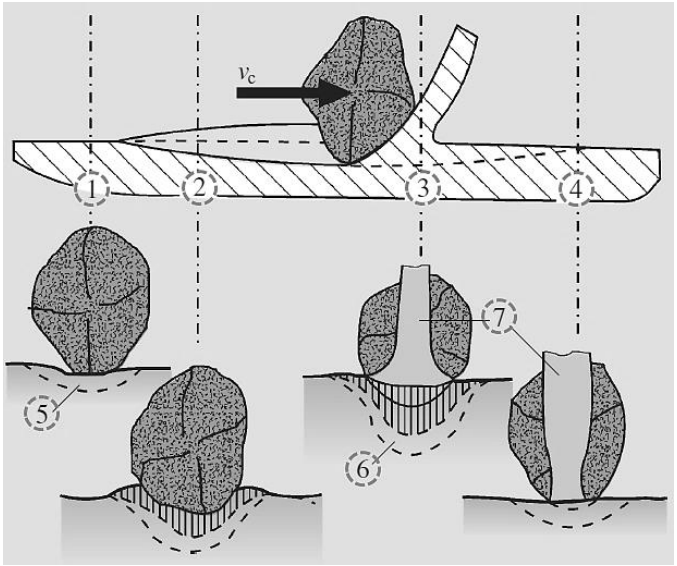

Figure 11 - Chip formation phases during grinding: 1) Elastic deformation; 2) Elastic and plastic deformation; 3) Ploughing and shearing of the chip; 4) Elastic deformation and chip shearing; 5) Zone of elastic deformation; 6) Zone of plastic deformation; 7) Chip – adapted from (Grote & Antonsson 2009)

Chip formation is accompanied by frictional and displacement processes due to the generally unfavourable cutting edge shape. The chip formation process is evaluated by means of statistically calculated averages. Figure 12 shows the formation mechanisms of a comma-shaped chip (red section) by the successive action of two cutting edges.

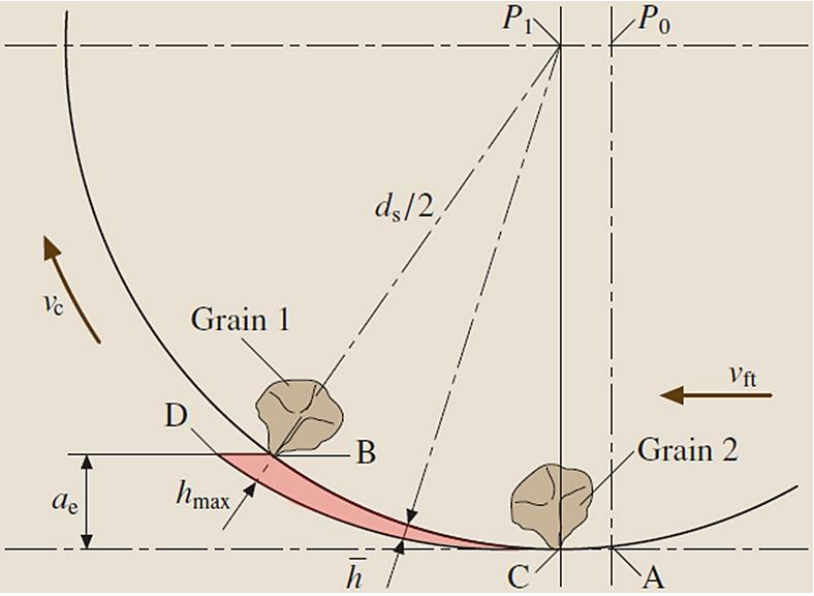

Figure 12 - Comma-shaped chip formation by two successive cutting edges during surface grinding - adapted from (Grote & Antonsson 2009)

While the centre of the grinding wheel moves from P_0 to P_1, Grain 1 travels along the path AB on the circumference of the grinding wheel. The successive grain, Grain 2, will then travel along the path CD, causing the thickness of the chip to increase from 0 up to h_{max}. By applying the continuity relationship, the average undeformed chip thickness, $\bar{h}$, can be calculated by,

$$v_{ft} a_e a_p = v_c C V_{sp} a_p \qquad \text{Eq. 2.1,}$$

which reduces to

$$\bar{h} = \frac{v_{ft}}{v_c} \frac{1}{\bar{b} C} \sqrt{\frac{a_e}{d_{eq}}} \qquad \text{Eq. 2.2,}$$

with $\bar{l} = \sqrt{a_e d_{eq}}$, $V_{sp} = \bar{l}\bar{b}\bar{h}$, $d_{eq} = \frac{d_w d_s}{d_w \pm d_s}$ (+ for external grinding and – for internal grinding). Further simplification of Equation 2.2 leads to,

$$\bar{h} = \sqrt{\frac{v_{ft}}{v_c} \frac{1}{rC} \sqrt{\frac{a_e}{d_{eq}}}} \text{ with } r = \frac{\bar{b}}{\bar{h}} \qquad \text{Eq. 2.3,}$$

The symbols used in Equation 2.1 to Equation 2.3 are as follows: $\bar{h}$ is the average undeformed chip thickness, $\bar{b}$ is the average undeformed chip width, $\bar{l}$ is the average undeformed chip

length, a_p is the grinding width (engagement width), a_e is the depth of cut, v_c is the cutting speed, v_{ft} is the workpiece feed speed, d_s is the grinding wheel diameter, d_w is the workpiece diameter (∞ for surface grinding), d_{eq} is the equivalent grinding wheel diameter and *C* is the number of active cutting edges per unit of surface area of the grinding wheel. The parameter *r* is the ratio of average chip thickness to average chip width. The maximum chip thickness, h_{max}, is double the average chip thickness, $\bar{h}$. The concentration of abrasive particles on the surface of the grinding wheel, *C*, affects the chip thickness to a great extent as illustrated in Figure 13. (Grote & Antonsson 2009)

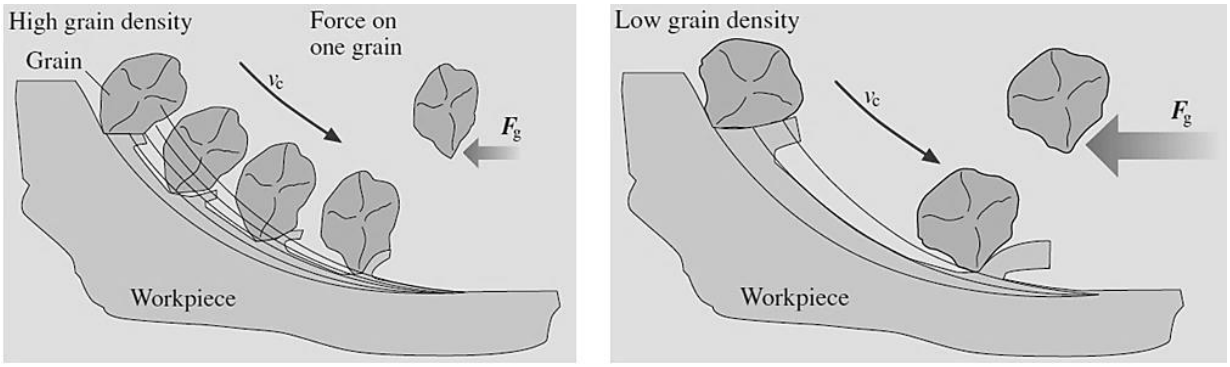

Figure 13 - Grain concentration, *C*, influence on chip formation mechanisms - adapted from (Grote & Antonsson 2009)

A higher grain density leads to smaller and thinner chips to be formed and as a result lower forces per grain. A lower grain density will produce larger and thicker chips with greater forces per grain. The grain size influences the grain density, which can influence the wear mechanisms of the grinding wheel. The equivalent chip thickness, h_{eq}, is often used as grinding process evaluation parameter due to the technical difficulties in measuring the amount and distribution of abrasive grains. The equivalent chip thickness parameter, h_{eq}, is directly related to the grinding forces and surface finishing by,

$$h_{eq} = a_e \left(\frac{v_{ft}}{v_c}\right) \qquad \text{Eq. 2.4}$$

The mean value of the removed chip thickness at any time is relatively constant, although these chips are small and of irregular size and shape. This mean value is dependent on the type of grinding operation. If a grinding wheel is producing larger chips, it could be due to two factors:

1. There is a higher loading on each cutting edge, thus higher specific forces. This increases the self-sharpening effect of the grinding wheel and gives it the characteristics of a softer wheel.

2. The surface texture of the workpiece after grinding is coarser. This can be seen in Figure 14 below.

If the average chip thickness is reduced, it represents the opposite, thus a perceived harder wheel and a smoother produced workpiece surface texture. (Uddeholm 2012)

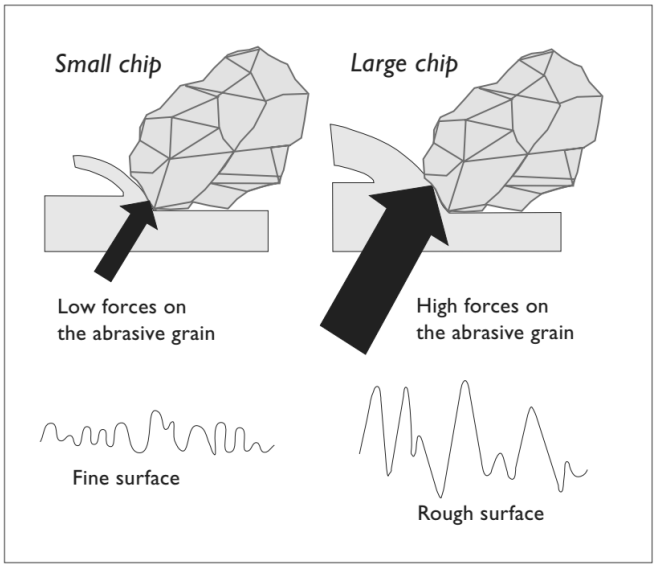

Figure 14 - Effects of chip size on workpiece surface finish (Uddeholm 2012)

There are two main material removal methods; brittle and ductile material removal. The distinction between these two material removal methods is important for the quality of the machined workpiece surface. Breaking and chipping is the main mechanisms of brittle material removal and leads to the generation of micro cracks in the workpiece surface. The ductile material removal method is characterized by plastic deformation and consequently produces a surface with greater quality and accuracy. The critical chip thickness, $h_{cu,crit}$, has the greatest effect on the transition from the ductile to brittle material removal regime. The critical chip thickness is a function of the Young's modulus E, Knoop hardness HK and critical fracture toughness K_c of the workpiece material. The critical chip thickness can be calculated with Equation 2.5. (Aurich et al. 2015)

$$h_{cu,crit} = 0.15\left(\frac{E}{HK}\right)\left(\frac{K_c}{HK}\right)^2 \qquad \text{Eq. 2.5}$$

The produced chip thickness should be lower than the critical chip thickness for ductile material removal. The mechanisms of material removal in grinding are however determined by a complex interaction between the process parameters, material response and the grinding wheel. The cutting speed has the greatest influence on the ductile-to-brittle transition of all the grinding parameters. (Aurich et al. 2015)

The supplied mechanical energy for grinding is almost entirely converted into heat. Most of the generated heat flows into the workpiece material while a small fraction of the heat flows into the abrasive particles, binder and the surrounding cooling lubricant (if present) and atmosphere. The rise in workpiece temperature could damage its surface by means of thermally induced residual stresses, structural changes or cracks, consequently influencing the behaviour of the workpiece. A qualitative heat flow distribution around an individual abrasive particle is shown in Figure 15. (Grote & Antonsson 2009; Oliveira et al. 2015; Heinzel et al. 2015; Klocke et al. 2005; Batako & Koppal 2007)

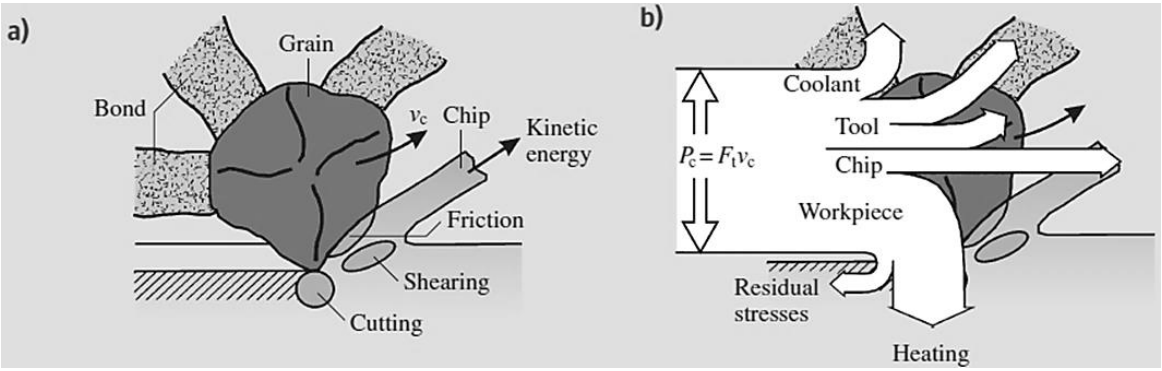

Figure 15 - Energy distribution and heat flow in a single particle during grinding: a) energy conversion effects; b) heat energy flows - adapted from (Grote & Antonsson 2009)

The use of cooling lubricants is important during grinding, which can reduce tool wear and reduce workpiece surface temperatures to avoid damage. Typical lubricants used are oils (water-immiscible) and emulsions or solutions (water-miscible), the effect of which can further be improved by the addition of polar and extreme pressure additives, anti-foaming agents, biocides and rust inhibitors. The cooling effect is dependent on physical parameters of the lubricants such as specific heat capacity c (kJ/kg*K), heat transmission coefficient α (W/m^2*K), thermal conductivity λ (W/m*K), heat of evaporation I_d (kJ/kg) and surface tension σ (N/m). The tribological parameters of the cooling lubricant are used to describe the lubricating effect. An improved workpiece surface finish and lower volumetric grinding wheel wear is achieved when a neat oil is used instead of a water-based lubricant. (Grote & Antonsson 2009; Oliveira et al. 2015; Heinzel et al. 2015; Klocke et al. 2015; Klocke et al. 2005; Batako & Koppal 2007)

Grinding wheel wear

The abrasive grains start off initially sharp, but wear down with usage and become blunt. When the grains become too blunt to penetrate the surface of the workpiece material, they cease to remove material and only generate frictional heat. The heating of the workpiece material by blunt grains is called burning and can cause stresses within the material. (Uddeholm 2012)

Grinding wheel wear takes place in the abrasive grains and the binder material. This relates to dulling and grain-bond breakage, as shown in Figure 16. When dulling (or attritious wear) occurs, flat wear areas form on the edges of the grains, leading to increased grinding forces and rise in temperature. This type of wear usually happens when the abrasive grains are submitted to gentle grinding conditions. When grinding conditions are rougher and higher grinding loads are present, the grain-bond breakage mechanisms will lead to high volumetric wear of the grinding wheel. This results in constant grinding forces and grinding temperatures, but might cause the deterioration of surface finish quality and form errors could increase. (Grote & Antonsson 2009)

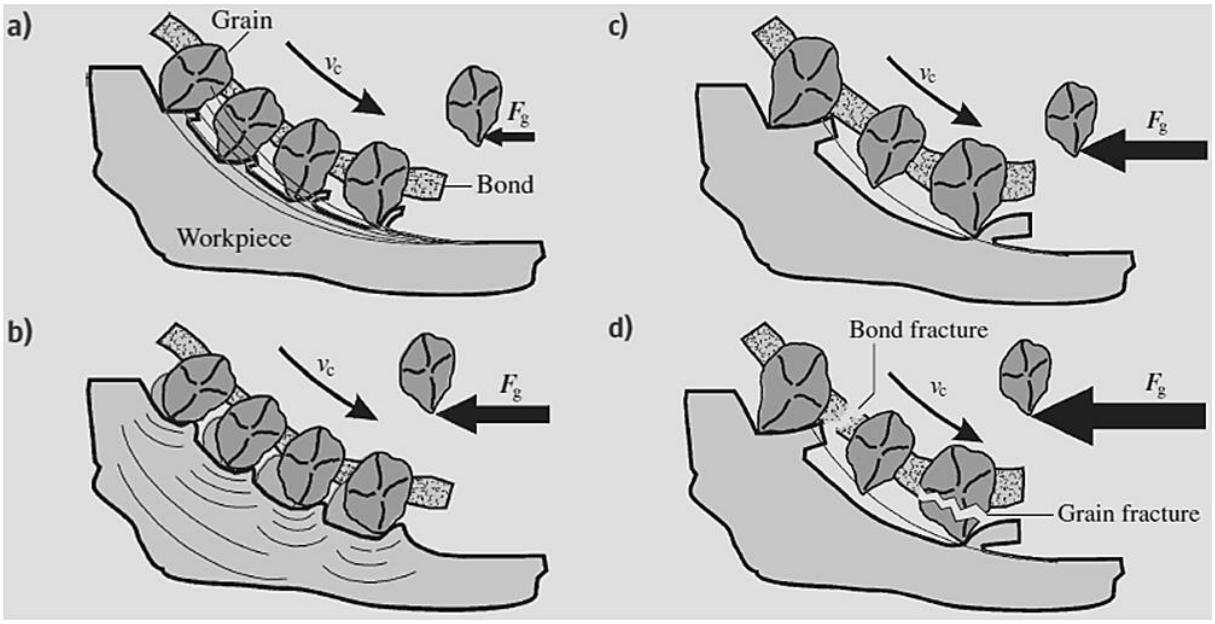

Figure 16 - Wear mechanisms of the grinding wheel: a) Sharp grains with low load per grain; b) dulling and loading; c) sharp grains with high load per grain; d) grain-bond fracture due to very high load – adapted from (Grote & Antonsson 2009)

To avoid damage to be incurred to the workpiece material, the grinding wheel binder requires the correct mechanical properties. The stresses in the binder and the strength of the binder must be balanced correctly so that as the grains become blunt due to wear, they are pulled out

of or broken from the binder, exposing new sharp grains. The grinding wheel will thus sharpen itself. This self-sharpening effect also occurs when grains are fractured, creating a new sharp cutting edge from the "old" grain. The degree of self-sharpening of a grinding wheel is thus dependent on the wheel's composition (its hardness or softness) and on the conditions at which it is operating (cutting speed, depth of cut, etc.). (Uddeholm 2012)

Grain fractures, attritious wear (dulling) and bond fractures are the three wear mechanisms that combine to cause the grinding wheel to wear as depicted in Figure 17. The first wear region is initially sharp grains undergoing grain fracture, which corresponds to the "break-in" period of conventional tool wear. The second wear region has a fairly constant wear rate, resulting in a linear wear relationship between the wheel and workpiece material volume removed. This second region has mostly attritious wear (dulling of grains) and some grain and bond fractures. During the third wear region, the grains become dull and the amount of ploughing and rubbing of grains increases relative to cutting. Additionally, some grinding chips get clogged in pores.

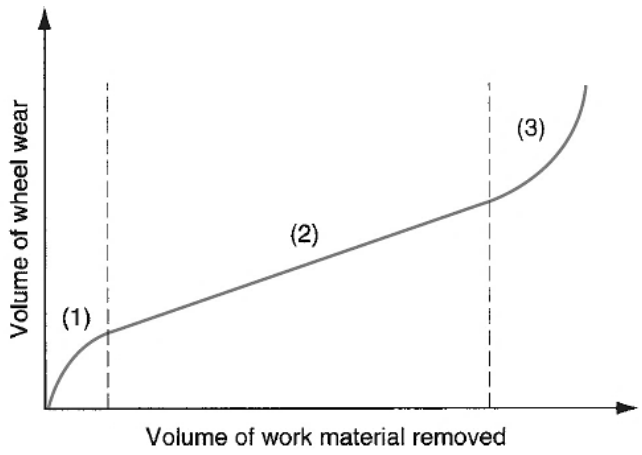

Figure 17 - Typical grinding wheel wear curve. Wear is plotted as a function of workpiece material volume removed

A grinding wheel's G-ratio (Grinding ratio) is the relationship between the *amount of material removed* and the *amount of grinding wheel consumed*. This ratio is a measure of the effectiveness of a grinding wheel with a certain workpiece material and is inversely related to the slope of the wheel wear curve ($slope = \Delta V_{wheel} / \Delta V_{workpiece}$). The ratio has the most significance in the linear second wear region of Figure 17. Typical ratio values range between 95 and 125, which can generally be increased by an increase of grinding wheel speed. The

equation for calculating the G-ratio is shown below with *GR* the G-ratio, V_w the workpiece material volume removed and V_g the grinding wheel volume worn. (Uddeholm 2012)

$$GR = \frac{V_w}{V_g} \qquad \text{Eq. 2.6}$$

Stock removal rate

Stock removal rate refers to the material that is ground away, or the amount of chips that is formed, per unit time. This rate can most easily be expressed as mm^3/s and is dependent on the machine feed rate, grinding wheel composition, peripheral cutting speed and the dimensions of the workpiece (in certain cases). The stock removal rate term is more meaningful to use as a single performance indicator when describing the grinding process, and to calculate its value, rather than the table feed speed, depth of cut, etc. (Uddeholm 2012)

The chip size produced by a grinding operation will increase when the stock removal rate is increased while the number of abrasive grains performing work is kept constant. One way this can be achieved is by increasing the infeed depth of the grinding wheel into the workpiece material. Machining efficiency usually dictates that the stock removal rate should be as high as possible in order to obtain the highest financial profit gain (less machining time at lower costs equals a greater profit margin).

Cutting speed

The peripheral speed of a grinding wheel has a direct effect on the amount of cutting edges in contact with the workpiece, since cutting occurs with the interaction of abrasive grains and the workpiece material. When, for example, the peripheral speed is doubled, twice the amount of cutting edges will be in contact with the workpiece material per unit time, if all other grinding parameters are kept constant. (Uddeholm 2012)

If the relative speed between the grinding wheel and the workpiece material is increased, the mean chip thickness will decrease because more grains are available to do the work. This also reduces the cutting forces on each grain, reducing the self-sharpening characteristic of the grinding wheel. The grinding wheel will be effectively harder, producing a finer surface finish, but with a greater risk of burning the surface. (Uddeholm 2012)

The opposite is true for when the relative speed between the grinding wheel and the workpiece material is reduced. This will cause an increase in produced chip thickness, resulting in the grinding wheel behaving like a softer wheel and thus producing a coarser surface finish. The change in relative speed between the grinding wheel and the workpiece material is illustrated in short in Figure 18.

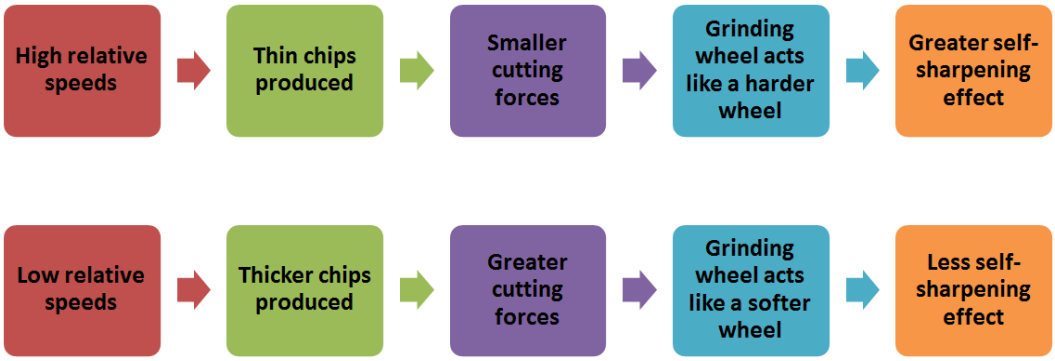

Figure 18 - Effects of cutting speed on grinding wheel performance

Grinding wheel contact surface

The cutting operation occurs at the interface of the grinding wheel and the workpiece material, called the grinding wheel contact surface (area). When the contact surface is large, a great number of cutting edges are participating in the cutting process, reducing the produced chip size and specific forces. Similarly, when the contact surface is small, the produced chips are larger and greater specific forces are present. (Uddeholm 2012)

The contact surface is in principle in the shape of a rectangle. The contact surface's extent in the direction of cutting is referred to as the *contact length* or *contact arc*, while its extent perpendicular to the cutting direction is referred to as the *contact width*. The contact length is mainly dependent on the type of grinding operation. Additionally, it is dependent also on the grinding wheel diameter, cutting depth and (excluding surface grinding) the dimensions of the workpiece. Due to afore mentioned parameters, the difference in contact length is the main reason for having to select different wheel compositions for different grinding operations. The differences in contact length for different grinding operations are shown in Figure 19. (Uddeholm 2012)

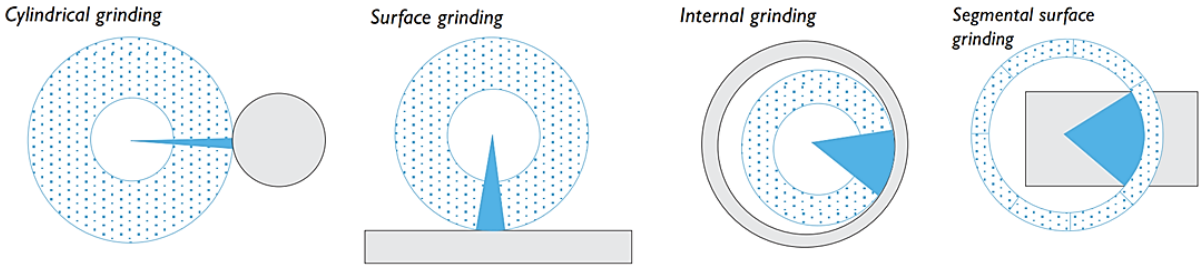

Figure 19 - Difference in contact length for different grinding operations (Uddeholm 2012)

If for example internal grinding is performed with a grinding wheel that has a diameter slightly less than that of the ground hole, the resulting contact length will be very large and thus low cutting forces per grain. If the wheel is to have good self-sharpening characteristics, it should be of a softer composition than a grinding wheel intended for external cylindrical grinding of a similar part. For the external cylindrical grinding case, the contact length is shorter, meaning that there are higher cutting forces on each grain. The effect of contact length is illustrated in short in Figure 20. (Uddeholm 2012)

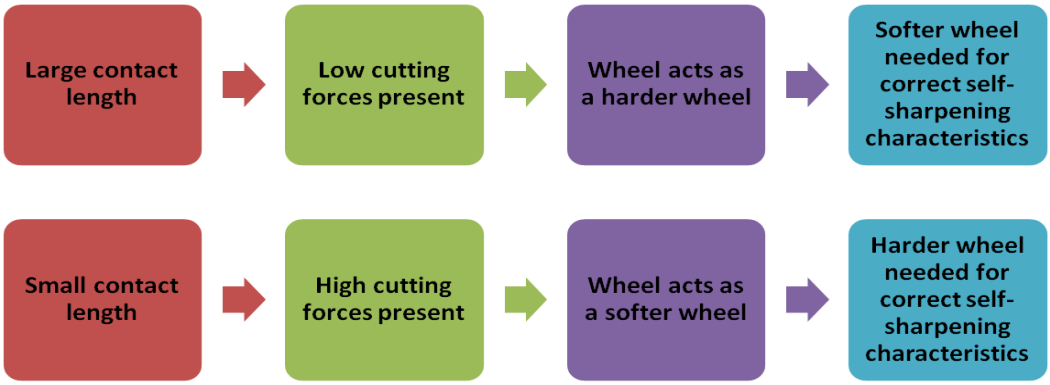

Figure 20 - Effects of contact length on grinding process

As for the contact width, it may be equal to the width of the grinding wheel for a grinding process such as plunge grinding. This is however not true for operations such as surface grinding, where only part of the grinding wheel might be in contact with the workpiece. It is possible to reduce the contact width of a grinding wheel by truing it. This reduces the contact surface, resulting in greater chip thickness, higher loads on the grains and an effectively softer grinding wheel. (Uddeholm 2012)

The chip thickness is greatly affected during grinding by the number of cutting edges in the contact area between the grinding wheel and workpiece material. A grinding wheel with a large amount of cutting edges per unit area reduces the chip thickness and specific forces

during grinding due to the work required to remove material being spread over a large number of grains. The abrasive grain size also affects the number of cutting edges, causing the common observation that fine-grained grinding wheels seem to be harder. (Uddeholm 2012)

Dressing and truing of grinding wheels

Dressing and truing of a grinding wheel are two different processes, but are often considered the same process because they are performed as a single operation. The process of truing produces any desired profile on the face of a grinding wheel and ensures concentricity. Dressing on the other hand is the process of conditioning the wheel surface so that it produces a desired cutting action by exposing sharp cutting edges. (Uddeholm 2012)

The grinding characteristics of a grinding wheel can be altered through the application of different dressing tools and methods. Dressing is consequently a particularly important parameter in achieving good grinding performance. The dressing of a grinding wheel that produces a smooth wheel surface results in the abrasive grains to be close together. A resulting rough surface leads to the grains to have a more open structure. Dressing thus provides a means of making the same grinding wheel having completely different grinding results. A grinding wheel that has a higher degree of self-sharpening has a greater open grain structure than one having a lesser degree of self-sharpening. (Uddeholm 2012)

Grinding wheel and workpiece speed

The cutting speed is often times restricted by the spindle speed of a grinding machine, especially in small grinding machines. A common peripheral speed safety limit for a vitrified bonded grinding wheel is 35 m/s, however some special application grinding wheels are approved for peripheral speeds of up to 125 m/s. The common cutting speed for surface and cylindrical grinding is 20 – 35 m/s. The grinding wheel's performance can be modified by varying the peripheral speed of the wheel:

- An increase in peripheral speed while keeping workpiece speed constant, results in a grinding wheel behaving as if it was harder.
- A reduction in peripheral speed with constant workpiece speed results in an apparent softer wheel.

For resin bonded grinding wheels, a suitable peripheral speed would be 30 – 40m/s. When a hard and tough metal is ground, such as high-carbide steel or a titanium alloy, the peripheral

speed of the grinding wheel should be high. The cutting speed thus has a considerable effect on the economics of grinding. (Uddeholm 2012)

Workpiece speed is the speed at which the workpiece moves with respect to the grinding wheel. During surface grinding, a workpiece speed of 10 – 20 m/min should be used, while for conventional cylindrical grinding a workpiece speed of 15 – 20 m/min would be sufficient. The performance of the grinding wheel can be modified by the varying of the workpiece speed. By increasing the speed of the workpiece, the grinding wheel will seem to be softer, while a decrease in workpiece speed will produce a grinding wheel that seems harder. (Uddeholm 2012)

Cross-feed and infeed

Cross-feed during grinding is the sideways motion of the grinding wheel with respect to the workpiece. The cross-feed speed is higher for rough grinding than for fine grinding. For cylindrical grinding, the cross-feed should be about 1/3 – 1/2 of the width of the grinding wheel for each revolution of the workpiece. For a fine surface finish, the cross-feed should be reduced to between 1/6 and 1/3 of the wheel width per wheel revolution. It should be noted that when the cross-feed is increased, the active contact surface area between grinding wheel and workpiece becomes larger, which results in the apparent increase in grinding wheel hardness.

Infeed is another term used to describe the depth of cut of a grinding wheel into the workpiece. The infeed of the grinding wheel depends on the type of wheel used and the rigidity of the grinding machine and workpiece clamp. Guide values for infeed during cylindrical grinding ranges from 0.05 mm/pass for a rough finish, to 0.005 – 0.01 mm/pass for a fine surface finish.

The infeed guide values for surface grinding with a straight grinding wheel ranges from 0.025 – 0.075 mm/pass for a rough surface finish to 0.005 – 0.01 mm/pass for a fine surface finish. When the grains of the grinding wheel are very fine, the infeed should be increased somewhat over the above values to achieve higher grinding pressures for the purpose of wheel self-sharpening. Only rotational machining processes such as grinding (or turning) can generate a workpiece surface without any feed marks. (Klocke et al. 2005)

2.3) Titanium and its alloy Ti-6Al-4V

2.3.1) Background and General Information

Titanium is a low density, strong, corrosion resistant metal with a silver-like colour and is nonmagnetic. It has an atomic number of 22 on the periodic table and occurs in several mineral deposits, most commonly as titanium dioxide (TiO_2), throughout the earth's crust and lithosphere. Titanium is the ninth most-abundant element and the fourth most-abundant structural metal. It was first discovered in 1791 in Great Britain by William Gregor, but only purified in the early 1900s. Titanium has only become widely used in industry in the second half of the 20th century and has up to now experienced about 50 years accumulated industry practice and use. Samples of titanium can be seen in Figure 21. (Encyclopædia Britannica Online 2013)

Figure 21 - Electrochemically produced pure titanium samples (Kummer n.d.)

Titanium is extracted from mineral ores, mostly with the use of the Kroll or Hunter process. The steps needed in the processing of titanium extraction are:

1) chlorination of titanium dioxide (TiO_2) to prepare titanium tetrachloride ($TiCl_4$)
2) reduction of $TiCl_4$ with magnesium metal (Kroll process), or
   reduction of $TiCl_4$ with sodium metal (Hunter process)
3) vacuum distillation of reduced mass

The by-product(s) of step 2, $MgCl_2$ and $NaCl_2$, is electrolysed to separate the elements for reuse in the process. (Nagesh & Ramachandran 2007)

The costs involved with these two processes are still high and alternative methods have been developed. The extensive study of electrochemical de-oxidation of titanium in a molten calcium chloride electrolyte led to the development of electrochemical reduction processes. The solid titanium dioxide is subjected to electrolysis in molten calcium chloride. Graphite is used as the anode and pressed and sintered TiO_2 pellets are used as cathode. When a DC voltage is applied, oxygen ions pass through the molten $CaCl_2$ and are diffused out of TiO_2,

reacting with the graphite to form CO and CO_2 gas at the anode. (Nagesh & Ramachandran 2007)

It should be noted that while numerous alternative methods for titanium extraction are investigated, none have yet reached the commercial production stage. Some are pilot, but most are still at the research and development level.

Titanium can be alloyed with iron, aluminium, vanadium, molybdenum and a few more metals to form alloys with specific characteristics and applications in industry. The use of titanium and its alloys were mostly for military applications, but more recently it is being used in aerospace, medical, automotive and even sports equipment. (Lide 2005)

Titanium has a few important and beneficial characteristics, adding to its widespread use. Some characteristics include:

- When compared with the density of steel and nickel-based superalloys, the density of titanium is only about 60% that of the mentioned metals.
- In alloy form, the tensile strength of titanium is comparable to lower-strength martensitic stainless steel and is better than austenitic or ferritic stainless steel.
- Depending on the alloy composition, the useful temperature limit of titanium is up to between 538°C and 595°C.
- The cost of titanium is comparable with superalloys, even if it is about four times the cost of stainless steel.
- Titanium has excellent corrosion resistance in most environments, often exceeding that of stainless steel, and exceptional biocompatibility in the human body (explaining its use as surgical implants).
- Forging, rolling and casting of titanium and its alloys with standard techniques are possible. (Investment casting being the preferred method and being cheaper than forged/wrought products)
- Joining of titanium parts can be achieved by means of fusion welding, brazing, adhesives, diffusion bonding and fasteners. Powder metallurgy of titanium is also possible.
- Titanium is formable (requiring high forces) and machinable, but with resulting rapid tool wear.

The physical and mechanical properties of elemental titanium can be seen in Table 4. (Donachie 2000)

Table 4 - Physical and mechanical properties of elemental titanium – adapted from (Donachie 2000)

Property	Description or Value
Atomic number	22
Atomic weight	47.90
Atomic volume	10.6 W/D
Covalent radius	1.32^{-}
Ionization potential	6.8282 V
Thermal neutron absorption cross section	5.6 barns/atom
Crystal structure	
Alpha (≤882.5 °C)	Close-packed hexagonal
Beta (≥882.5 °C)	Body-centred cubic
Colour	Dark grey
Density	4.51 g/cm^3
Melting point	1668°C
Solidus/liquidus	1725°C
Boiling point	3260°C
Specific heat (@ 25°C)	0.5223 kJ/kg.K
Thermal conductivity	11.4 W/m.K
Heat of fusion	440 kJ/kg (estimated)
Heat of vaporization	9.83 MJ/kg
Specific gravity	4.5
Hardness	70 to 75 HRB
Tensile strength	240 MPa
Young's modulus	120 GPa
Poisson's ratio	0.361
Coefficient of friction	
At 40 m/min	0.8
At 300 m/min	0.68
Coefficient of linear thermal expansion	8.41 µm/m.K
Electrical conductivity	3% IACS (where copper = 100% IACS)
Electrical resistivity (@ 20°C)	420 nΩ.m
Electronegativity	1.5 Pauling's
Temperature coefficient of electrical resistance	0.0026/°C
Magnetic susceptibility (volume, at room temperature)	180(±1.7) . 10^6 mks

2.3.2) Titanium Metallurgy

Titanium exists in more than one crystallographic form, making it an allotropic element. Pure titanium, however, has two crystal structures. A hexagonal close-packed (HCP) structure, existing at room temperature and is referred to as alpha phase. At 882°C, the HCP structure transforms to a body-centred cubic (BCC) crystal structure, referred to as beta phase. The cubic structure is found only at high temperatures, unless the metal is alloyed to maintain this cubic crystal structure at lower temperatures. Figure 22 is an illustration of the two crystal structures. (Donachie 2000)

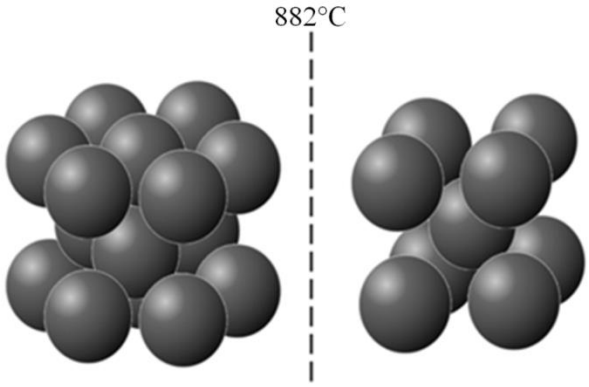

Figure 22 - Crystal structures of titanium: (a) HCP and (b) BCC – adapted from (Donachie 2000)

Alloying of titanium leads to four classes of titanium: alpha, near-alpha, alpha-beta and beta. They generally denote the type of crystal microstructure (phase and grain structure) after processing. Figure 23 represents some of the effects alloying elements have on the structure of titanium and Figure 24 shows the pseudo-binary phase diagram of titanium and some alloys. (Donachie 2000)

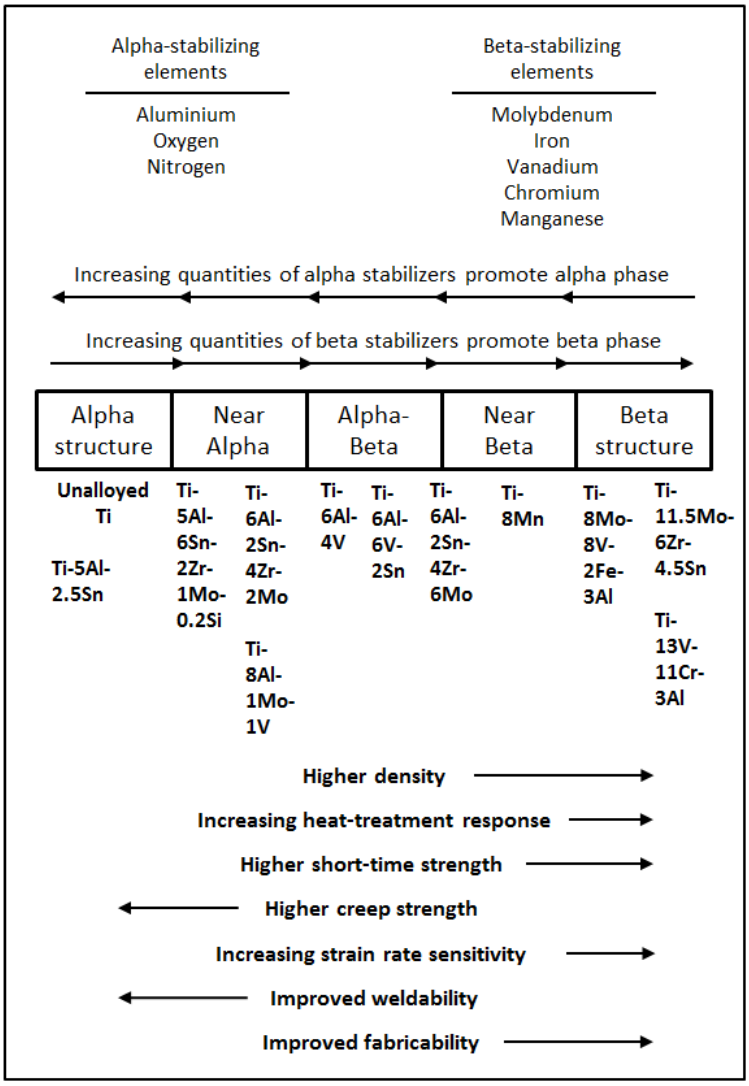

Figure 23 - Effects of alloy elements on the structure of titanium (Donachie 2000)

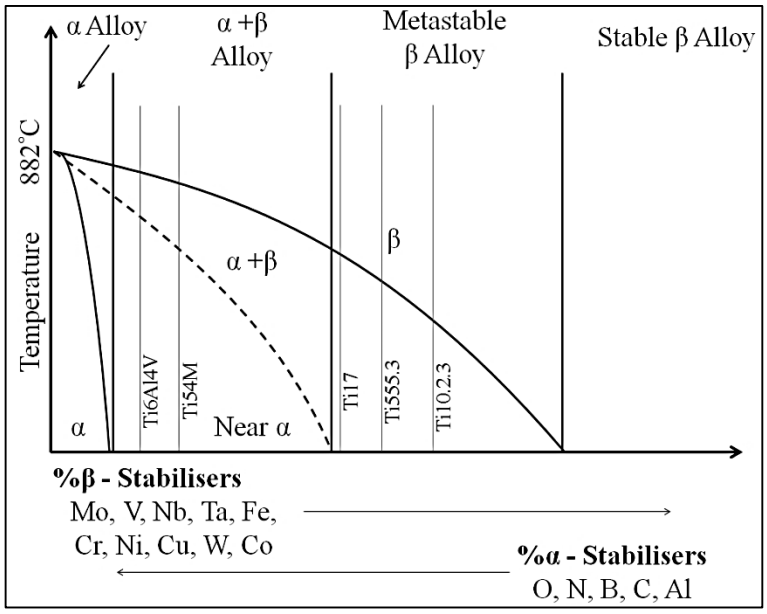

Figure 24 - Pseudobinary phase diagram of titanium with various alloys – adapted from (Donachie 2000)

Commercially pure titanium consists of an alpha phase structure. As seen from Figure 23 and Figure 24, a range of possible microstructures can be formed by the addition of alloying elements. The best high temperature oxidation resistant alloys are the alpha and near-alpha alloys containing high amounts of aluminium. These alpha alloys cannot be heat treated for the development of greater and improved mechanical properties, because of their single phase. The properly treated alpha-beta phase alloys exhibit an excellent combination of strength and ductility and are stronger than both alpha and beta single-phase alloys. (Donachie 2000)

The beta phase structures should rather be referred to as metastable beta phases because they tend to transform to an equilibrium structure, but mostly beta phase, upon cooling. The strength of the (metastable) beta phase is generated from the intrinsic beta structure strength and precipitation of alpha phase (and other phases) after heat treatment of the alloy. The beta phase structure benefits from increased formability, relative to alpha and near-alpha structure types (hexagonal structures). (Donachie 2000)

An alpha alloy normally does not form beta phase on heating, but a near-alpha alloy forms limited amounts upon heating. This causes the near-alpha alloy to look similar in microstructure to an alpha alloy when viewed at lower temperatures. The composition of an alpha-beta alloy permits complete beta phase transformation upon heating, but transforms back to alpha phase plus retained/transformed beta phase at cooling to lower temperatures. Beta alloys indefinitely retains beta phase, regardless of temperature, but forms metastable beta phase on initial cooling. In Figure 25 typical titanium microstructures are shown. The actual microstructure of titanium alloys depends on chemistry and processing, and the figures are only generally representative. (Donachie 2000)

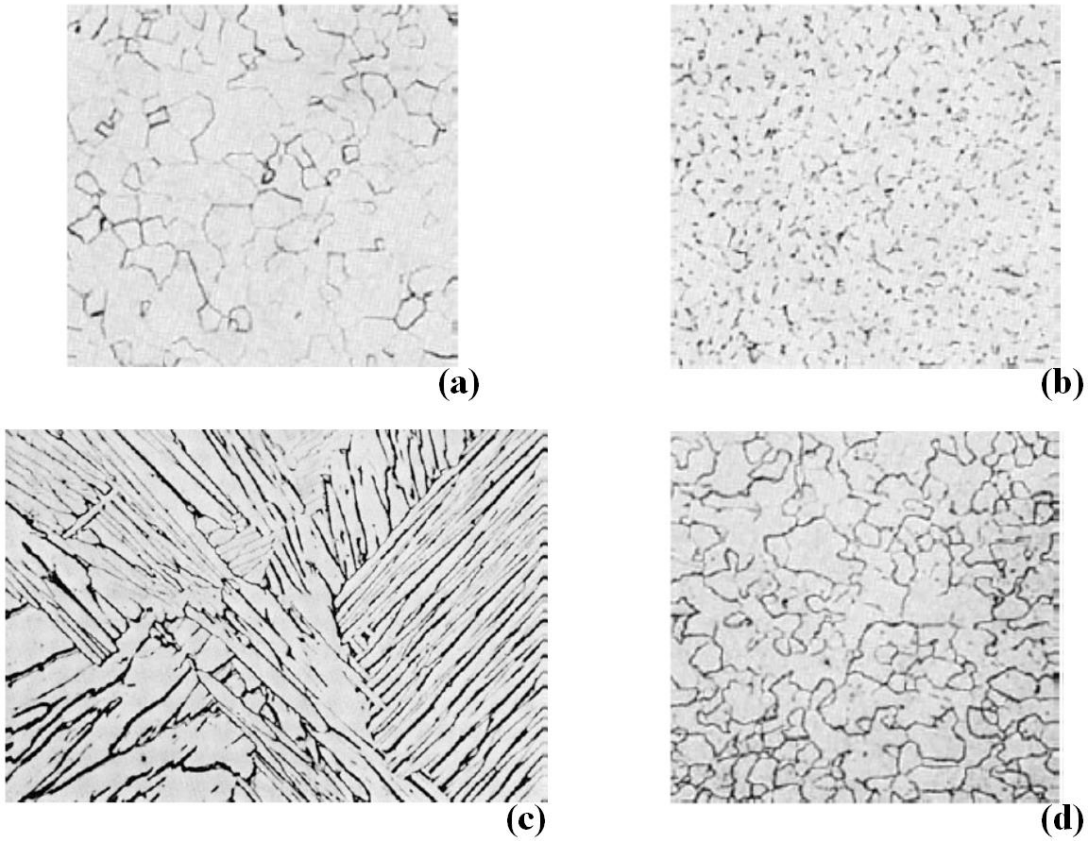

Figure 25 - Typical titanium alloy microstructures: (a) alpha phase, (b) near-alpha phase, (c) alpha-beta phase, (d) beta phase – adapted from (Donachie 2000)

2.3.3) Titanium Alloys

For the past 50 years, a great variety of titanium alloys were produced, each alloy with its own unique set of characteristics and for specific applications in industry. Many alloy compositions have been invented, but never seen the commercial success of Ti6Al4V. This specific alloy accounted for about 45% of the total titanium alloy weight production in the last half of the 20th century. Ti6Al4V is composed of 6 wt% aluminium, 4 wt% vanadium, ±1 wt% impurities and the rest (~89 wt%) titanium. The aluminium stabilizes the alpha phase (HCP phase/structure), while the vanadium stabilizes the beta phase (BCC phase/structure). It is a unique alloy in that it combines attractive properties with inherent characteristics. Ti6Al4V can be produced into all types of mill products (due to its good workability), both large and small sizes, which can then be made into complex components. (Donachie 2000; Patankar et al. 2001; Dimitrov et al. 2013)

Ti6Al4V has become such a popular and easily obtainable alloy, that it is the standard against which other titanium alloys are measured. This applies for wrought and casting alloy considerations as well. Ti6Al4V is also used in powder metallurgy processes and will

continue to be the most widely utilised titanium alloy for many years. The only major drawback of this alloy is its temperature limitation, restricting use to about 500°C temperature threshold, beyond which oxidation readily occurs. (Donachie 2000)

3) Research Methodology

This chapter explains and describes the steps taken towards designing, manufacturing, testing and evaluating the performance of a tungsten carbide based grinding wheel by the grinding of a titanium alloy.

3.1) Grinding Wheel Production

3.1.1) Determination of grinding wheel shape and size

In order to evaluate the performance of tungsten carbide as abrasive medium for use in grinding wheels, a custom grinding wheel had to be manufactured since there are no commercial grinding wheels containing WC as abrasive medium available. The large amount of data required for the performance evaluation led to the decision of using mounted points. These are smaller grinding wheels rather than the larger, more common sized grinding wheels. The selected design is a combination of a WPL 13 13 06 (former W185) and a WPL 20 10 03 (former W202) mounted point from the ISO 603-17 document (Addendum A); having a diameter of 20 mm, a thickness of 13 mm and a spindle diameter of 3 mm. The mounted point design can be seen in Figure 26.

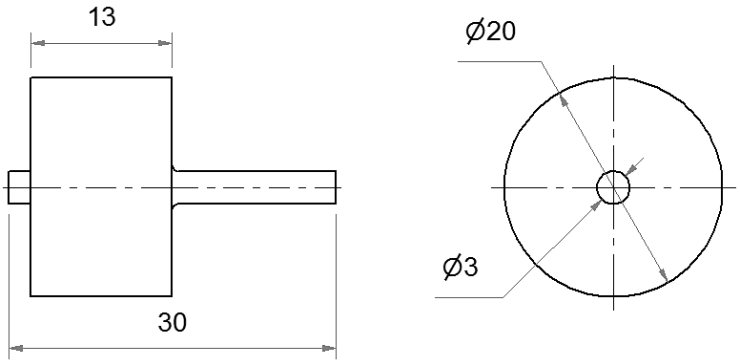

Figure 26 - Mounted point design (dimensions in mm)

This design allows for minimal abrasive material usage (~4.084 cm^3) during manufacturing when compared to large grinding wheels (282.74 cm^3 to 1767.14 cm^3). The amount of tungsten carbide powder to be used as abrasive material is thus reduced, lowering the cost of experimentation by lowering the amount of expensive WC-12wt%Co powder to be used. The smaller mounted points can thus also be used in a micro-machining process, as mentioned later. These smaller mounted points will also allow for a larger amount to be produced during a single production process, rather than one larger grinding wheel at a time.

3.1.2) Abrasive particles

The abrasive material used for the manufacturing of the mounted points is, as mentioned previously, WC-12wt%Co. This specific composition has a favourable combination of hardness and toughness (see Figure 1), which is preferred for use in the grinding processes. The WC-12wt%Co powder used in the study was obtained from Global Tungsten and Powders from the USA and is their SX408 powder type. The powder has a spherically agglomerated shape, which is manufactured with a spray drying process. The powder was analysed by Global Tungsten and Powders after manufacturing to certify it is of highest quality standard. The analysis produced the data in Table 5 regarding the powder characteristics.

Table 5 - Experimental WC-12wt%Co powder characteristics

Characteristics	Value
Tungsten content	Balance
Cobalt content	12.1 wt%
Carbon content	5.2 wt%
Iron & other impurities	<1 wt%
Particle size	<31 μm

3.1.3) Determination of the type of binder

From the section on grinding wheel binders, it is apparent that there is a multitude of binders that could be used to bind the abrasive grains in a grinding wheel. Each binder type has its own production requirements in terms of procedure and equipment, and leads to usage limitations. Resin as binder has shown successful usage in grinding hard metals such as titanium alloys. This binder type is also the most cost effective in terms of purchasing cost, manufacturing method and necessary production equipment. For this reason and the relatively safe production process and handling of resin, it is the chosen binder type for this research study.

Normally in the production of resin bonded grinding wheels, a phenolic resin is preferred above that of an epoxy resin. These two types of resins have similar tensile and compressive strengths and preparation methods, but different thermal decomposing temperature thresholds. Phenolic resins have a slightly higher decomposing temperature than epoxy resins, but are

harder to come by. Economically, epoxy resin is less expensive than phenolic resin. Phenolic resin contains phenols, which are toxic, leading to strictly controlled exposure limits. (Enever et al. 2015)

It thus becomes apparent that an epoxy resin is preferred for use in the manufacturing of the mounted point grinding wheels. This is due to lower cost, increased safety, greater availability and comparable mechanical properties when compared with phenolic resin, despite the drawback of having a slightly lower decomposing temperature. The epoxy resin used in this study is the AR 600 resin and AH 2336 hardener from Aerontec.

3.1.4) Abrasive to binder ratio

Literature suggests that the amount of resin to be used in the manufacture of a resin bonded grinding wheel in order for functional and efficient grinding is not to exceed 30 wt% (Gardziella et al. 2000). This amount is based on grinding wheels that have abrasive particles of grain size numeral 100, or 110 μm – 150 μm. These particles are much larger than the WC-12wt%Co particles that will be used in the experiments. For the surface of a relatively large abrasive particle to be covered in resin during production requires a greater resin-to-abrasive ratio. To cover the surface of a relatively small abrasive particle would then require less resin. The particles need to be fully covered in resin in order to bind them together into a shape. It thus leads to the amount of resin used in the production of the tungsten carbide based mounted points to be decreased in order to achieve an optimal resin-to-abrasive mixture.

With the optimal resin-to-abrasive ratio unknown for production of the mounted points, tests were conducted to determine potential “candidate” ratios. On a structural scale, for a grinding wheel to be able to grind effectively it should be strong and not shatter during operation. For this purpose, strength tests had to be conducted on a few resin-abrasive samples. To determine the strength testing method, the stresses within a grinding wheel should be analysed. For the purpose of determining the stresses within a to-be-produced mounted point, it can be visualized as a full size grinding wheel.

The grinding wheel can be modelled as a rotating disc with a central hole, with inner and outer radius. During operation, the wheel will rotate at high angular velocity and thus undergo high centrifugal forces. By modelling the centrifugal forces in the abrasive particle section of the grinding wheel only, the principal stresses can be determined which act on the powder-

resin composite material. Consider Figure 27 below which indicates the mechanics during centrifugal loading.

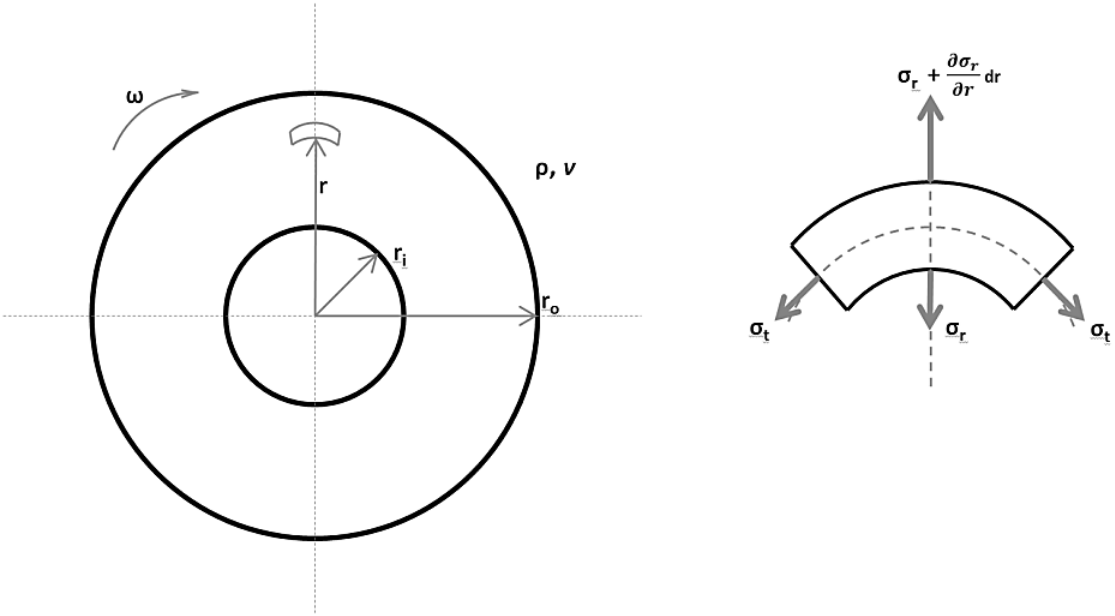

Figure 27 - Stresses induced during centrifugal loading of a rotating disk with central hole (Enever et al. 2015)

The disc section rotates at an angular velocity $\boldsymbol{\omega}$ (rad/s), has a relative composite density $\boldsymbol{\rho}$ (g/cm^3), a Poisson's ratio $\boldsymbol{\nu}$ (dimensionless), inner radius $\boldsymbol{r_i}$ (m) and outer radius $\boldsymbol{r_o}$ (m). At any radial distance $\boldsymbol{r}$ from the inner to the outer radius of the disc, a section can be taken where stress equilibrium expressions indicate the stresses within the disc. The stress in the radial direction is radial stress ($\boldsymbol{\sigma_r}$) and stress along a circular path is tangential stress ($\boldsymbol{\sigma_t}$). (Enever et al. 2015)

At equilibrium, the stress in the tangential direction is equal in opposite directions for a given radius. The radial stress on the other hand increases as the radius increases. Thus, on the section, the outermost radial stress is equal to the inner most radial stress plus an additional change in radial stress over the change in radial length of the section. The radial and tangential stress in the disc at any radius within the inner and outer radial range, can be calculated with Equation 3.1 and Equation 3.2 as follows (Benham et al. 1996; Budynas & Nisbett 2008; Zhang et al. 2011):

$$\sigma_r = \frac{3+\nu}{8}\rho\omega^2\left(r_i^2 + r_o^2 - \frac{r_i^2 r_o^2}{r^2} - r^2\right) \qquad \text{Eq. 3.1}$$

$$\sigma_t = \frac{3+\nu}{8}\rho\omega^2\left(r_i^2 + r_o^2 + \frac{r_i^2 r_o^2}{r^2} - \frac{1+3\nu}{3+\nu}r^2\right) \qquad \text{Eq. 3.2}$$

For these equations of radial and tangential stress, the total composite density and Poisson's ratio is required. The density and Poisson's ratio of each material need to be known as well as the weight and volume ratios of each component. An initial computation is done to determine the stresses by using a mixture with 10 wt% resin content. The densities and Poisson's ratios of both WC-12wt%Co and epoxy resin are shown in Table 6. Equations 3.3 and Equation 3.4 for calculating the composite density and Poisson's ratio are shown below Table 6. (Ohoud et al. 1988; Callister 2010)

Table 6 - Material characteristics of WC-12wt%Co and epoxy resin (Enever et al. 2015)

	Density (g/cm^3)	**Poisson's ratio**	**wt%**	**vol%**
WC-12wt%Co	14.88	0.23	90	74
Resin	1.1	0.31	10	26

$$\rho_{composite} = \frac{1}{\frac{wt\%_{WC-12Co}}{\rho_{WC-12Co}} + \frac{wt\%_{resin}}{\rho_{resin}}} \qquad \text{Eq. 3.3}$$

$$\nu_{composite} = vol\%_{WC-12Co}.\nu_{WC-12Co} + vol\%_{resin}.\nu_{resin} \qquad \text{Eq. 3.4}$$

To calculate the tangential and radial stress in the rotating grinding wheel during operation, the variables in Table 7 below are used in Equation 3.1 and Equation 3.2. The apparent density of WC-12wt%Co is used as it is assumed that the resin would fill the spaces between abrasive particles. The resulting tangential and radial stress curves are shown in Figure 28 below Table 7.

Table 7 - Variables used for tangential and radial stress calculations (at 10wt% resin) (Enever et al. 2016)

Composite density (ρ_c)	6.6 g/cm^3	
Composite Poisson's ratio (ν_c)	0.278	
Rotational speed (ω)	20 000 rpm	2094.39 rad/s
Inner radius (r_i)	0.003 m	
Outer radius (r_o)	0.02 m	

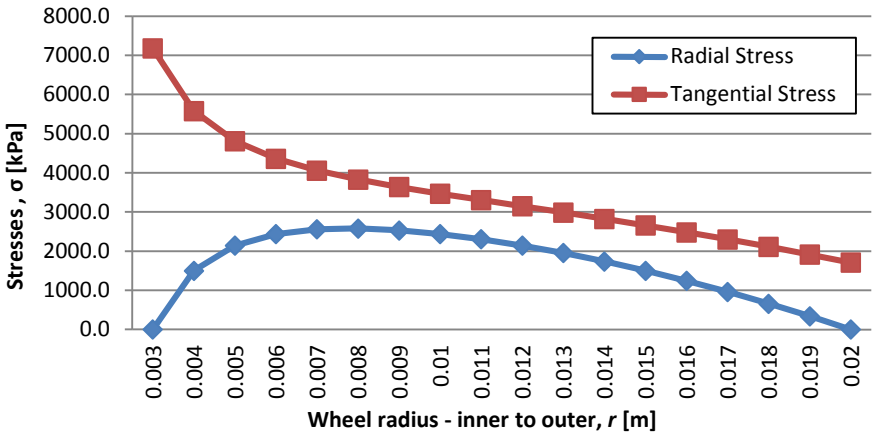

Figure 28 - Tangential and radial stress distribution along mounted point radii at 20 000 RPM (Enever et al. 2015)

It is evident from the stress distribution in Figure 28 that the tangential stress has a greater effect on the mounted point. Since the tangential stress is in the circumferential direction, it imparts a tensile stress. With the radial stress in the outward direction away from the axis of rotation, the tensile stress is intensified. It can thus be accepted that the major stress within the rotating grinding wheel is a tensile stress.

For the case when the grinding wheel is grinding a workpiece, a compressive force is imparted to the wheel equivalent to the applied downward grinding force. The induced compressive stress due to grinding will not have a significant effect on the large tensile stress present in the grinding wheel during operation. This is due to the small grinding force that will be applied to the mounted point for micro grinding. The grinding parameters for experimentation purposes will be discussed later, but for now only the tensile stress will be considered for the analysis.

The amount of resin in the grinding wheel has an effect, but not to a great extent, on the distributed stresses as the density of the resin is low compared to the density of the WC-12wt%Co powder. The theoretical and simulated effect of four different resin contents (10 wt%, 12 wt%, 14 wt% and 16 wt%) on the tangential and radial stress in a mounted point is shown in Figure 29 and Figure 30.

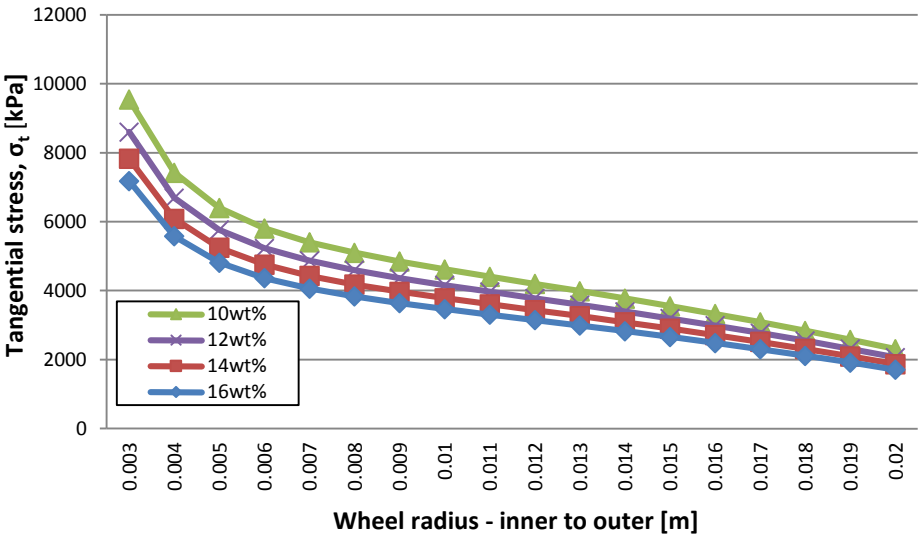

Figure 29 - Tangential stress distribution for various resin contents

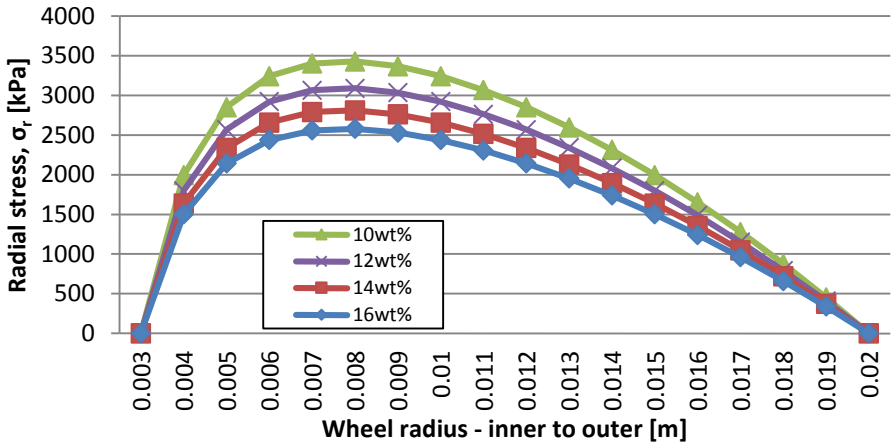

Figure 30 - Radial stress distribution for various resin contents

From the analysis on the stress distribution within an operating grinding wheel leading to the major stress being a tensile stress, a tensile strength test can be planned and conducted on samples to determine the strength of the various resin contents. When the resin and powder is mixed, moulded and cured, the final composite product will resemble a material similar to stone or set concrete. For this purpose, the Brazilian Disk test, which is an indirect tensile strength test, is chosen as the method for testing the tensile strength of cured resin-power samples. In order to conduct the Brazilian Disk test, the samples should be moulded into a disk of known diameter and thickness. (Wang & Xing 1999; Li & Wong 2012)

For the determination of the optimal resin-to-powder ratio, the four ratios similar to the simulated theoretical analysis is used (10 wt%, 12 wt%, 14 wt% and 16 wt%). The resin and powder is mixed in these ratios and moulded into circular disks with a mould having a

diameter of 30 mm. The thicknesses of the disks are not specifically controlled as the Brazilian Disk test takes into account the geometry of the disks. After the four resin-powder mixtures are placed in the moulds, they are left to pre-cure in ambient room temperature for a minimum of 12-hours. Thereafter, the samples are thermally cured in a hotbox at the resin manufacturers' specifications of 2-hours at 80^{o}C, then 3-hours at 150^{o}C followed by 4-hours at 180^{o}C. After the thermal curing process, the samples are removed and are ready for strength testing.

The Brazilian Disk test is conducted by diametrically compressing a relatively thin circular disc (thickness < disk radius) to failure. This is an indirect method for testing the tensile strength of brittle materials such as concrete, rock, and rock-like material (Li & Wong 2012), which the fully cured resin-powder composite material resembles. The Brazilian Disk test method assumes that failure will occur within the material at the point of maximum tensile stress. The failure point, under good testing conditions, occurs at the centre of the disk where the tensile stress is greatest (Li & Wong 2012).

Another assumption is that the sample disk experiences a uniformly applied pressure over a short strip of the circumference at each end of the disk. This assumption leads to the perception that the sample will split along the compressive diametral line, starting in the centre and propagating outward along the diameter. If this split does not occur, it is regarded as exhibiting an invalid failure mode. The short strip over which the force is applied covers an area defined by a loading angle of 2α. The applied load, loading angle and failure mode is schematically shown Figure 31. (Li & Wong 2012; Wang & Xing 1999)

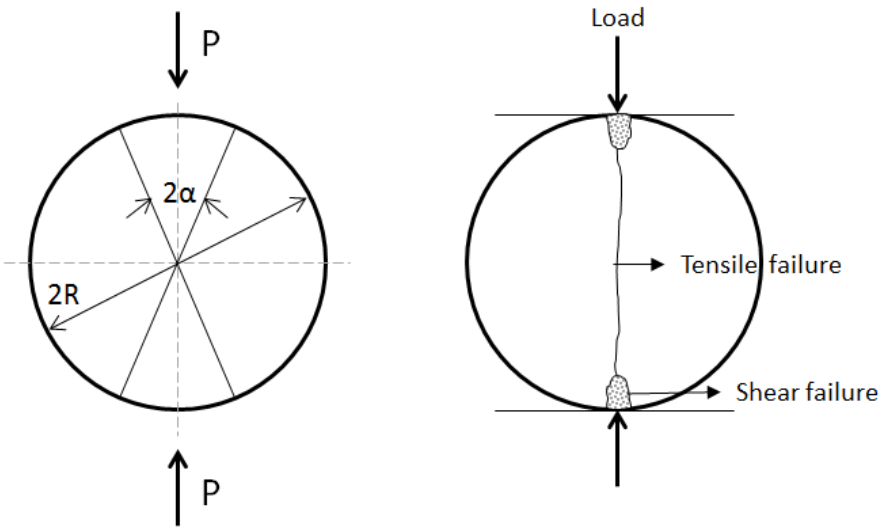

Figure 31 - Disc orientation, loading direction, loading angle and failure mode during the Brazilian Disk test – adapted from (Li & Wong 2012; Wang et al. 2004)

The loading angle 2α is taken as 20º as suggested in literature for central crack initiation and flat plate loading of the disks (Wang & Xing 1999). A segment section of nearly 5 mm is formed over the loading angle of 20º, which is roughly the observed length over which the loading force is applied during testing.

The test apparatus used for compressive testing is a hydraulic lab press. The instrument provides a pressure reading in mega Pascal (MPa) and need to be converted to applied force in Newton (N). This conversion can easily be done when the thickness of each sample being compressively tested is measured before the test is conducted. The loading angle over the disk is 2α, which was measured to be 20°. The disk segment length can be calculated with Equation 3.5a, which is a function of the disk diameter.

$$segment\ length = \frac{2\alpha\pi D}{360} \qquad \text{Eq. 3.5a}$$

The segment surface over which the load is applied, is simply the segment length multiplied by the disk thickness. The conversion from applied pressure to applied force can be calculated by Equation 3.5b.

$$applied\ force = segment\ surface \times applied\ pressure \qquad \text{Eq. 3.5b}$$

During testing, a steel support plate is used above the sample. This plate's weight is also accounted for in the total overall load applied to the test specimens. With the applied load known, Equation 3.5 can be used to calculate the tensile strength of the samples (Li & Wong 2012).

$$\sigma_t = 0.636\frac{P}{Dt} \qquad \text{Eq. 3.5}$$

In the equation, ***P*** is the applied load at failure (N), ***D*** the disk diameter (m) and ***t*** the disk thickness (m). The four sample disks were compressed to failure and the data collected. The failed samples can be seen in Figure 32. Note the upper and lower loading points (flattened area on outside periphery of disks), shear failure area (triangular failure section adjacent to loading points) and central crack. (Enever et al. 2016)

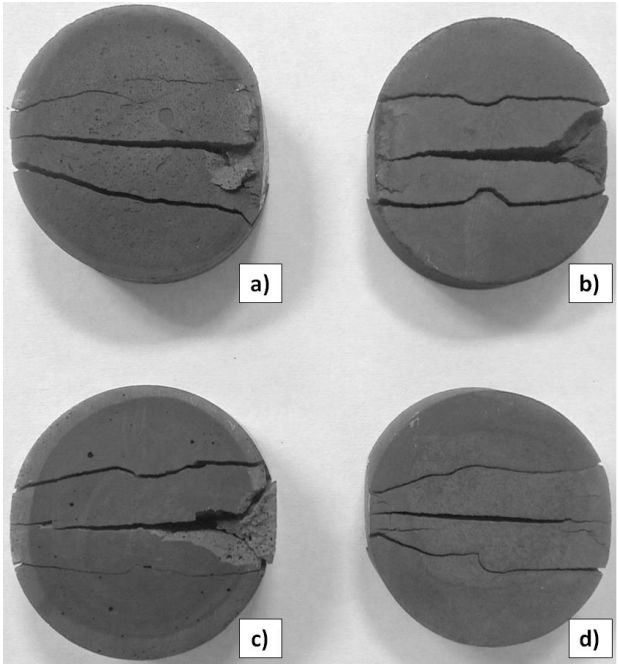

Figure 32 - Brazilian disk test samples after failure: a) 10wt%; b) 12wt%; c) 14wt%; d) 16wt% (compressive load in the direction of the cracks) (Enever et al. 2016)

The resulting geometrical, applied load at failure and calculated tensile strength information of the four samples can be seen in Table 8 below and the tensile strength results are graphically illustrated in Figure 33. (Enever et al. 2015)

Table 8 - Disc thickness, measured failure pressure and tensile strength data for powder-resin samples (Enever et al. 2015)

wt% Resin	10wt%	12wt%	14wt%	16wt%
Disc thickness (mm)	8.94	9.5	9.9	11.6
Measured Pressure (MPa)	3.8	4.1	6	6
Tensile strength (kPa)	446	478	688	685

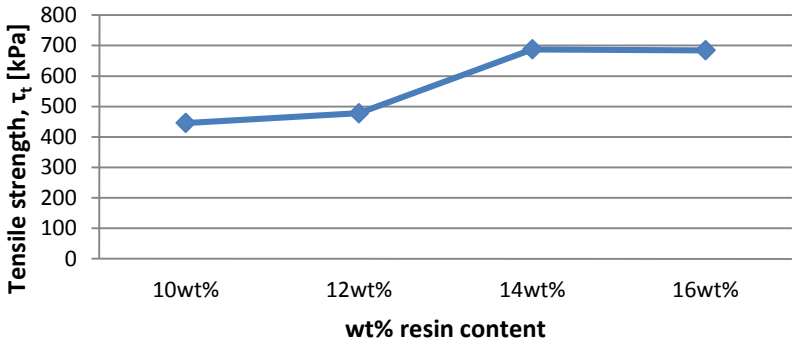

Figure 33 - Resulting tensile strength of powder-resin test samples (Enever et al. 2015)

From the data in Figure 33, it is decided to use the **12wt%** and **16wt%** resin ratios for experimental purposes. The 12wt% resin content was chosen because of its low resin content and being marginally stronger than the 10wt% resin content. The low resin content will ensure that the abrasive particles are able to grind the workpiece material effectively without the resin "getting in the way" and prohibiting optimal grinding. The 12wt% resin content sample is relatively easily mixable and mouldable, adding to the decision to use it.

The 16wt% resin content was chosen mainly for its strength, but also for its internal structure. The internal structure of this sample produced air bubbles, caused by the resin expelling gas during curing. This sample has enough resin to capture these air bubbles, whereas the lower wt% resin samples does not have enough resin to capture the air bubbles, but releases them during the curing process. The air bubbles, or voids, are needed in a grinding wheel to help with cooling of the wheel during operation as well as to aid in the removal of grinding swarf.

The 16wt% resin content sample is easily mixable and mouldable due to its higher resin content. The higher resin content is a trade-off that is accepted for the induced air bubbles that are created. The amount of resin is still low enough to allow for good grinding characteristics of the abrasive particles and will be analysed during the experiments. A microscope photograph of the internal structures of the two samples can be seen in Figure 34 below.

Notice the difference in internal structures of the two samples and the air bubbles or voids on the right in the 16wt% resin content sample.

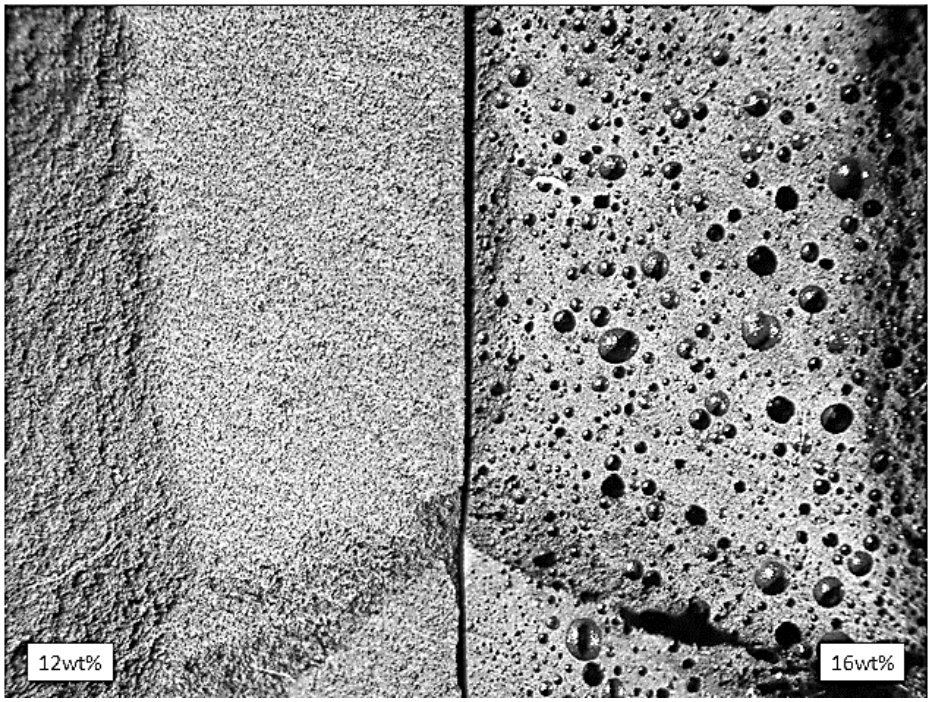

Figure 34 - Comparison of the 12wt% and 16wt% resin content samples (Enever et al. 2016)

3.1.5) Production of mounted points

The mounted points have specific dimensions to which they are constrained. In order to achieve these dimensions, the mounted points were produced in a mould that conformed to these dimensions. For experimentation, the mounted points are cast around spindles that serve as the central shaft of the mounted point and transfer the rotational energy to the mounted point. The spindle is designed in such a way as to allow for maximum grip of the resin-powder mixture during grinding operations and is produced from stainless steel. The design of the spindle can be seen in Figure 35.

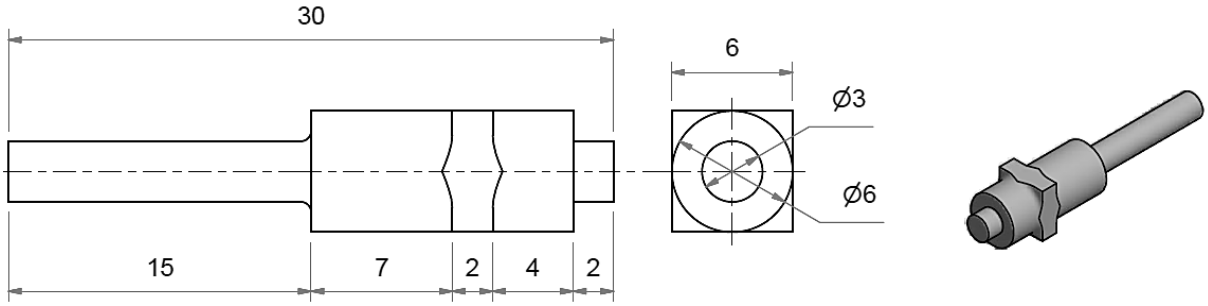

Figure 35 - Mounted point spindle design (dimensions in mm)

The spindles have a short 2mm protruding end which is intended to centre the spindle in the mould. This protruding end is inserted in a centring/aligning hole situated on the base plate of the mould. The base plate (see Figure 36) is bolted to the main body of the mould, which has nine equally spaced Ø20mm diameter holes serving as individual mounted point moulds (see Figure 37). The centre line of the holes in the main mould body and the base plate are aligned to high tolerances, in order to ensure the produced mounted points are balanced along its axis of rotation. To ensure the top part of the spindle also stays centre, an end cap with a hole drilled through it is placed over the spindle. The base plate, main mould body and end cap design can be seen in Figure 36 to Figure 38.

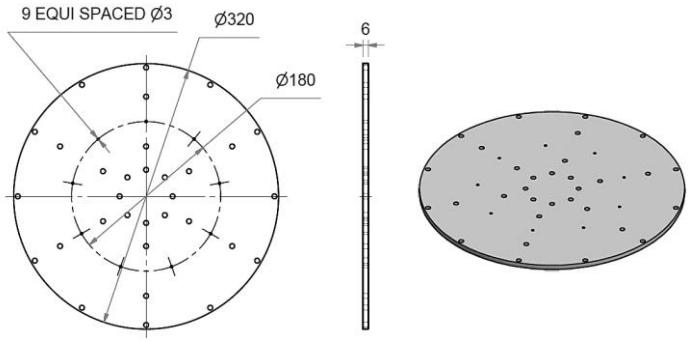

Figure 36 - Mould base plate design

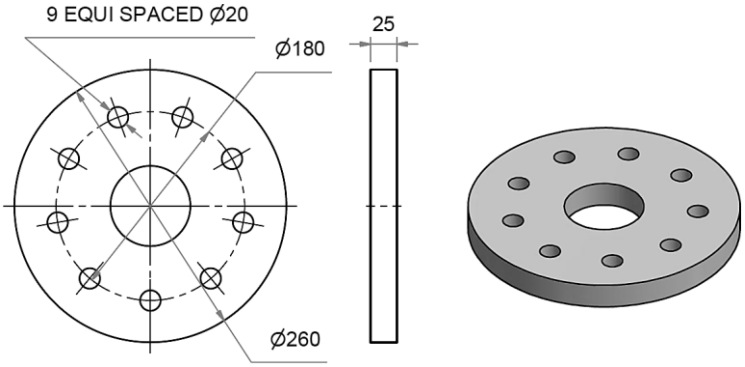

Figure 37 - Main mould body design

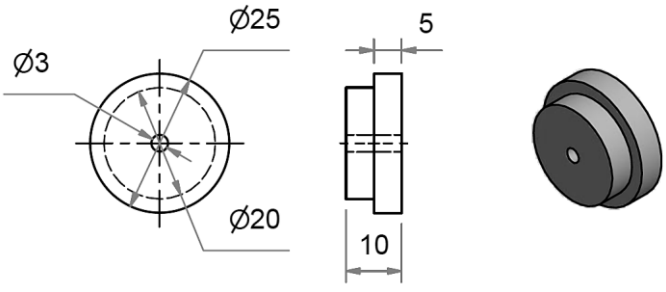

Figure 38 - Mould centring end cap design

In the design drawings of the main mould body and base plate, some features do not have any dimensional annotations. This is due to these two parts being repurposed parts from a previous project. The complete engineering drawings for all parts can be seen in Addendum B and the mould assembly can be seen in Figure 39.

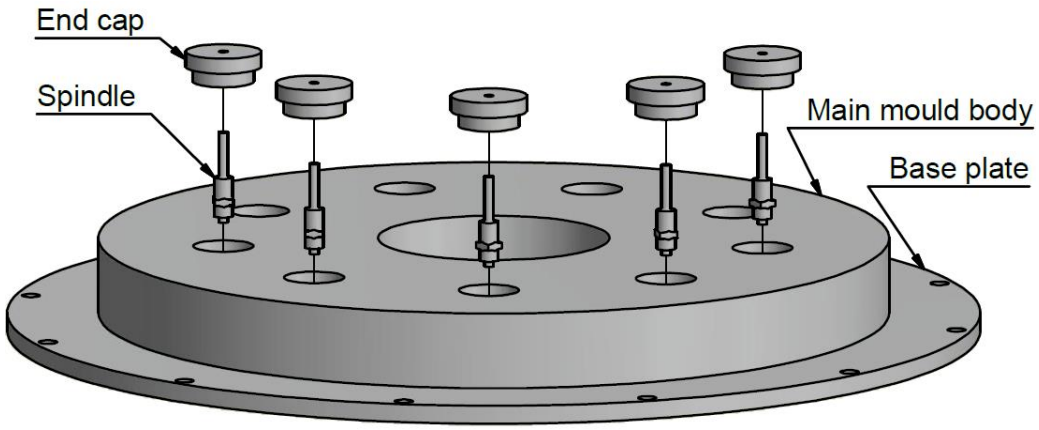

Figure 39 - Mounted point mould assembly (Enever et al. 2016)

The process of producing the custom mounted points is time consuming and requires as much precision as possible in order to ensure consistency throughout. The first phase in the production of mounted points was to prepare the mould. This was done by giving the mould a light sanding with very fine sanding paper to remove possible dirt, followed by cleaning with alcohol to remove oiliness. The mould could then be coated with a non-stick release agent (such as the Airtech Safelease30 release agent from Aerontec resin suppliers) that allowed the finished mounted points to be easily removed. The non-stick coating was left to dry completely for about 15 minutes after which the main mould body and base plate were bolted together. It was important to not cover the spindles in the non-stick coating as this would defeat the purpose of obtaining a good bond between the resin-abrasive mix and the spindle. The spindles were cleaned with alcohol before use to remove any oil and/or dirt.

The next phase was to prepare the resin and abrasive powder composite and to mould this composite mixture. The resin and powder is mixed in their specific quantities to produce a mixture with either a 12wt% or 16wt% resin content. These mixtures are thoroughly mixed to ensure all abrasive powder particles are covered with resin and that the resin is distributed evenly. The spindles are then inserted into the guide holes in the base plate and the resin-abrasive composite mix is dispensed in the produced cavity between the base plate, main mould body and spindles. The mixture is filled up to the top of the 6mm diameter part of the

spindle, causing the height of the mixture to be 13mm as the design suggests. The end caps are placed over the spindles to ensure the axis of the spindle is centred and aligned with the axis of the hole in the main mould body. A cross sectional view of this setup can be seen in Figure 40.

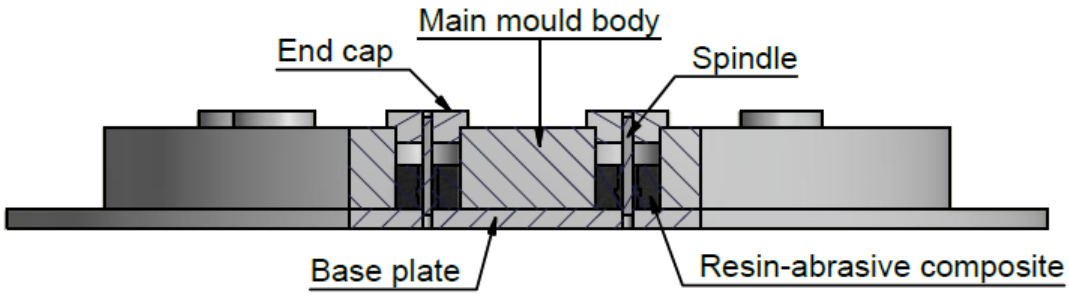

Figure 40 - Cross section of resin-abrasive composite mix in mounted point mould (Enever et al. 2016)

The resin-abrasive composite mix is left to cure at ambient room temperature for a minimum of 12 hours, similarly to the strength test samples. After this initial curing stage, the entire mould is placed in a hot box resin curing oven to thermally treat the resin so that it can attain its full mechanical strength. The thermal curing process takes place at different temperatures for different time intervals, as suggested by the resin manufacturer. These intervals and temperatures are as follows: 2 hours at 80^{o}C, 3 hours at 150^{o}C and 4 hours at 180^{o}C. The hot box is switched off after the 9 hour period and the mould left inside to slowly cool down to ambient room temperature to avoid thermal shock.

The shrinkage of the resin-abrasive mixture during curing is limited due to the high WC-12wt%Co powder content, as such the final cured dimensions are similar to the mould. The mounted points can then be removed from the mould and are ready to be machined with. Figure 41 shows the finished mounted points.

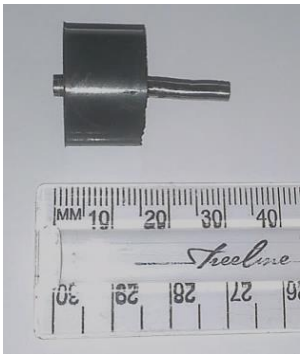

Figure 41 - Cured mounted point

3.2) Experimentation

3.2.1) Experimental design

To determine the performance of the mounted points, they are subjected to grinding experiments and their performance measured. The grinding is done by rotating the mounted point and controlling its x,y,z-axis movement with a micro-CNC machine. The mounted point is then moved along the face of the workpiece material at a specified interference depth, which would cause it to abrasively remove material from the workpiece. An illustration of the movement path of the mounted points is shown in Figure 42.

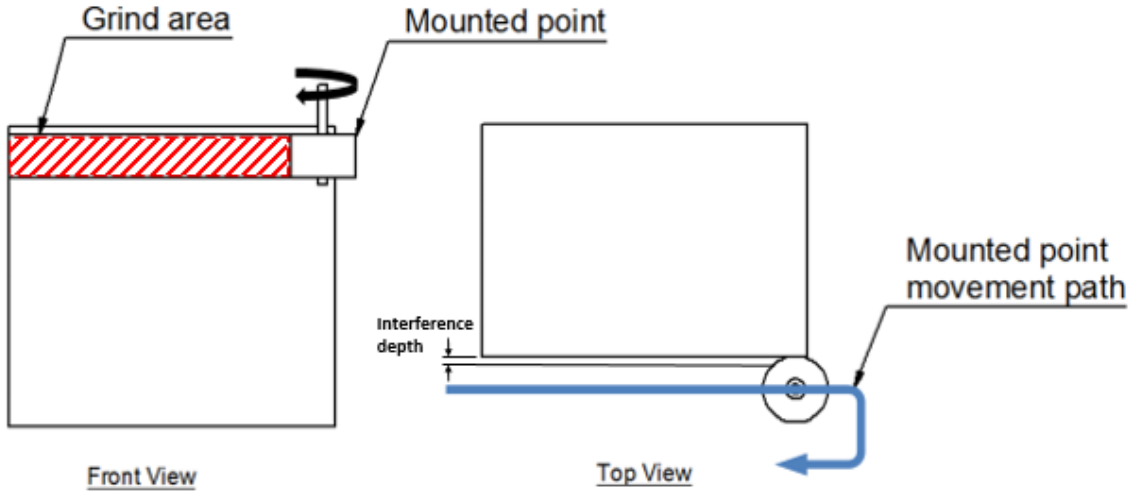

Figure 42 - Mounted point movement path with respect to workpiece

The grinding process, as described earlier, has many variables that will affect the effective working of a grinding wheel. For this reason, some variables will be changed for different experimental runs and the effects measured, while other variables are kept constant throughout. Only two variables are chosen that will be changed; spindle rotational speed and transverse feedrate. The only other variable which changes during experimentation is the resin content, which is either 12wt% or 16wt%. The spindle speed is varied between 15 000 and 20 000 RPM and the feedrate is varied between 30 and 90mm/min.

This means that nine experimental runs combining different spindle speeds and feedrates need to be conducted for each resin content value. For the 18 combinations of variables, a new mounted point is used for each test to ensure each set starts with the same initial mounted point geometrical conditions. For statistical reasons, three grinding runs were conducted per set of test variables. Thus, 54 experimental grinding runs were conducted in total. The

variable combinations are randomized and assigned a number and tests are executed in numerical order. This randomized order is shown in Table 9.

Table 9 - Randomized execution order for mounted point experiments

Execution #	Spindle speed (RPM)	Feedrate (mm/min)	
1	20 000	30	
2	20 000	90	
3	17 500	30	
4	17 500	90	
5	15 000	60	12wt%
6	15 000	30	
7	17 500	60	
8	20 000	60	
9	15 000	90	
10	17 500	30	
11	17 500	60	
12	15 000	30	
13	17 500	90	
14	20 000	30	16wt%
15	15 000	90	
16	20 000	60	
17	20 000	90	
18	15 000	60	

The variables that were kept constant are depth of cut, abrasive particle size and applied grinding power. The depth of cut will be 100µm for every grinding run with respect to the previous run. That means that from a surface reference point, the first run will have a depth of cut of 100µm, the second run will have a depth of cut of 200µm and the third run will have a 300µm depth of cut. The three cutting depths per mounted point are illustrated in Figure 43.

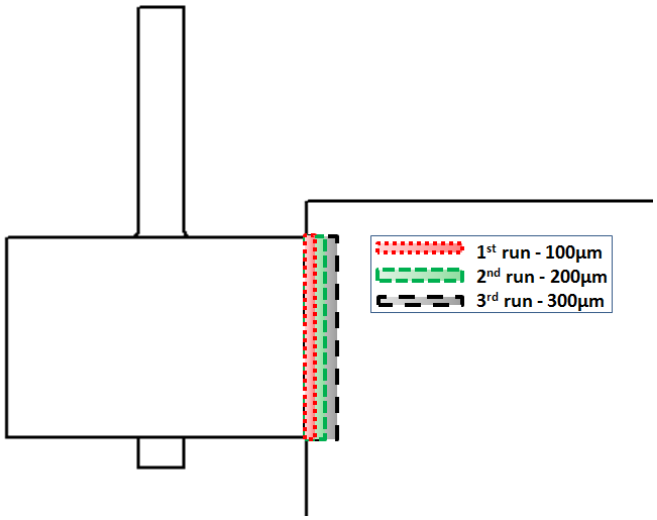

Figure 43 - Cutting depth per grinding run (exaggerated view)

With the depth of cut being kept constant with respect to the ground surface, the applied perpendicular grinding force was also kept constant. The transverse grinding force will vary with and depend on every combination of spindle speed and transverse feedrate. The abrasive particle size can also affect the performance of the mounted points, but is not varied since the WC-12wt%Co powder being used to produce all mounted points has its origin from the same batch of powder. The applied grinding power is also constant as the machine used does not have the capability of varying its power consumption. This will affect the rotational speed of the machine when it encounters some form of resistance. There are however machines that have the ability to vary power consumption to regulate rotational speed as resistive loads increase, but these machines were not available for this study.

The rotational direction of the mounted point, with respect to the direction in which the mounted point moves, is specifically chosen to produce an up-grinding process. The up-grinding process requires less grinding energy to remove workpiece material and is a more suitable grinding method for finishing processes. The Ti6Al4V workpiece has the dimensions as shown in Figure 44 which also shows the location of the grinding paths.

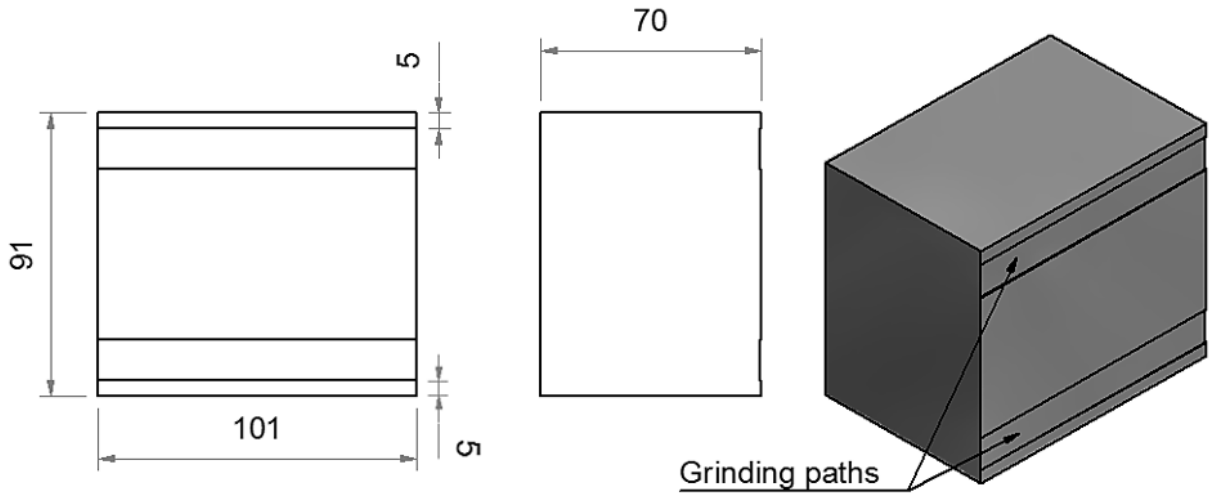

Figure 44 - Workpiece dimensions and locations of grinding paths

The performance of the mounted points is characterized by their rate of wear during grinding and the workpiece surface integrity and finish due to the grinding process. The wear of the mounted points will be an indicator to the rate at which the mounted points lose abrasive material. When all material is lost, grinding cannot be done with the mounted point and thus a replacement is needed. The rate of wear can then also be an economic indicator to the suitability of use of WC-12wt%Co as abrasive material.

The surface integrity of the workpiece is an indicator of the influence of the grinding process on the workpiece. This is determined by the induced stresses on the surface due to the rise in temperature during grinding and the applied perpendicular grinding force. The quality of surface finish is an indication of the abrasive particles being uniformly distributed within the resin matrix and their uniform material removal. It is thus an indication of the appropriateness of the abrasive particle size for the intended and required surface finish. As a result, the parameters that will be measured to determine the effectiveness and performance of the mounted points are the wear of the mounted points and the surface finish and surface hardness of the workpiece.

3.2.2) Experimental equipment and setup

The machine used to provide the rotational power to the mounted points is a Dremel 4000 high performance rotary tool, and is shown in Figure 45. It has variable speed control of 5 000 - 35 000 RPM and has a rated power consumption of 175W.

Figure 45 - Dremel 4000 high performance multi-tool

Due to the design of the Dremel, it is mounted vertically to allow for grinding along the horizontal plane. To control the movement of the rotating mounted points in the x,y,z-planes, an in-house custom manufactured Computer Numerical Control (CNC) machine is used onto which the Dremel is securely fixed. The CNC machine has the ability to move the Dremel much further in distance than the geometrical size of the workpiece and is thus suitable for use. The movement is controlled by stepper motors having a resolution of 2µm, hence the process being called micro-grinding (or micro-machining). This is well within the limits required to ensure accurate positional control of the mounted point's movement.

The CNC machine is controlled with a standard desktop computer that has specific software installed on it. The software used for controlling the CNC machine is Artsoft Mach3 v2.0. To control the CNC machine, the software makes use of machine code to interpret geometrical positioning as bits to control the stepper motors accurately. The machine code used to control the path the mounted point should follow to grind the titanium alloy at the correct depth and correct transverse feedrate is based on a reference point. This reference point is located at the top right backside of the titanium alloy workpiece. Figure 46 shows the reference point as viewed from the top with a clockwise rotational direction of the mounted point, a feed direction from right to left and the positive x- and y-axis as indicated. The positive z-axis is out of the page, while the negative z-axis is into the page. The machine code used to control the CNC machine can be seen in Figure 47.

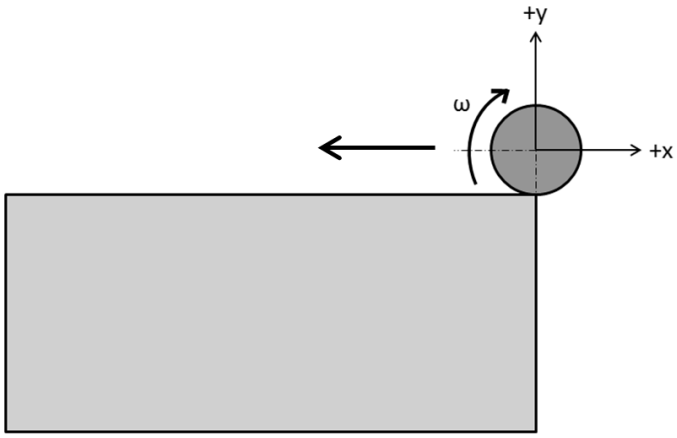

Figure 46 – Top view indicating the reference point position (Enever et al. 2016)

```
G90
G01 X0 Y0 Z0 F1100
G01 X0 Y30 Z0 F1100
G01 X0 Y30 Z-5 F1100
G01 X0 Y1 Z-5 F600
G01 X0 Y-0.1 Z-5 F80
G01 X-102 Y-0.1 Z-5 F60
G01 X-102 Y30 Z-5 F1100
G00 Z40

M30
%
```

Figure 47 - Machine code used to control mounted point movement path and speed (Enever et al. 2016)

From the code it can be interpreted that the mounted points grind 5mm below the top horizontal surface of the titanium workpiece (from the highlighted z-axis positional indication) also seen in Figure 42 and Figure 43. This is simply to ensure that there is material available on all sides of the mounted point to grind. The highlighted *y* and *F* parameters in the code indicate the depth of cut in the y-direction and the transverse feedrate. x, y and z positional indications are in mm and feedrate in mm/min.

During grinding, dust particles are produced as abrasive and binder material wear from the mounted points and titanium alloy particles are ground from the workpiece. This is a health and safety concern which needs addressing. The solution to this problem is the installation of an industrial vacuum system to remove as much ground material as possible from the immediate grinding area. As a secondary precaution, a ventilation system is used to continuously ventilate the air in the room where the experiments are carried out as to remove the remaining airborne dust particles.

The equipment used in the recording of mounted point wear data, is a Mitutoyo STRATO-Apex coordinate measurement machine (CMM). This machine measures positional coordinates to determine the geometry of objects with a resolution of up to 1µm. The surface hardness of the post-ground workpiece surface is measured with a micro hardness testing machine and works by optically measuring the size of an induced micro indentation. The surface roughness is measured with a Surftest SJ-210 surface roughness testing machine. It uses a stylus that is moved over the workpiece surface being tested to measure the vertical displacement of the stylus point. The data measuring equipment are further described in the *Data analysis* section.

For the experimental setup, the Dremel is securely fixed to the CNC machine with the mounted point securely fixed to the Dremel. The pipe of the industrial vacuum system is mounted as close to the mounted point as possible in order to vacuum the maximum amount of dust particles. The workpiece is positioned and clamped in place on the bed of the CNC machine. With the control software running, the mounted point is manually positioned to the reference point. The Dremel rotational speed is selected, switched on and the machine code executed at specified variable values as in Table 9. Figure 48 shows the Dremel, workpiece and vacuum setup, while Figure 49 shows the CNC machine and control computer setup.

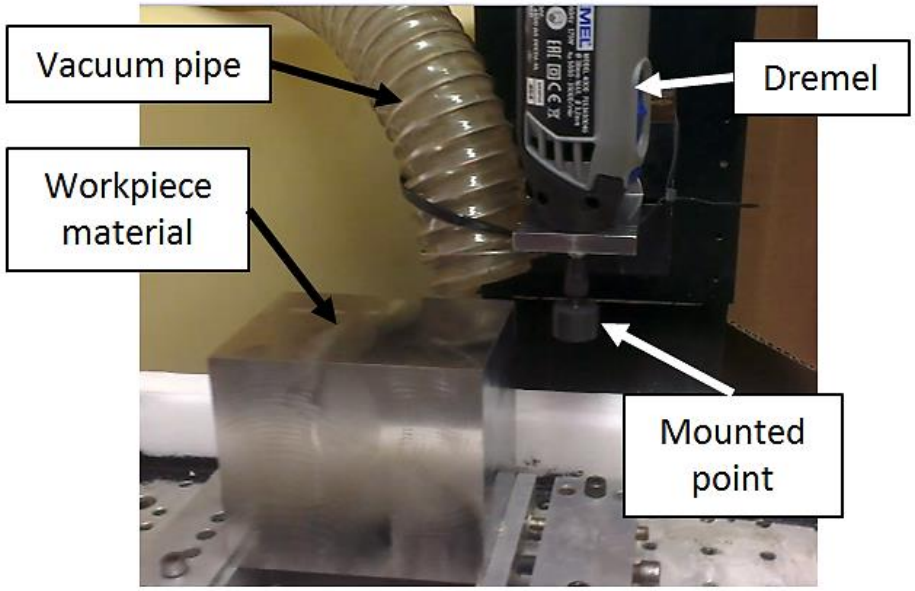

Figure 48 - Dremel, workpiece and vacuum system setup (Enever et al. 2016)

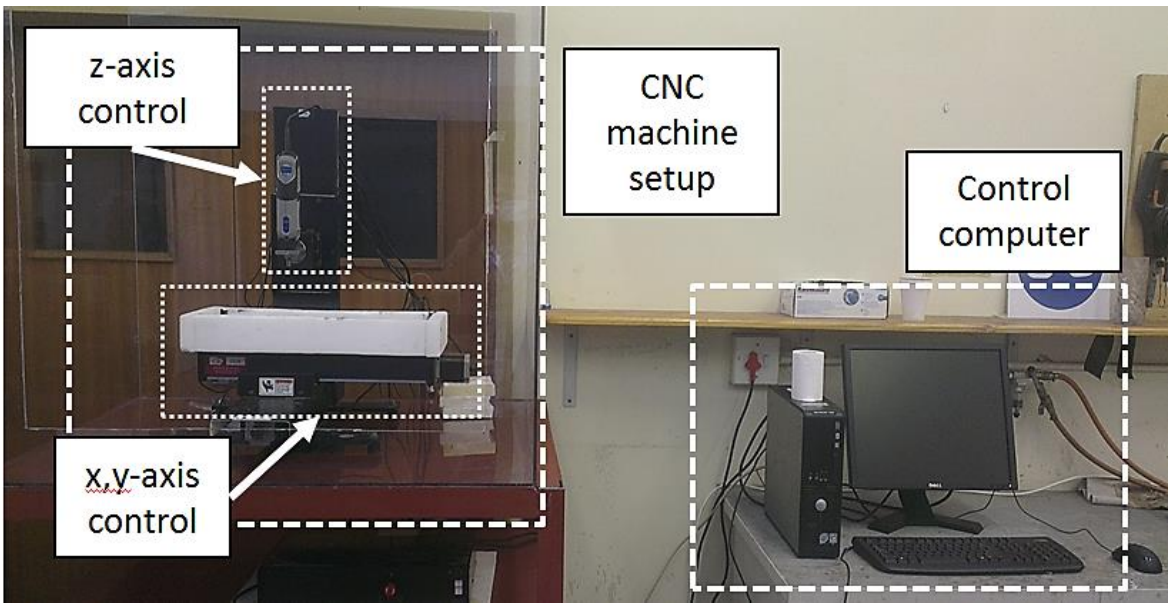

Figure 49 - CNC machine and control computer setup (Enever et al. 2016)

Since the workpiece has only four sides of 101mm in length, only eight experimental runs are executed before the workpiece needs to be cleaned with a milling machine. This is due to the maximum negative z-axis distance the experimental setup can reach before component interference occurs. This leads to the workpiece being cleaned twice in total to complete all eighteen experimental runs. Only the surfaces being ground are machined so as to keep the grinding distance constant at 101mm.

3.2.3) Ti6Al4V workpiece material analysis

The performance characteristics of the tungsten carbide mounted points are tested by grinding the titanium alloy Ti6Al4V. This alloy contains 6wt% aluminium, 4wt% vanadium and titanium constituting the rest. To analyse the alloy, a small test sample is cut from the main block of Ti6Al4V, mounted in a resin base and polished to a high degree. The section is then analysed by Electrodispersive Spectroscopy (EDS) by using a Scanning Electron Microscope (SEM) and the surface photographed with an Olympus GX51 optical microscope. An image acquired from the SEM/EDS is shown in Figure 50.

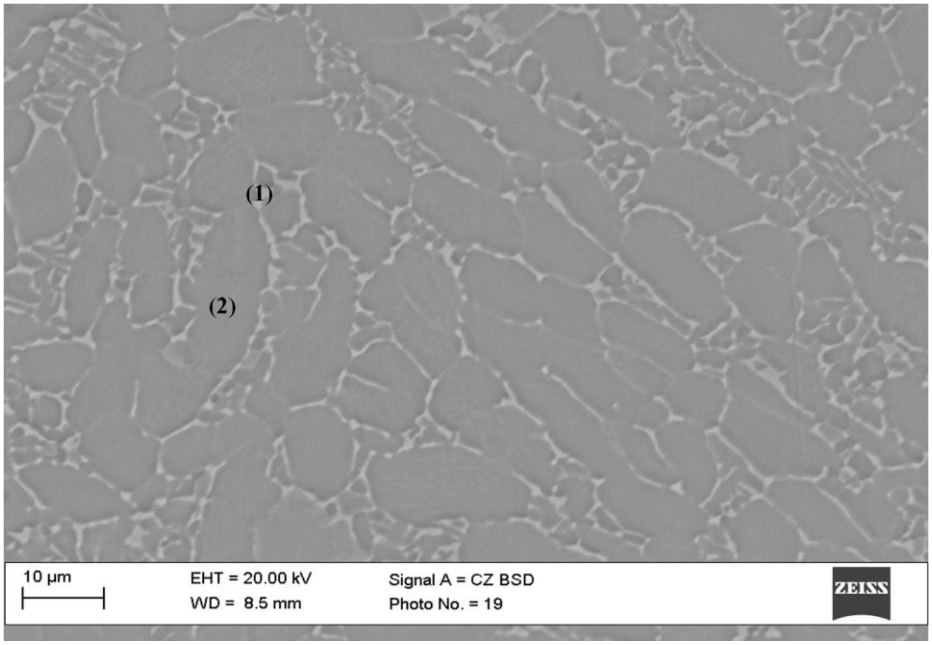

Figure 50 - SEM imaging of Ti6Al4V workpiece material (as-polished)

In the SEM image, there are two phases of the titanium alloy present. The lighter area resembling veins, denoted with the number (1), is the beta-phase, while the darker area resembling clusters or islands, denoted with the number (2), is the alpha-phase. The specific compositions of each phase can be seen in Table 10 below, which represents the information retrieved from the SEM/EDS analysis.

Table 10 - Ti6Al4V SEM/EDS analysis results (Donachie 2000)

Spectrum	Al (wt%)	V (wt%)	Ti (wt%)	Fe (wt%)	Total (wt%)
Lighter area (1)	4.2	10.2	84.7	0.8	100
Darker area (2)	7.2	1.7	91.1	0	100
Literature Ref. Values	6	4	89.7	0.3	100

In the lighter beta-phase area, the concentration of vanadium is much higher than in the darker alpha-phase area. This is an expected occurrence, because the vanadium is a beta-phase stabilizer. In the darker alpha-phase area, the concentration of aluminium is higher than in the lighter beta-phase area. This is once again expected, because of the alpha-phase stabilization characteristics of the aluminium. The analysis technique is however restricted to a resolution of $1\mu m^3$ and the composition of the alloy can thus not be taken as these values. The actual composition of the alloy is as indicated in Table 10 as obtained from literature.

For each phase of the alloy, the specific weight fraction of each alloying metal is inconsistent with the overall fractions of the alloy. The reason for this is the occurrence mentioned above.

To stabilize each phase, the specific alloying metal must bind into that phase, thus diffusing the alloying metals into uneven concentration densities. The weight fractions closer resemble the overall alloy weight fractions when the average weight fractions are calculated for each alloying metal.

In the composition of the lighter beta-phase, it can be seen that there are trace amounts of iron. This impurity in the alloy could be contributed to the manufacturing process. There will always be to some extent impurities mixed in together with the alloying metals. It is the responsibility of the quality controllers to ensure minimal contamination of alloys. For the tested sample, the amount of iron impurity is less than the amount specified in literature for this alloy and will thus not have any significant influence on any aspect of experimentation. The sample sent for SEM analysis was also photographed under a normal optical (Olympus GX51) microscope. The photo can be seen in Figure 51. (Donachie 2000)

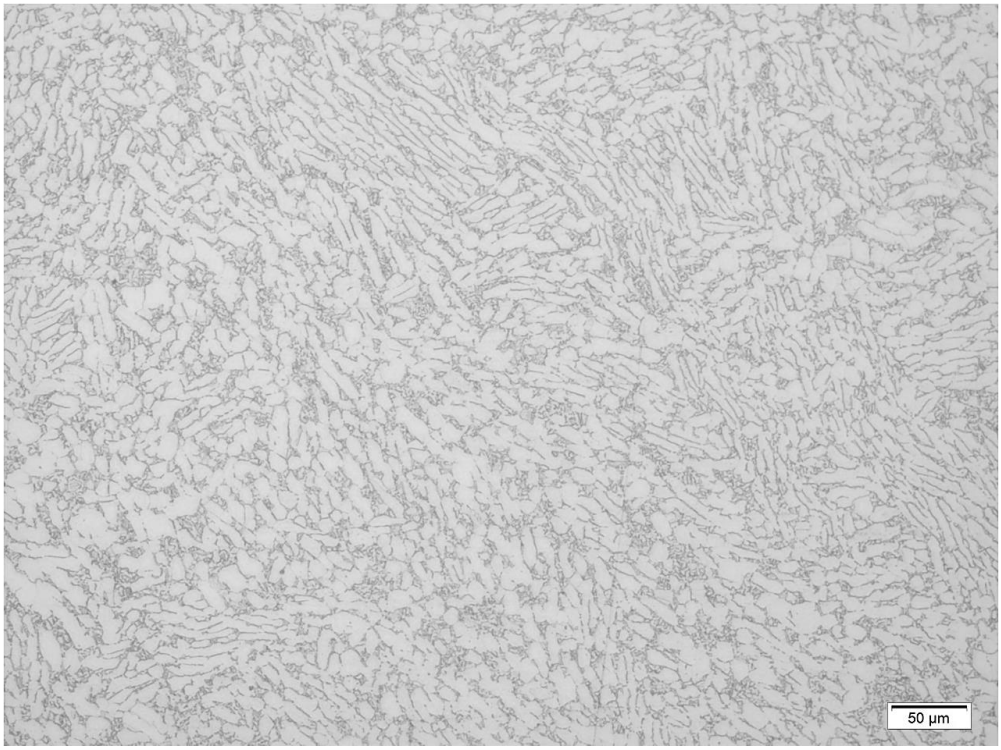

Figure 51 - 200x Magnification optical microscope image of Ti6Al4V

The surface was polished and etched with Kroll's solution. This image has inverted colours to that of the SEM image in Figure 50. This means that the darker areas are the beta-phase and the lighter areas are the alpha-phase. It could be noted that the alpha-phase areas are much larger in size. This is due to Ti6Al4V being closer to a pure alpha-phase alloy rather than a pure beta-phase alloy. Refer to Figure 24, the pseudo-binary phase diagram of titanium alloys, to locate the position of Ti6Al4V on this specific diagram.

3.2.4) Safety

Safety is the highest priority which should be pursued during execution of experiments since the mounted points do not have a safety speed rating and are rotating at high rotational velocities. For this reason, the entire CNC machine is placed in a Perspex box to prohibit any possibly created debris from doing damage to persons and property. The Perspex box is closed prior to the Dremel being switched on and is only opened again after the Dremel is switched off.

The experimental layout is also set up in such a manner that the mounted point moves along the back side of the workpiece between it and the CNC machine. This setup will also aid in deflecting debris from the grinding process away from the front side of the CNC machine where the operator is positioned. In addition to the special setup and Perspex safety box, the operator is to wear safety glasses during experimentation. For respiratory health issues, the vacuum and ventilation system is implemented as described earlier.

3.2.5) Pilot experiments

Pilot experiments were conducted with both 12wt% and 16wt% resin content mounted points. The purpose of the pilot experiment was to determine whether the specific setup works and if the custom mounted points are indeed able to grind the titanium alloy workpiece. For this initial experiment, the same setup parameters were used as described in the *Experimental design* section for the main experiments. The spindle speed and feedrate variables was only tested at a single setting, namely 20 000 RPM and 60mm/min. The depth of cut was kept at 100µm for consistency and eight machining runs were chosen for each mounted point. The wear of the two mounted points was less accurately measured with a Vernier calliper while the surface hardness and roughness was not measured.

The 12wt% resin content mounted point failed during its second run and could not produce any significant wear data. The 16wt% resin content mounted point persisted for all eight machining runs. Wear was determined by measuring the change in diameter and calculating the volume of the mounted point for each machining run. When compared with the initial diameter, the change in volume thus indicated the wear. The measurement of change in diameter and calculation of wear is better explained in the following section *Data analysis*. The two mounted points, after the pilot experiments were conducted, are shown in Figure 52 and the wear data in Figure 53.

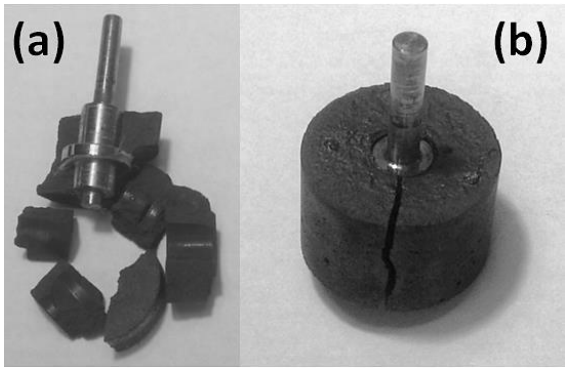

Figure 52 - Post pilot experimentation condition of the (a) 12wt% and (b) 16wt% mounted points (Enever et al. 2015)

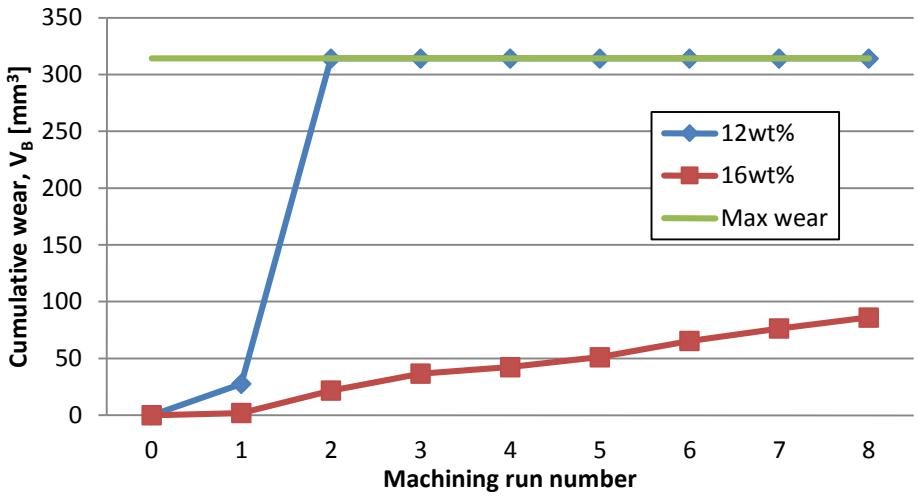

Figure 53 - Cumulative wear data of the pilot experiment mounted points (Enever et al. 2015)

The 12wt% resin content mounted point in Figure 52 experienced catastrophic failure and shattered into multiple pieces. The 16wt% resin content mounted point cracked at the end of its eighth grinding run, possibly due to overheating. The crack might have affected the wear results of the last data entry of this mounted point and should thus not be taken into account even though it is shown in Figure 53.

The data in Figure 53 shows the failure of the 12wt% resin content mounted point after its first grinding run (during its second grinding run) while the 16wt% resin content mounted point produced wear results up to its eighth grinding run. Wear rate of this mounted point was steady and did not exceed 100mm^3 of wear in the eight grinding runs. The green line indicating *maximum wear* is when the maximum volume of the mounted point is lost due to grinding wear and only the stainless steel spindle remains.

The grinding parameters used in the pilot experiment and those to be used for full scale experimentation equate to grinding peripheral speeds of roughly between 15 and 20m/s and workpiece speeds of between 0.03 and 0.09m/min. The peripheral speed is below the suggested 30 to 40 m/s for resin bonded grinding wheels, but will not be increased to these values due to excessive vibration and chatter of the mounted points as experienced during the pilot experiments. The workpiece speed is very low compared to what literature indicates, but this is due to this study investigating micro-grinding and thus low feed rates are used.

3.3) Data Analysis

A coordinate measurement machine (CMM) is used to accurately measure the geometry of the mounted points after grinding to determine the rate of wear. The CMM uses the coordinates of the object being measured to calculate and determine its geometry. In the case of the cylindrical mounted points the CMM probes around the mounted points in a circular pattern and uses a mathematical algorithm to calculate the dimensions of the circle. This concept can be utilized to determine the volume of the mounted point by two methods. The first is incremental circular segment volume calculation and the second is cylindrical volume estimation.

The incremental circular segment volume calculation method measures points around the mounted point's circumference and calculates an average diameter of a circle that fits the coordinate points. This process is repeated at 0.5mm increments along the height of the mounted point. By calculating the volume for each section of measured circle of 0.5mm height and summing the volumes of all sections, an average volume for the mounted point can be determined.

The cylindrical volume estimation method measures coordinate points in a circular pattern around the mounted point and along its height. A mathematical algorithm then calculates an average cylinder that would fit the measured coordinate points and produces its volume as one of the outputs. Both of these methods are used for determining the volume of the mounted point after each grinding run. It thus becomes apparent that the measurement process is time consuming.

The surface roughness of the workpiece, after the three grinding runs have been executed, is measured with a Mitutoya surface roughness tester. It measures the peaks and valleys created by abrasive grains as they pass over and grind the workpiece surface. These peaks and valleys are on the micron scale and thus a stylus with micrometer dimensions is used. The stylus measures the deflection due to the peaks and valleys and an average surface roughness, R_a, is calculated from this data.

The roughness of the workpiece surface is measured at the end of the three grinding runs of each mounted point. The direction of measurement is perpendicular and parallel to the grinding direction. For each ground area, the R_a value is measured at multiple points and an average R_a value is calculated for the post-grinding surface. This value is compared to the unground workpiece surface R_a average value measured on the same surface of the workpiece. The roughness of the post- ground surface should be less than the unground surface. The positions of measuring and measuring directions are shown in Figure 54.

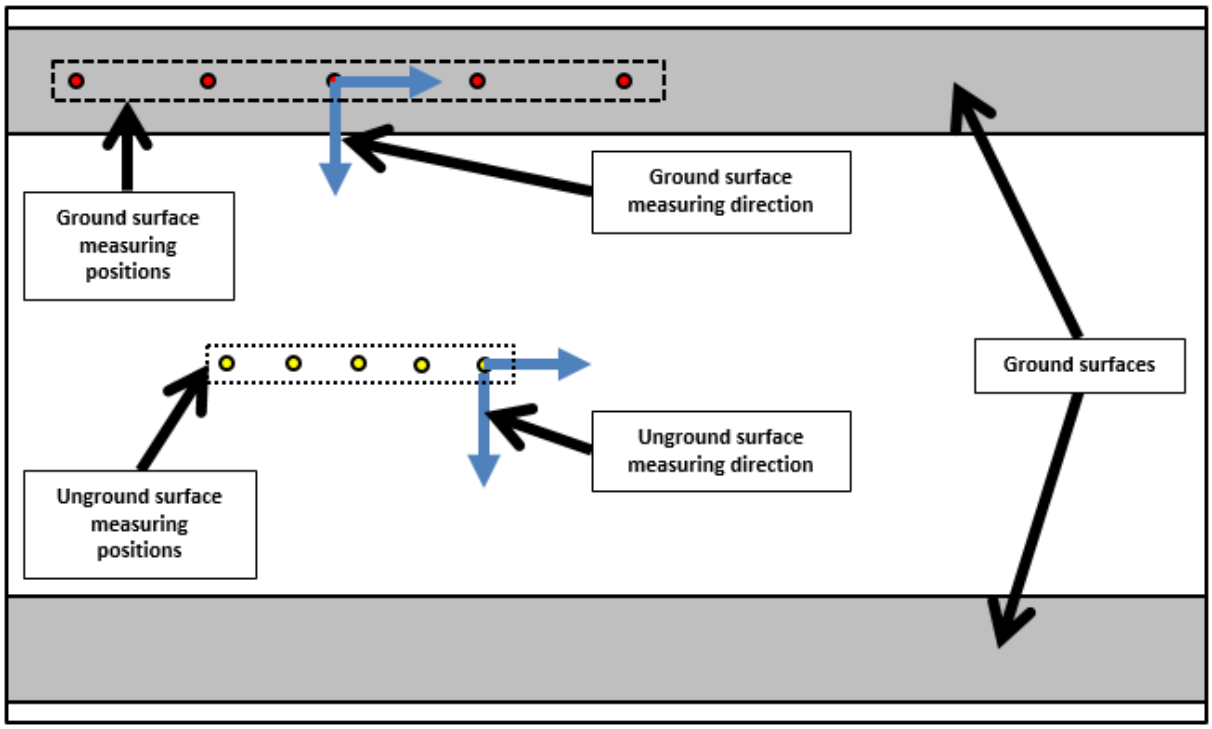

Figure 54 - Location and direction of surface roughness measurements taken which was produced by each mounted point after grinding (top view)

The surface hardness of the post-ground workpiece surface is measured with a Struers DuraScan Vickers micro-hardness tester under an indentation load of 1kg. This device calculates the surface hardness based on the size of an indentation made on the surface with a

synthetic diamond with known geometrical dimensions and applied load. The hardness of the ground and unground surfaces is measured at multiple positions and an average hardness calculated.

It is expected that the surface hardness of the workpiece should be greater after grinding than prior to grinding. This is due to the work hardening that takes place during grinding which is in turn caused by the grinding forces and elevated temperatures. The grinding forces and elevated temperatures also cause residual stresses to be induced on the workpiece surface, leading to the higher surface hardness. For critical parts it is important that post grinding material treatments are carried out to relieve the residual stresses and to remove some of the work hardening. The locations of surface hardness measurements are shown in Figure 55.

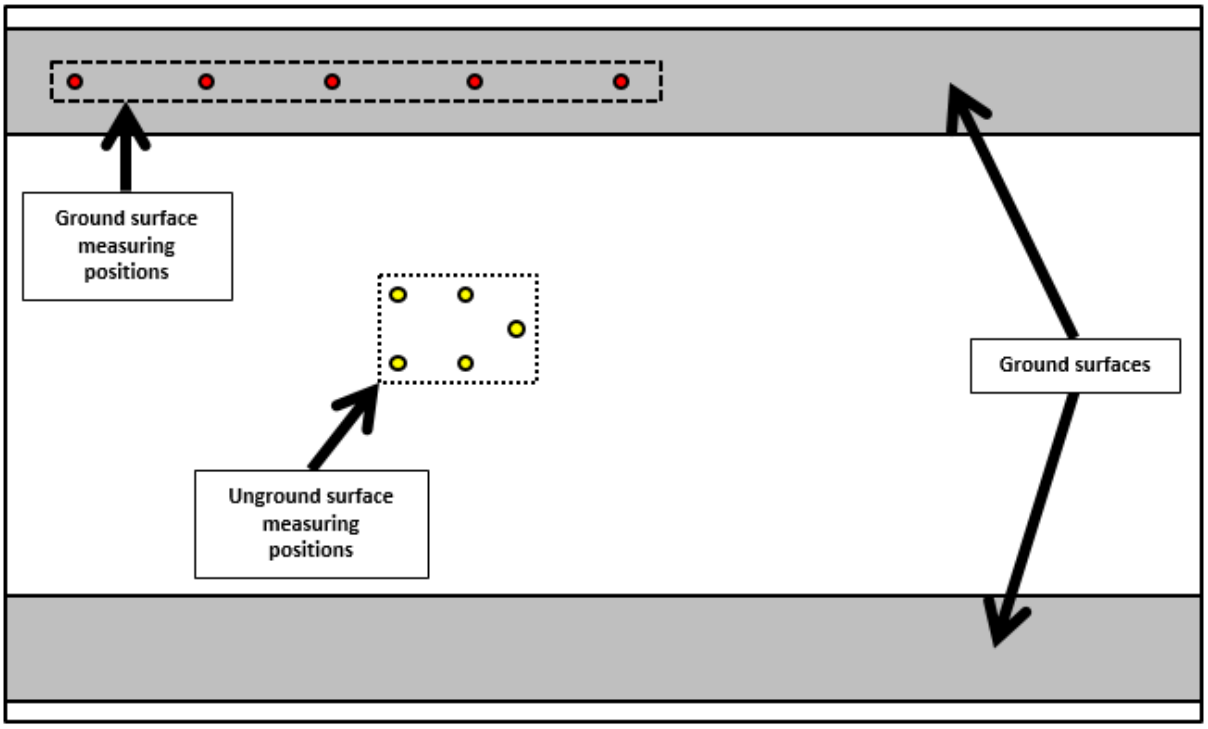

Figure 55 - Locations of surface hardness measurements taken which was produced by each mounted point after grinding (top view)

4) Experimental Results and Discussion

During experimentation to determine the performance of mounted point grinding wheels containing WC-12wt%Co as abrasive medium, three out of eighteen mounted points failed catastrophically. Two of the three mounted points failed during the first grinding run, after some grinding was done, and did not produce any measurable wear results. The surface roughness and work hardening effect due to grinding could, however, be measured on the areas that were ground prior to mounted point failure. The third mounted point failed during its third grinding run. It was thus able to produce measurable wear results as well as surface roughness and hardness measurements. It is important to mention that these three failed mounted points contained 12wt% resin.

The wear measurements were done with two methods (as mentioned in the section *Data analysis*), incremental circular segment volume calculation and cylindrical volume estimation, which produced slightly different wear results for most of the mounted points. The wear results from the two measurement methods are shown in Figure 56 and Figure 57. Figure 56 shows the wear measurements for the mounted points containing 12wt% resin and Figure 57 shows the data for the 16wt% resin content mounted points.

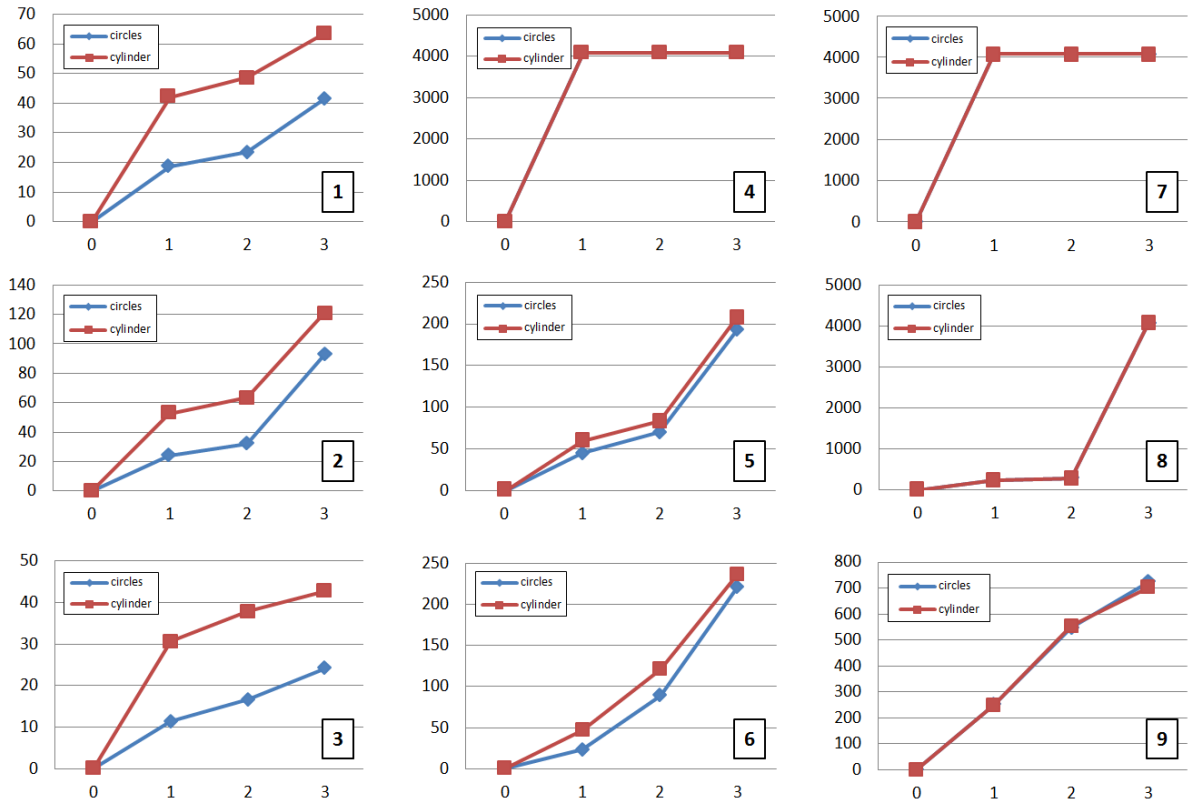

Figure 56 - Wear measurement data comparison for 12wt% resin content mounted points. Vertical axis indicates volumetric wear, horizontal axis indicates grinding run number and figure numbers represent corresponding mounted point numbers (see Table 9).

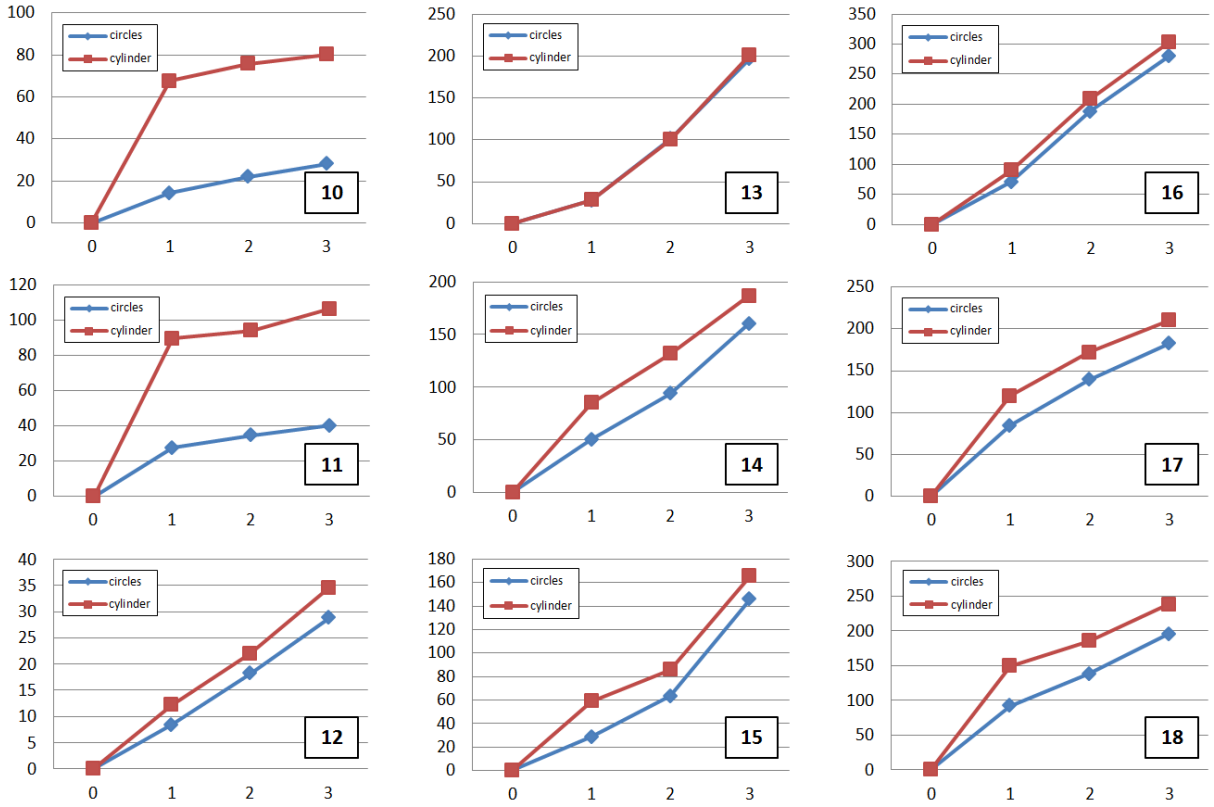

Figure 57 - Wear measurement data comparison for 16wt% resin content mounted points. Vertical axis indicates volumetric wear, horizontal axis indicates grinding run number and figure numbers represent corresponding mounted point numbers (see Table 9)

In Figure 56 and Figure 57, the red lines indicate the mounted point volumetric wear estimated with the cylindrical volume estimation method, while the blue lines indicate the mounted point volumetric wear with the incremental circular segment volume calculation method. The wear curves calculated in the graphs in the two figures show that the shape of the curves for both estimation methods match, but has for some mounted points a large offset value. For most of the wear data curves the two methods produced very similar, if not exactly the same, wear data. Since the incremental circular segment volume calculation method uses smaller increments to more accurately calculate the wear, its data will be used to represent the wear of the mounted points.

The wear data of the mounted points are represented in terms of grinding runs. This can also be converted into distance ground as the grinding distance for every grinding run stays constant. The wear of all mounted points cannot be represented on a single graph in terms of grinding time, since the transverse feedrate is not the same for each mounted point. The wear of corresponding feedrates can however be compared to each other on a single graph, but not

shown here. Figure 58 and Figure 59 show the complete wear data for the 12wt% and 16wt% resin content mounted points respectively.

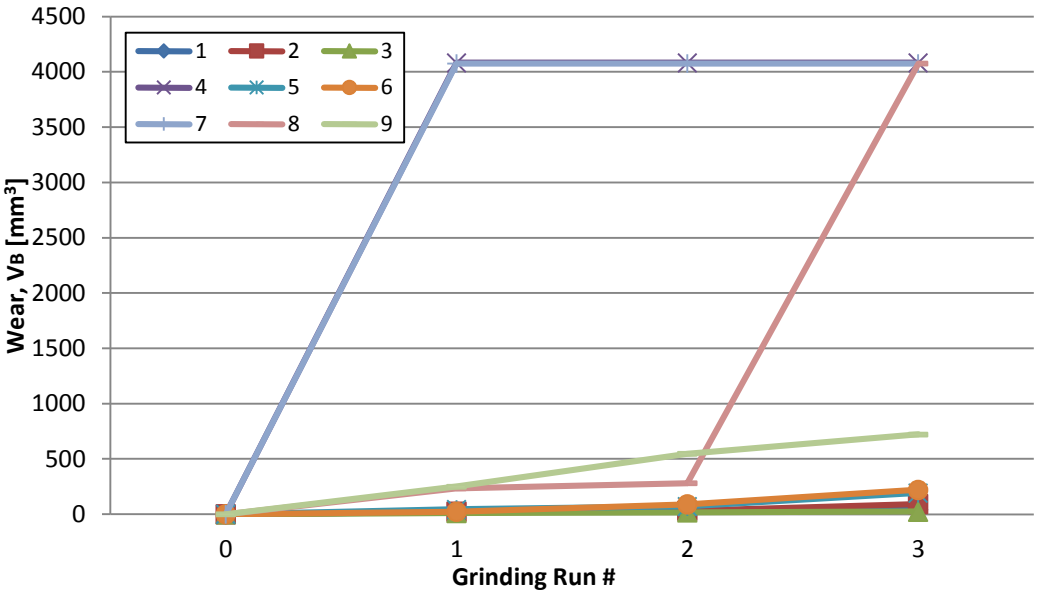

Figure 58 - Cumulative wear data of the 12wt% resin content mounted points

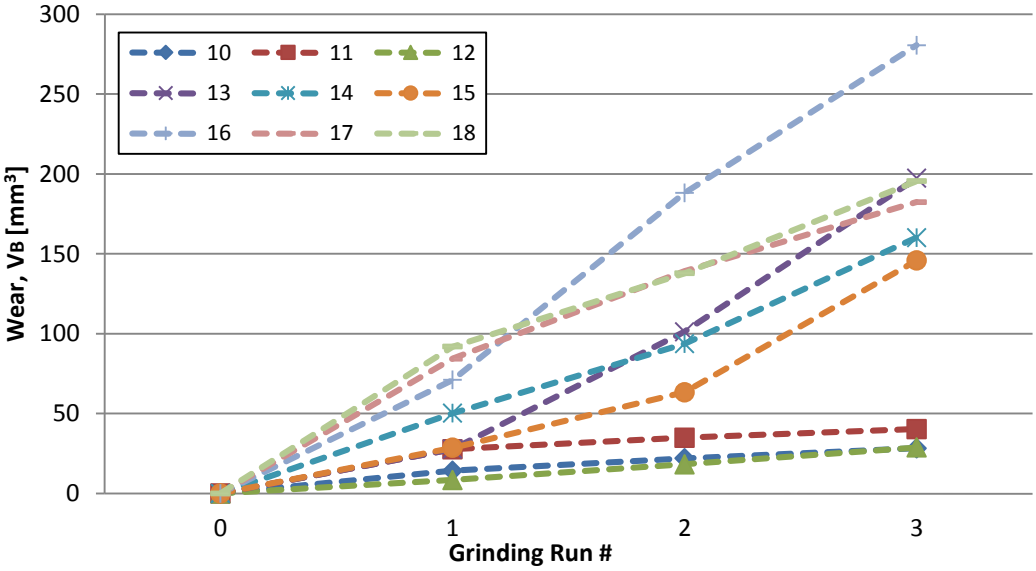

Figure 59 - Cumulative wear data of the 16wt% resin content mounted points

The failed mounted points can be seen in Figure 58 (as well as in Figure 56) to be number 4, 7 and 8, with number 8 failing during its final grinding run. The maximum wear the mounted points could reach (just over 4000mm^3), is the total volume of the mounted point. Figure 60 is the adapted graph of Figure 58 where the failed mounted point data is not included. These failed mounted points could be seen as 'flukes' and their wear data considered as outliers and are thus not used further on.

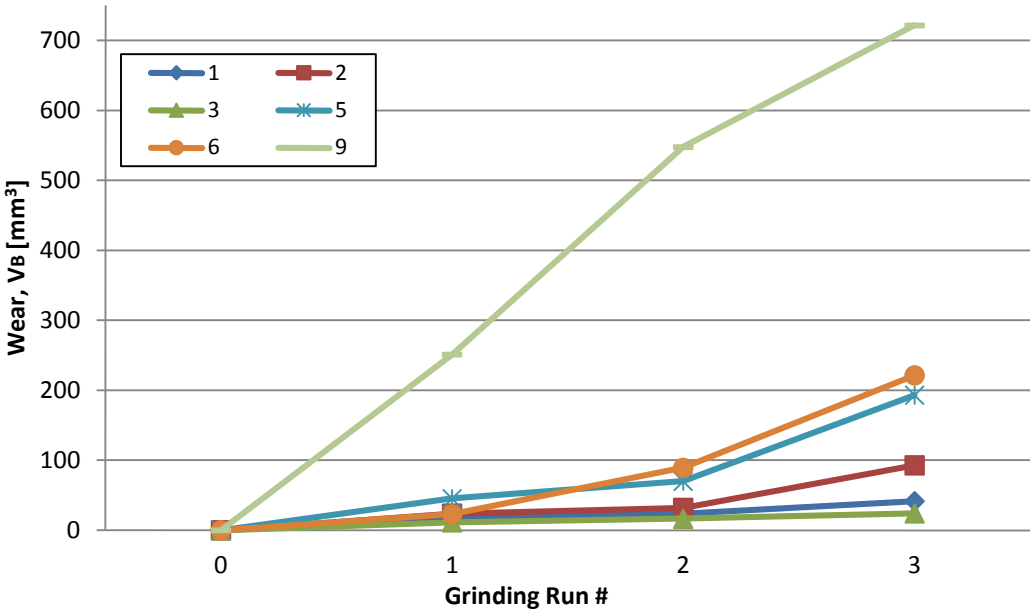

Figure 60 - Cumulative wear data of non-failed 12wt% resin content mounted points

The wear of most of the mounted points is not more than 200mm^3 after three grinding runs. With the exception of the three failed mounted points, only three mounted points had wear of more than 200mm^3. The rate of wear is gradual and consistent and future wear can be predicted without too much effort. Figure 61 shows the combined wear data of all mounted points.

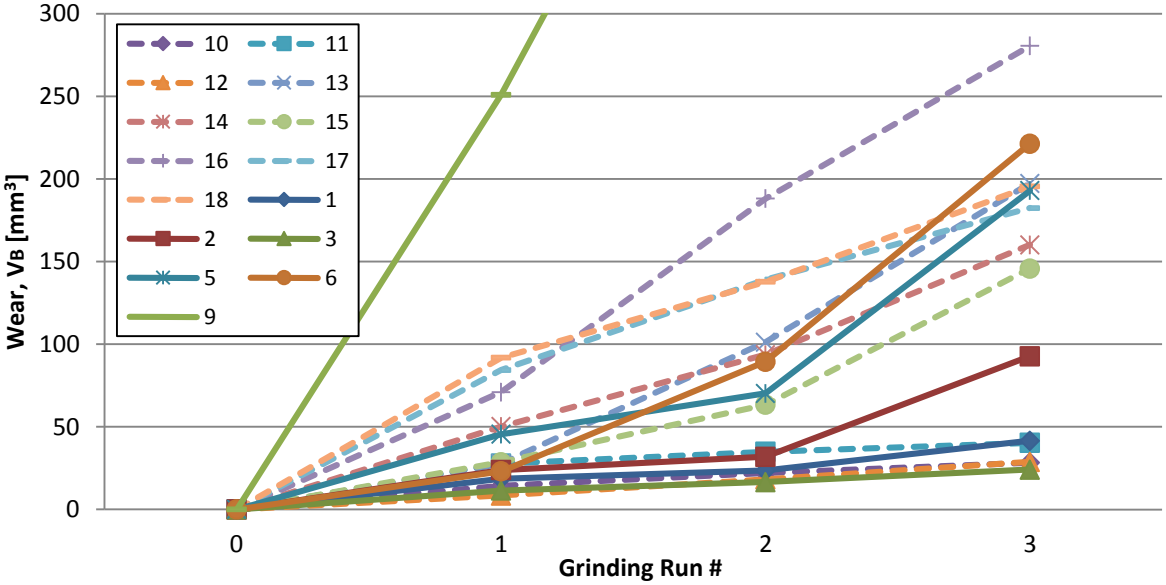

Figure 61 - Combined wear data for both 12wt% and 16wt% resin content mounted points

Mounted points having wear of greater than 300mm^3 are not shown in Figure 61 for comparison purposes between the wear of the 12wt% and 16wt% resin content mounted points. To clarify, each data point in the graphs depicting mounted point wear represents a single experimental test. There should thus be 54 data points in total between Figure 58 and Figure 59, and Figure 61 contains 45 data points. It is interesting to note that after the third grinding run there seems to be a spike in the wear rate of most of the 12wt% resin content mounted points. This might be explained by workpiece strain hardening during grinding, but cannot be the final conclusion from the available data and further testing should be conducted. It is expected that when each test is repeated, the wear graphs of corresponding parameters should match up.

The purpose and design of the mounted points are to remove a small amount of workpiece material in a micro grinding process and produce a smooth, but not polished, surface. The surface roughness of the workpiece should be less after grinding has taken place than before the surface was ground. The surface roughness measurement data is shown in Figure 62.

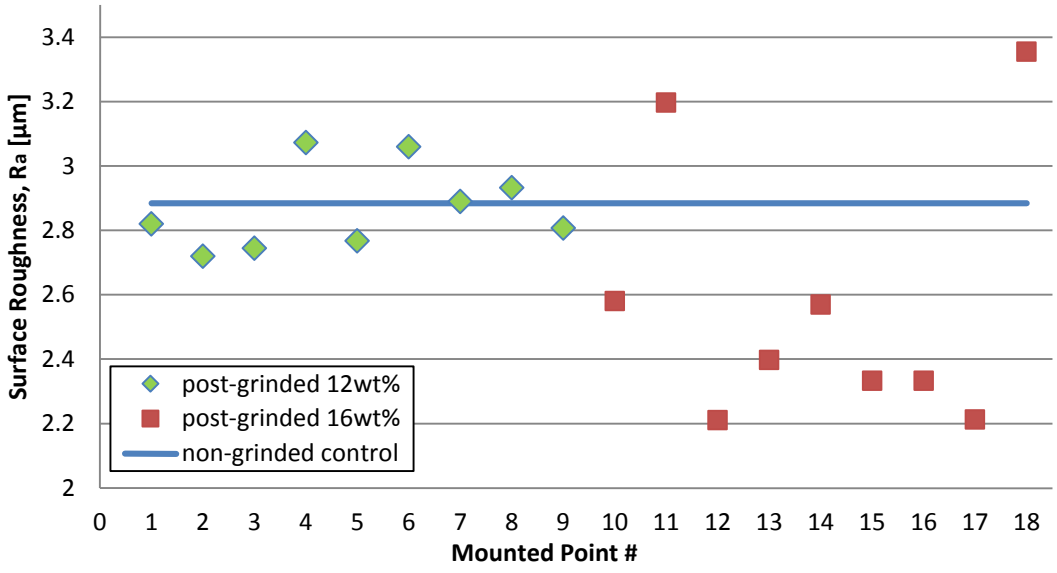

Figure 62 - Surface roughness measurement data of the post-ground workpiece surface (as measured after the 3rd grinding run)

As mentioned earlier, the surface roughness measurements were taken after the third grinding run of each mounted point. From the data in Figure 62 it is clear that most spindle speed to feedrate combinations produced a better and smoother surface finish for both 12wt% and 16wt% resin content mounted points. The 16wt% resin content mounted points produced overall a smoother surface finish than the 12wt% resin content mounted points. The reason

might be due to more resin being present in the mounted points that does not specifically grind, but helps polish the ground surface. This could be either advantageous or disadvantageous, depending on the intended application of the mounted points. The effects of resin content should thus be considered in future studies.

In total, 66% of the mounted points produced a smoother workpiece surface roughness. The blue line in Figure 62 is the average surface roughness of the workpiece on areas where grinding was not performed. The green diamonds are the surface roughness data points for each respective 12wt% resin content mounted point on ground areas while the red squares are the data points for each respective 16wt% resin content mounted point. The data for the average surface roughness (the blue line) and each point indicated in Figure 62 are the average values of a minimum of three measurements. The reason for some of the produced R_a values to be greater than the average could be due to a variety of factors such as grinding system deflection, vibrations/chattering, grinding parameters or defects incurred during mounted point manufacturing. Further analysis is required to determine the specific cause.

During grinding, the effect of work hardening is expected due to elevated temperatures and grinding forces that cause residual surface stresses. These stresses cause the surface hardness of the workpiece material to be greater than the material below the surface. The surface hardness measurements are shown in Figure 63. As mentioned earlier, the hardness measurements were conducted using a Vickers micro-hardness tester under an indentation load of 1kg.

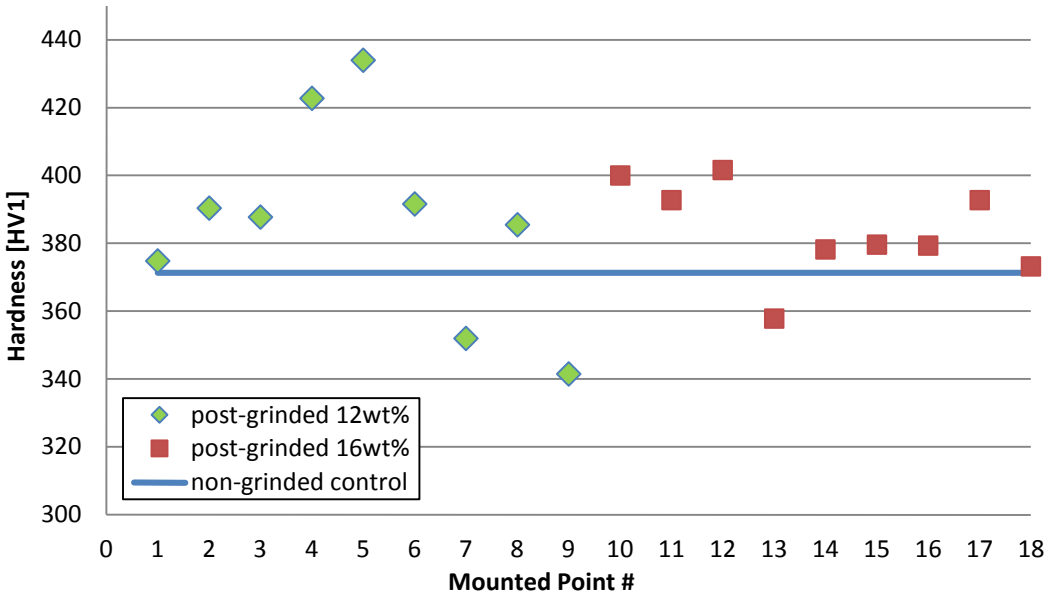

Figure 63 - Surface hardness measurement data for the post-ground workpiece surface

The surface hardness is also measured after the third grinding run of each mounted point. As expected, the surface hardness has increased for most of the areas where grinding took place. In total, about 83% of the mounted points caused work hardening on the surface of the workpiece. The blue line in Figure 63 is the average surface hardness of the workpiece on areas where grinding was not performed. The green diamonds are the surface hardness data points for each respective 12wt% resin content mounted point on ground areas while the red squares are the data points for each respective 16wt% resin content mounted point. The data for the average surface hardness (the blue line) and each point indicated in Figure 63 is the average values of a minimum of three single indentation measurements.

The grinding ratio of the mounted points can be calculated which would indicate whether the mounted points have similar wear to conventional grinding wheels. Even though the mounted points are manufactured with the highest possible consistency in a custom process, they are not perfect. The grinding ratio is calculated from Equation 2.6 as the ratio between the volumes of workpiece material removed and the wear of the mounted point. The individual grinding ratios for each mounted point is shown in Figure 64 and Figure 65.

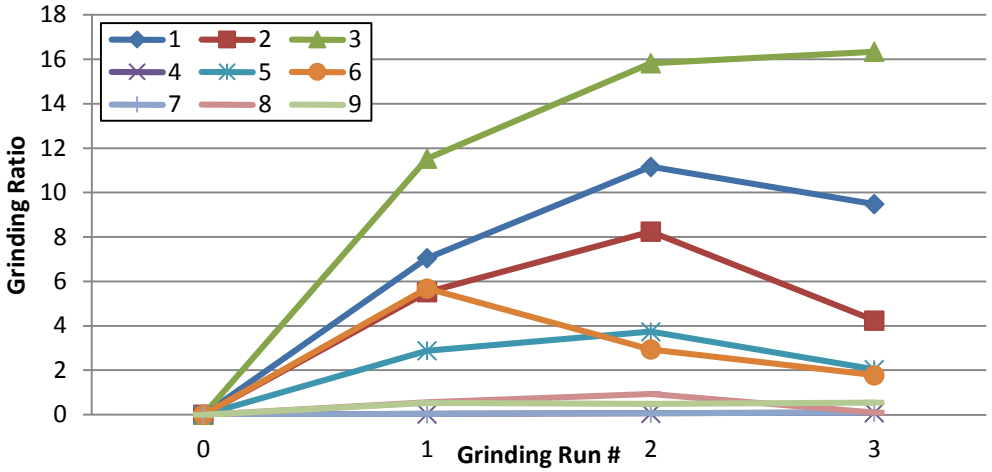

Figure 64 - Grinding ratio for the 12wt% mounted points

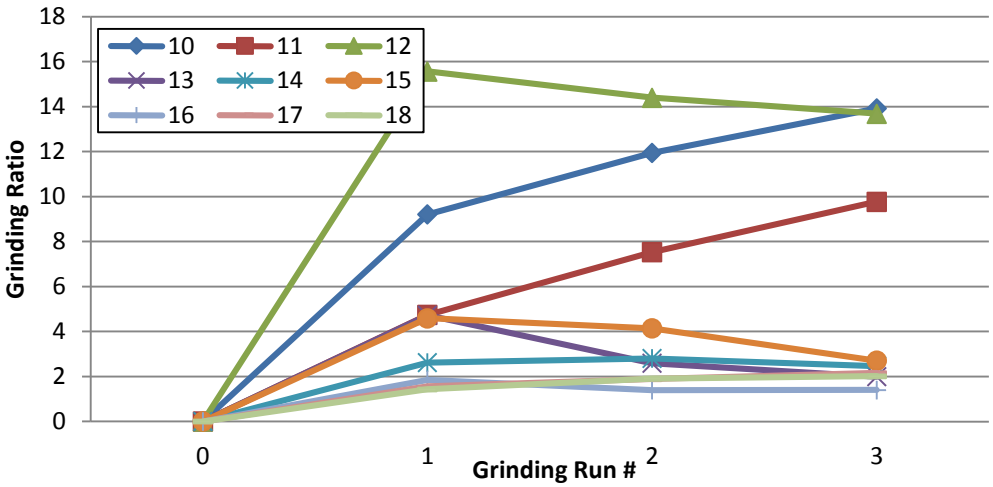

Figure 65 - Grinding ratio for the 16wt% mounted points

The grinding ratios of the mounted points in Figure 64 and Figure 65 show that there is a non-linear increase in some of the mounted points, but a decrease for most. The mounted points with a non-linear increase in grinding ratio is number 3, 10 and 11, all three having a steady wear rate as depicted in Figure 59 and Figure 60. The rest of the mounted points do not have steady wear rates, some having sharp increases in wear rate, and thus produces grinding ratios that decreases after the second grinding run. The grinding ratio data is insufficient for concluding that these custom produced mounted points performed similarly to conventional grinding wheels when comparing grinding ratios.

It would be very useful to measure the produced chip thicknesses, calculate the theoretical thicknesses as suggested in literature and compare the values. This could however not be done as the amount of material removed was very little and chips produced would most certainly

have been too small for evaluation purposes. However, to have gathered the chips for analysis, the vacuum system should not have been used. This was however not considered as the health and safety of the machine operator and any other person in the room was of greater importance. The analysis of chips produced with the grinding of WC-12wt%Co abrasives is thus strongly suggested for future work.

5) Conclusion and Future Work

Custom designed and manufactured mounted points containing WC-12wt%Co as abrasive medium and bonded with epoxy resin were used in grinding experiments to determine the performance characteristics of these mounted points. The grinding experiments consisted of grinding with two sets of resin content mounted points; consisting of 12wt% and 16wt% resin content. The workpiece being ground, at three different spindle speed and transverse feedrate values, was Ti6Al4V. Performance data measurements taken include the wear rate of the mounted points and the surface roughness and hardness of the workpiece material before and after grinding.

The mounted points ground the workpiece material and performed like grinding wheels, as expected. The wear rate of most of the mounted points is steady and predictable. The abrasive particle size allowed for the mounted points to be designed and implemented with micro-grinding as finishing process where low material removal rates are needed while a smooth workpiece surface finish is produced without polishing. This was supported by the workpiece surface roughness data where 66% of the tested mounted points produced a smoother surface finish compared to the workpiece surface prior to grinding. The workpiece surface hardness increased as expected over areas where grinding took place due to elevated temperatures during grinding and grinding forces causing residual stresses in the ground surfaces.

From the selected grinding parameters, no specific conclusion can be made as to the influence these parameters have on the resulting ground workpiece surface. The only conclusion that can be drawn from this finding is that more experiments should be conducted and thus more data recorded. From the increase in wear data, a more accurate conclusion could be made with respect to the influence of each parameter and their influences on each other and the wear of the mounted points.

Given the grinding parameters used in this study, the grinding process with WC-12wt%Co as abrasive medium can be used as an intermediate micro-grinding step (minimal material removal, high geometrical accuracy) before final polishing. Based on the experimental results, the micro-grinding with the mounted points is suitable for generating tight tolerances on highly accurate geometrical parts and part components. The application of producing these tight tolerances would most certainly require the mounted points to have improved geometries, which would require alternative mould designs. By altering the grinding

parameters to some extent and lowering the abrasive particle size, the grinding process can also be used for part or surface polishing. More experimentation should be conducted though to confirm the effectiveness of a polishing process.

The use of WC-12wt%Co as abrasive medium in mounted points, or grinding wheels in general, is not known as far as commercial applications go. There are thus many improvements that can be incorporated for future research. The abrasive particle size and shape can be changed so that other grinding applications such as high material removal rates or workpiece polishing could be investigated. The binder could be changed to vitrified, but then more specialized equipment would be needed for manufacturing of the mounted points. The implementation of a vitrified binder requires high temperatures for the vitrified binder to bind the abrasive particles, which are high enough for the WC-12wt%Co to undergo sintering, causing possible unforeseen issues such as large scale WC-*x*Co agglomeration.

For the continuation of development of resin bonded mounted points, the mould could be redesigned to allow for easier and more efficient mounted point production. Such alterations could include a more effective spindle design that takes up less space while the resin bonds better to it. The use of a phenolic resin should also be considered as it might allow for easier handling and moulding of mounted points. The amount of resin used should also be investigated as it might improve or hamper the grinding ability of the abrasive particles as was the case with the surface roughness of the higher resin content mounted points. There is also the possibility of producing a large grinding wheel, test its performance and compare it to the performance data of the smaller mounted points.

The grinding machine setup used during experimentation has some degree of flexing and this should be improved in future experimentation. Flexing could cause the grinding forces to be inconsistent along the grinding path as suggested by the system deflection data illustrated in Figure 10. The grinding machine setup could be made stiffer by improved clamping and the use of rigid spacers where needed. Another, possibly better, solution would be to use a larger grinding machine that is designed for the purpose of grinding and has a high degree of structural rigidity.

The use of cooling and lubricating fluids should be investigated to determine its effect on the grinding with WC-12wt%Co abrasive particles/grains. The use of the fluids might lead to a

better surface finish being produced or the prevention of surface hardness increase. These fluids could also reduce the grinding forces and reduce the wear rate of the mounted points. The dressing of the mounted points to produce an even grinding surface should also be investigated. It has the potential of improving the surface finish due to the grinding face having new sharp abrasive grains after each grinding run from the dressing process.

The use of carbides is vast in the manufacturing industry, ranging from tool inserts to end mills. The worn inserts and end mills usually end up as scrap and are sold off at low prices for recycling and reusing. There thus exists the possibility of using the recycled tungsten carbide as abrasive medium for grinding wheel or mounted point experimentation. This would reduce the product cost considerably and could make WC-Co in general a good competitor as abrasive material for the abrasives industry.

The grinding ratios of the mounted points showed that these mounted points operated in the initial wear region of conventional grinding wheels. The secondary wear region is linear and more gradual. This would cause the mounted points to wear at a lower rate and have an extended predicted working life. It is thus suggested that future experiments should be conducted with more grinding runs as to reach the second wear region. More grinding runs and wear rate calculations would allow for more accurate behaviour characterisation of the mounted points and thus allowing their type of abrasive and wear rates to be more comparable to that of conventional grinding wheels.

6) References

Aurich, J.C., Carrella, M. & Walk, M., 2015. Micro grinding with ultra small micro pencil grinding tools using an integrated machine tool. *CIRP Annals - Manufacturing Technology*, 64(1), pp.325–328.

Batako, A.D.L. & Koppal, S., 2007. Process monitoring in high efficiency deep grinding-HEDG. *Journal of Physics: Conference Series*, 76, pp.1–6.

Benham, P.P., Crawford, R.J. & Armstrong, C.G., 1996. *Mechanics of Engineering Materials* 2nd ed., Harlow: Pearson Education Limited.

Budynas, R.G. & Nisbett, J.K., 2008. *Shigley's Mechanical Engineering Design* 8th ed., New York: McGraw-Hill.

Callister, W.D., 2010. *Materials Science and Engineering* 8th ed., John Wiley &Sons, inc.

Dimitrov, D., Conradie, P.J.T. & Oosthuizen, G., 2013. A Process Planning Framework for Milling of Titanium Alloys. In *International Conference on Competitive Manufacturing*.

Donachie, M.J., 2000. *Titanium: a technical guide* 2nd ed., ASM International.

Encyclopædia Britannica Online, 2013. titanium (Ti). Available at: http://www.britannica.com/EBchecked/topic/597135/titanium.

Enever, A.A., Oosthuizen, G.A. & Sacks, N., January 2016. Performance evaluation of WC-12Co as grinding wheel abrasive material for machining titanium alloys. In *Proceedings of the 16th International Conference on Competitive Manufacturing*.

Enever, A.A., Oosthuizen, G.A. & Sacks, N., 2015. WEAR EFFECTS OF CUSTOM TUNGSTEN CARBIDE GRINDING WHEEL. In *Proceedings of the 11th International Tribology Conference*. Pretoria, p. 041 : 1–10.

Ferreira, J.A.M., Amaral, M.A.P, Antunes, F.V., Costa, J.D.M., 2009. A study on the mechanical behaviour of WC/Co hardmetals. *International Journal of Refractory Metals and Hard Materials*, 27(1), pp.1–8.

Gardziella, A., Pilato, L.A. & Knop, A., 2000. *Phenolic Resins - Chemistry, Applications, Standardization, Safety and Ecology* 2nd ed., Heidelberg: Springer.

Grinding Techniques, 2013. ABRASIVE PRODUCTS CATALOGUE. , pp.14–19. Available at: http://www.grindtech.com/pdf/TECHCATALOGUE_EBOOK.pdf.

Grote, K.-H. & Antonsson, E.K., 2009. *Springer Handbook of Mechanical Engineering*, New York: Springer.

Heinzel, C. et al., 2015. Advanced approach for a demand-oriented fluid supply in grinding. *CIRP Annals - Manufacturing Technology*, 64(1), pp.333–336.

Kim, J.C. & Kim, B.K., 2004. Synthesis of nanosized tungsten carbide powder by the chemical vapor condensation process. *Scripta Materialia*, 50(7), pp.969–972.

Klocke, F., Soo, S.L., Karpuschewski, B., Webster, J.A., Novovic, D., Elfizy, A., Axinte, D.A., Tönissen, S., 2015. Abrasive machining of advanced aerospace alloys and composites. *CIRP Annals - Manufacturing Technology*, 64(1), pp.581–604.

Klocke, F., Brinksmeier, E. & Weinert, K., 2005. Capability Profile of Hard Cutting and Grinding Processes. *CIRP Annals - Manufacturing Technology*, 54(2), pp.22–45.

Koc, R. & Kodambaka, S.K., 2000. Tungsten carbide (WC) synthesis from novel precursors. *Journal of the European Ceramic Society*, 20, pp.1859–1869.

Kummer, J., Chemical Elements, A Virtual Museum. Available at: http://images-of-elements.com/titanium.php [Accessed February 1, 2016].

Li, D. & Wong, L.N.Y., 2012. The Brazilian Disc Test for Rock Mechanics Applications: Review and New Insights. *Rock Mechanics and Rock Engineering*, 46(2), pp.269–287.

Lide, D.R., 2005. *CRC Handbook of Chemistry and Physics* 86th ed., Boca Raton, Florida: CRC Press.

Medeiros, F.F.P. et al., 2001. Synthesis of tungsten carbide through gas–solid reaction at low temperatures. *Materials Science and Engineering: A*, 315(1-2), pp.58–62.

Nagesh, C.H. & Ramachandran, C.S., 2007. Electrochemical process of titanium extraction. *Transactions of Nonferrous Metals Society of China*, 17(2), pp.429–433.

Ohoud, M.B., Obrecht, F., Gatineau, L., Levitz, P., Van Damme, H., 1988. Surface Area , Mass Fractal Dimension , and Apparent Density of Powders. *Journal of colloid and interface science*, 124(1), pp.156–161.

Oliveira, J.F.G., Silva., E.J., Coelho, R.T., Brozek, L., Bottene, A.C., Marcos, G.P., 2015. Dry grinding process with workpiece precooling. *CIRP Annals - Manufacturing Technology*, 64(1), pp.329–332.

Oosthuizen, G.A., Akdogan, G., Dimitrov, D., Treurnicht, N.F., 2010. A Review of the Machinability of Titanium Alloys. *R & D Journal of the South African Institute of Mechanical Engineering*, (26), pp.43–52.

Patankar, S.N., Kwang, Y.T. & Jen, T.M., 2001. Alpha casing and superplastic behavior of Ti–6Al–4V. *Journal of Materials Processing Technology*, 112, pp.24–28.

Picas, J.A., Xiong, Y., Punset, M., Ajdelsztajn, L., Schoenung, J.M., 2009. Microstructure and wear resistance of WC-Co by three consolidation processing techniques. *International Journal of Refractory Metals and Hard Materials*, 27(2), pp.344–349.

Saito, H., Iwabuchi, A. & Shimizu, T., 2006. Effects of Co content and WC grain size on wear of WC cemented carbide. *Wear*, 261(2), pp.126–132.

Shetty, D.K., Wright, I.G., Mincer, P.N., Clauer, A.H., 1985. Indentation fracture of WC-Co cermets. *Journal of Materials Science*, 20(5), pp.1873–1882.

da Silva, A.G.P., Schubert, W.D. & Lux, B., 2001. The role of the binder phase in the WC-Co sintering. *Materials Research*, 4(2), pp.59–62.

Uddeholm, 2012. *Grinding of Tool Steel*, Available at: http://www.uddeholm.com/files/TB_grinding-english.pdf [Accessed May 20, 2015].

Wang, Q. & Xing, L., 1999. Determination of fracture toughness K IC by using the flattened Brazilian disk specimen for rocks. *Engineering Fracture Mechanics*, 64, pp.193–201.

Wang, Q.Z., Jia, X.M., Kou, S.Q., Zhang, Z.X., Lindqvist, P.-A., 2004. The flattened Brazilian disc specimen used for testing elastic modulus, tensile strength and fracture toughness of brittle rocks: analytical and numerical results. *International Journal of Rock Mechanics and Mining Sciences*, 41(2), pp.245–253.

Zhang, X., Yan, P. & Shen, H., 2011. Study on the Stress Distribution of Grinding Wheel Based on ANSYS under Multi-operating Modes. In *2011 Second International Conference on Digital Manufacturing & Automation*. Ieee, pp. 1184–1186.

Addendum A

Dimensions in millimetres

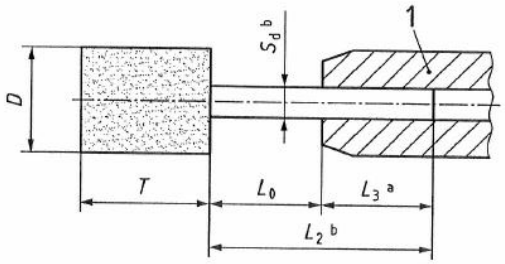

Key

1 collet

a $L_3 \geq 10$.

b $S_d = 3$ and $L_2 = 30$ or $S_d = 6$ and $L_2 = 40$ or $S_d = 8$ and $L_2 = 40$.

Figure 1 — Wheel plain, Shape WPL

Table 1 — Wheel plain, Shape WPL, $S_d = 3$ mm and $L_2 = 30$ mm or $S_d = 6$ mm and $L_2 = 40$ mm or $S_d = 8$ mm and $L_2 = 40$ mm

Dimensions in millimetres

Designation	Former code	D	T
WPL 03 06 03	W144	3	6
WPL 03 10 03	W145		10
WPL 03 13 03	W146		13
WPL 05 06 03	W152	5	6
WPL 05 10 03	W153		10
WPL 05 13 03	W154		13
WPL 06 06 03	W160	6	6
WPL 06 10 03 WPL 06 10 06	W162		10
WPL 06 13 03 WPL 06 13 06	W163		13
WPL 06 20 03	W164		20
WPL 08 10 03 WPL 08 10 06	W169	8	10
WPL 08 13 03	W170		13
WPL 08 20 03	W171		20
WPL 10 10 03 WPL 10 10 06	W175	10	10
WPL 10 13 03 WPL 10 13 06	W176		13
WPL 10 20 03 WPL 10 20 06	W177		20
WPL 10 25 03 WPL 10 25 06	W178		25
WPL 10 32 06	W179		32

Table 1 *(continued)*

Designation	Former code	*D*	*T*
WPL 13 03 03 WPL 13 03 06	W182	13	3
WPL 13 06 03 WPL 13 06 06	W183		6
WPL 13 13 03 WPL 13 13 06	W185		13
WPL 13 20 03 WPL 13 20 06	W186		20
WPL 13 25 03 WPL 13 25 06	W187		25
WPL 13 40 06	W188		40
WPL 16 20 03 WPL 16 20 06	W195	16	20
WPL 16 25 03 WPL 16 25 06	W196		25
WPL 16 50 06	W197		50
WPL 20 06 03 WPL 20 06 06	W201	20	6
WPL 20 10 03 WPL 20 10 06	W202		10
WPL 20 20 03 WPL 20 20 06	W204		20
WPL 20 25 06	W205		25
WPL 20 32 06	W206		32
WPL 20 38 06	W207		38
WPL 20 50 06	W208		50
WPL 25 03 03 WPL 25 03 06	W215	25	3
WPL 25 06 03 WPL 25 06 06	W216		6
WPL 25 10 06	W217		10
WPL 25 13 06	W218		13
WPL 25 20 06	W219		20
WPL 25 25 06	W220		25
WPL 25 32 06 WPL 25 32 08	W221		32
WPL 25 50 06 WPL 25 50 08	W222		50
WPL 32 06 06	W225	32	6
WPL 32 10 06	W226		10
WPL 32 20 06	W228		20
WPL 32 32 06 WPL 32 32 08	W230		32
WPL 32 50 06	W232		50
WPL 38 06 06	W235	38	6
WPL 38 13 06	W236		13
WPL 38 38 06 WPL 38 38 08	W238		38

Addendum B